SIMULATION OF AGONIST AND ANTAGONIST MUSCLE ACTIVATION PATTERNS IN BIDIRECTIONAL POSTURAL PERTURBATION IN CATS

A Thesis
Presented to
The Academic Faculty

by

Alexander Koenig

In Partial Fulfillment
of the Requirements for the Degree
Master of Science in the
School of Electrical and Computer Engineering

Georgia Institute of Technology
August 2006

SIMULATION OF AGONIST AND ANTAGONIST MUSCLE ACTIVATION PATTERNS IN BIDIRECTIONAL POSTURAL PERTURBATION IN CATS

Approved by:

Dr. Lena H. Ting, Advisor
School of Biomedical Engineering
Georgia Institute of Technology

Dr. Robert Lee
School of Biomedical Engineering
Georgia Institute of Technology

Dr. Magnus Egerstedt
School of Electrical Engineering
Georgia Institute of Technology

Date Approved: 7th July 2006

Für meine Eltern – Danke für Wurzeln und Flügel!

ACKNOWLEDGEMENTS

The final version of this thesis turned out to be very different from what I intended it to be in the beginning. I thank my advisor Dr. Lena Ting for introducing me to the world of science and trusting in me during the changes my work underwent. I have the highest respect for her professional skills and want to thank her for pushing me in the right direction at the right time. Thanks to my reading committee, Dr. Robert Lee and Dr. Magnus Egerstedt for investing their time and commitment. I also want to thank to my colleagues: Dr. Anindo Roy, who mentored me until he left the Neurolab, Lucas McKay for great help with Matlab, Torrence Welch and Kartik Sundar for all their suggestions and improvements, Keith van Antwerp for explaining me the world of muscle contraction and my colleagues Jevin Scrivens, Nate Bunderson and Gelsy Torres-Oviedo for their tips and for proof reading - literal German translations sometimes just don't do it.. Thanks to my roommates for allowing me to mess up their party schedule by asking for quiet on the weekends.

Finally, I want to thank Danie Meyer for all her commitment to me, to my work and for her patience with me.

TABLE OF CONTENTS

LIST OF TABLES

LIST OF FIGURES

SUMMARY

We studied the effects of varying perturbation magnitude and direction on the postural control process of the central nervous system (CNS) caused by perturbation, before and after sensory loss. The electromyogram (EMG) response to a postural perturbation can be composed by a weighted sum of the center of mass (CoM) kinematics. We extended an existing CoM feedback model which predicted EMG of one muscle for unidirectional perturbations; we used recorded data of bidirectional perturbations, which caused muscle activity in anterior as well as posterior muscles. Modeling the CNS as two delayed feedback controllers, we reconstructed the EMGs of two antagonistic muscles simultaneously that were recorded during postural perturbation experiments on cats. Minimizing the error between predicted and recorded EMG and CoM kinematics, we were able to identify controller gains that would result in the best prediction of the recorded EMGs.

We hypothesized that the weights on the CoM kinematics remained constant independent of variations in perturbation magnitude or reversed perturbation direction. We applied our model to data from bidirectional perturbations with varying magnitude, with which the cats were perturbed for a short time in one direction and a longer time in the opposite direction.

The gains showed small variation for EMG predictions following long perturbations; however, the prediction of EMG following the initial displacement resulted in large gain variations. We showed that these variations were caused by our optimization methods, which was not able to consistently identify controller gains for short initial movements. Using the weights identified for unidirectional perturbations, we were able to predict muscle activity for both directions with the same gains. This suggests that the weights of the CoM kinematics for each muscle did not change for varying perturbation magnitude. We conclude that varying EMG shapes were induced solely by the variation of the CoM kinematics.

We repeated the investigations on data that was recorded from cats suffering from sensory loss and found reduced CoM acceleration feedback.

CHAPTER I

INTRODUCTION

1.1 Motivation

Upright posture in humans and animals is inherently unstable due to the effects of gravity and perturbations; the body will fall when no active control is applied. 30% of persons over 65 experience at least one fall pear year, of which one out of every ten results in serious injury (Tinetti 2003). The body's attempt to stabilize upright posture is controlled by the central nervous system (CNS). As the consequences of a fall are not predictable and can be fatal, the CNS is responsible for ensuring the body's stability: during each movement and after each perturbation. The mechanisms, through which the CNS controls movements of humans and animals, are not yet completely understood. In case of a perturbation to stability, sensors throughout the body deliver information to the CNS. We have a good understanding of the functionality of the sensors which detect a perturbation of balance, as well as on the dynamics of the muscle-skeleton-apparatus, which translates the control commands of the CNS into movements. However, it is still widely unknown how the CNS integrates sensory information, and how it uses this integrated information to generate the control signal to the muscles. Also unknown is how sensory loss affects the generation of the control signal. Although the magnitude of a perturbation has an impact on the generation of the control signal (Park et al. 2004); up to now, the influence of the characteristics of the perturbation on the generation of the control signal is also not completely understood.

In order to stabilize the body, the CNS uses sensory information and integrates this information to generate the control signal to the muscles. The influence of sensory sources, supplying the CNS with information on the stability and position of the body, is weighed differently during the integration process (Peterka and Loughlin 2004).

Somatosensory information, the sensory feedback on muscle force, length and contraction velocity, is estimated to contribute about 60-75% of the information, which the CNS uses to compile the postural control signal (Horak et al. 2002). As diabetes can cause somatosensory loss (Horak et al. 2002), investigations on diabetes patients revealed a 35 times increased risk of falling compared to non diabetic persons (Tinetti and Williams 1998). This raises the questions: which are the consequences of the loss of one or several sensory information sources used for postural control and how does the CNS stabilize the body with decreased feedback information?

Modeling and simulation give insight into the functionality of the CNS as means to better understand how the CNS stabilizes the body. In modern control theory, controller design can be accomplished fairly easily, as precise models of manmade systems are commonly available. The state space representation of a helicopter can be calculated with a high degree of accuracy as the laws of physics are very well understood, and it is possible to create mathematical models of all of the subsystems with which the helicopter is built. Once the dynamic behavior of the subsystems is known, the behavior of the overall model can be predicted very accurately and a controller can be calculated using the methods of modern control theory.

Compared to a technical system like that of a helicopter, the controller design of the CNS model can be difficult due to the incomplete knowledge on the human system. A mathematical derivation of a model of the body can only be done partially using the laws of physics – a ‘divide and conquer’ approach to the body in order to investigate controllable subsystems is not possible. Additionally, in comparison to a helicopter, reverse engineering of the CNS is impossible, since subsystems cannot be removed in order to separately investigate their functionality. This lack of mathematical representability therefore must be replaced by observations and measurements.

One possible measurement of the CNS activity is the control signal generated by the CNS, which is reflected indirectly as muscle activity in the electromyogram (EMG). Lockhart showed that there exists evidence that the EMG response to a postural perturbation is composed due to feedback of a weighted sum of the center of mass (CoM) kinematics (Lockhart 2005).

But how does the CNS scale its reaction with varying perturbation velocities and accelerations? What role does the sensory information play during the composition of the EMG? How are perturbation velocity and acceleration incorporated into the EMG when one or more sensors do not deliver feedback anymore? Deeper understanding of the dependency between perturbation and CNS reaction as well as a better understanding of adaptation behavior of the CNS to sensory loss could potentially lead to controllers that sense destabilization in elderly people, analyze the perturbation and intervene intelligently in the control process to prevent falling. Results of these controllers have the potential to be neural prostheses which bridge damaged parts of the CNS and might partially restore functionality of the CNS in spinal cord injury patients. Perhaps, one day paraplegics could overcome their handicap or injury, and death rate due to fatal falls of old people could find a drastic reduction.

1.2 Research Question

We were interested in the effects of different magnitudes and directions of perturbation displacement on the postural control process of the CNS, before and after somatosensory loss. We based our work on the research of Lockhart (2005), who predicted EMG data that was recorded during perturbation experiments on cats standing at rest, using a feedback model. He simulated one muscle at a time and predicted the muscle activity for a unidirectional ramp and hold translation. Since postural control in real life involves several muscles at a time, we wanted to predict more than one muscle EMG simultaneously. We extended Lockhart's model and reconstructed the EMGs of two antagonistic muscles simultaneously that were recorded during postural perturbation experiments.

Perturbations occur during quiet standing and during movement. We wanted to investigate if Lockhart's hypothesis on the EMG composition via summation of CoM kinematics would still hold, when the body was not initially at rest when a perturbation occurred. By using a variety of different perturbations magnitudes and reversed

translation direction, we investigated the effects of initial movement on the postural control process

Cats were used as test subjects, since we wanted to investigate the effect of sensory loss. The sensory loss was induced by an overdose of Pyridoxine and was permanent. We directed special attention to the following questions:

- Can we predict two antagonist muscles that act during one perturbation, at the same time with a simple model?
- What is the effect of reversed perturbation direction or altered displacement magnitude on the parameters of the model when the subject is initial not at rest?
- What effect does sensory loss have on the EMG and on the parameters of our model?

CHAPTER II

BACKGROUND

2.1 Overview

Although several studies have been published on postural control, to our best knowledge there exists no theoretical study that simulates postural behavior and treats two antagonistic muscles simultaneously in one model using uni- and bi-directional perturbations. We developed a model for investigation of postural stabilization after perturbation in cats and predicted two antagonistic EMG traces simultaneously. We investigate the dependency of the perturbation, its magnitude, its velocity and acceleration on the resulting EMGs of the muscles responsible for postural stabilization. We developed muscle models of different complexity and studied their impact on the EMG prediction. In the following, the basic background information on perturbation experiments, up to date literature on simulation models, EMG patterns, muscle models and sensory loss will be reviewed.

2.2 Introduction to perturbation experiments and models

A body is considered stable when the body's Center of Mass (CoM) lies within the base of support (BoS) and when the current velocity vector will not push the CoM out of these bounds (Roy 2004). The BoS is the area underneath the feet which has contact with the ground. When a perturbation of balance occurs, the CNS has to compensate for the perturbation and bring the body back to an upright position. As long as the CoM does not leave the BoS, the perturbation can be intercepted without stepping. In perturbation experiments, humans or animals stand on a perturbation platform; they are disturbed by ramp plus hold translation of the platform. The platform movement destabilizes the body

by pulling the BoS away underneath the CoM. Depending on the perturbation, sensors throughout the body sense a stretch or shortening of muscles and send sensory information to the CNS. Compiled with further information like muscular contraction speed or force, the CNS creates a control signal which is sent to the muscles. Due to the finite signal conduction speed of nerves, this information transfer and processing results in a time delay. In humans, the delay lies around 100ms (Horak and Macpherson 1996), in cats between 30 and 50ms. Together with the moment arms, the muscles then translate this control signal into corrective torque around the joints. The muscle activity is called electromyogram (EMG) and can be measured using EMG sensors. Furthermore, using a motion analysis system, the position of single body segments (shank, thigh, upper body and head) and of the angles at the ankle, knee and hip joint can be recorded.

Though we worked with cat data, a review of results on human postural stabilization is relevant, since we used simulation concepts on cats that were previously employed on humans, and since sensomotori mechanisms are similar in cats and humans. For stabilization after perturbation, the human CNS can select between three general strategies (Horak et al. 1989). Smaller perturbations can be accounted for by the “ankle strategy”. Hip and knee joints remain almost stiff, and the perturbation is compensated by moments around the ankle joints. Larger perturbations often demand compensatory movements of the hip, known in the literature as the “hip strategy”. Additionally, flexion of the knees can be used.

2.3 Review of previous research on postural control modeling

2.3.1 Postural control models of body dynamics, time delays and muscle models

Several researchers used feedback models to predict kinematic or EMG data that was recorded during perturbation experiments. The models simulated the kinematics of the stabilization movements that the test subject performed after a perturbation. Amongst other information, sensory models provide feedback information to the CNS on muscle contraction velocity, muscle length or muscle contraction force. Together with time

delays accounting for the neural time delays, the CNS controller performed the sensorimotor transformation, i.e. compiling the control signal to the muscles from the timed delayed sensory information. The muscles were simulated as transfer functions that translate the CNS control signal into forces. Moment arms transformed these forces into torque around the joints (Horak and Macpherson 1996).

Previous researchers simulated the physiology of the test subject and included different levels of complexity some modeling one, two or three link inverted pendula, sensory systems, time delays or muscle models. While most researchers predicted kinematics and matched them to recorded data, only few predicted EMGs. Conclusions were then drawn from the simulation parameters of the system and from their behavioral reactions to changing perturbation magnitudes and directions or changing sensory information.

To theoretically investigate perturbation experiments, the body's dynamics have been modeled as an inverted pendulum. To investigate the ankle strategy in humans, the body was modeled as a one link inverted pendulum (Lockhart 2005; Peterka 2000). Hip movements were accounted for by extending the pendulum by one joint (Park et al. 2004). Additionally, the three link inverted pendulum modeled knee movements (Jo and Massaquoi 2004; Kuo 1995; Kuo and Zajac 1993; Peterka 2000; 2002). Cats have been modeled as a one link inverted pendulum (Lockhart 2005), the dynamics of a cat limb have been modeled as a three link inverted pendulum (He et al. 1991).

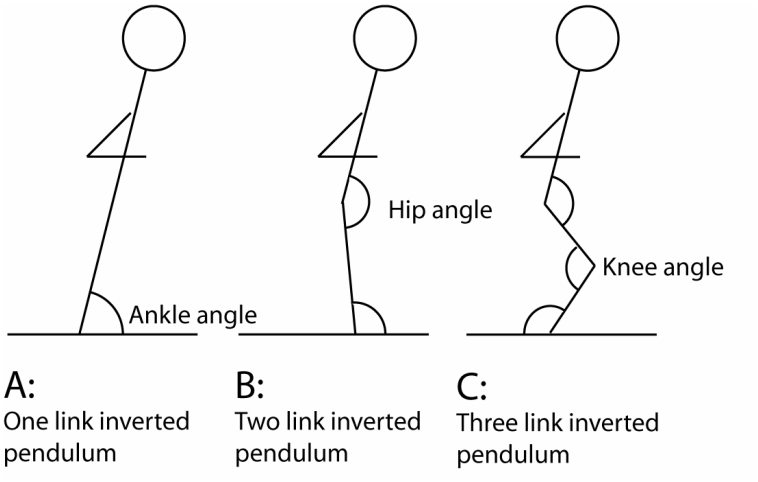

Figure 1: Stick figure models for perturbation experiment. A - Ankle strategy model, B - Hip strategy model, C: additional joint for knee modeling

Besides the body dynamics, previous simulation models included sensory systems, time delays and muscle models and employed optimal control to identify parameters of the CNS model. As for models of sensors throughout the body, the complexity of sensory systems ranged from full state feedback (Park et al. 2004) without employing sensory models to sophisticated sensor models. If sensors were modeled, they could include muscle spindles, otolith organs, semicircular canals, skin afferents and the visual system (van der Kooij et al. 1999; van der Kooij et al. 2001). He et al. modeled the system states of the limb dynamics to represent the physiological outputs of sensors throughout the limb: muscle forces, muscle length and velocity, joint angles and velocities and motoneuron activities. By multiplying the output of the dynamical system with gain matrices, his model was able to provide state feedback (He et al. 1991). Time delays simulated the neural time delays inherent in every test subject. Variable (Peterka 2000, Kuo 1995) or fixed time delays (van der Kooij et al. 1999; van der Kooij et al. 2001) have been used; there also exist studies that neglected time delays (Park et al. 2004). If muscle models were employed, models of different complexities have been developed: Lockhart used a first order model (Lockhart and Ting 2004) to predict one muscle at a time; Jo and Massaquoi employed second order muscle models(Jo and Massaquoi 2004), He et al. predicted the EMG of 10 muscle tendon actuators simultaneously using complex, nonlinear models. Optimal control in form of a Linear Quadratic Gaussian Regulator (LQG) (He et al. 1991; Kuo 1995; Kuo and Zajac 1993) or with hybrid switching (Jo and Massaquoi 2004) was used to stabilize a three link inverted pendulum against perturbations. The cost function used on the optimization process penalized deviation of the states from the desired reference trajectory as well as from the neural control effort. Using a similar cost function, Lockhart employed optimal control using optimal feedback gains of a PID controller.

2.3.2 Postural control models of the CNS

The model of the CNS used delayed feedback information from the sensors and integrated it to generate the control signal to the muscles models. Since the functionality of the CNS has not been clearly understood, the development of the CNS model was difficult. Van der Kooij had modeled the CNS as a PD controller, wheresas He et al. had modeled the CNS using gain matrices which weighed and summed the sensory output.

Lockhart showed that recorded EMG can be reconstructed in a simulation via a linear combination of delayed CoM kinematics. In order to simulate CoM kinematics for EMG reconstruction, he developed a biomechanical model of the dynamic, muscular and neural properties of a cat during perturbation experiments. As models of human or animal physiological can become complex, he chose a model with which he would strike a balance between simplistic and realistic behavior. Peterka had shown that a one link inverted pendulum approximated the dynamics of a test subject well enough for postural perturbation experiments (Peterka 2000). Using the recorded platform acceleration

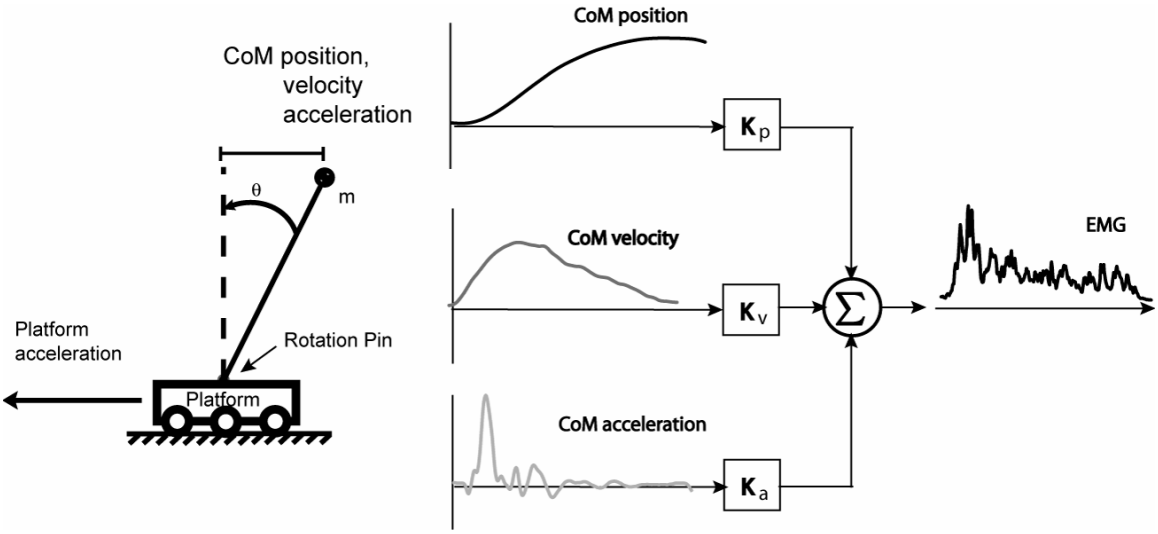

Figure 2: EMG composition via weighed sum of CoM kinematics. A - Inverted pendulum as model for the cat dynamics. B - Composition of EMG from CoM feedback components. Note the difference between results of Szturm or Siegmund, who investigated the dependency of the EMG on the platform kinematics and the findings of Lockhart, who showed that the EMG can be composed by a weighted sum of CoM kinematics.

as input data, Peterka was able to compute the simulated CoM kinematics of the model. By theoretically predicting data that was recorded in cat experiments, he found that the

first burst of an EMG was mainly dependent on the acceleration of the CoM, whereas the EMG plateau would scale with the CoM position and velocity. Peterka mentioned that an acceleration signal would rise faster in magnitude than velocity or position on a continuous time signal and that this information could therefore be used until velocity and position information became available. (Lockhart 2005).

2.3.3 Modeling critiques and our extension

We wanted to close the gaps between the publications described above regarding magnitude and direction of perturbation, number of predicted muscles and simulation models. We investigated the effects of bidirectional perturbations on the composition of the EMG. Park investigated the effect of changing perturbation magnitudes (Park et al. 2004) and predicted a gradual, linear scaling of feedback parameters with varying platform displacement magnitude. Park concluded that constant feedback gains would be inappropriate to predict perturbations of different magnitudes and that the gains would scale linearly with perturbation magnitude. She did not investigate the effect of changing perturbation magnitude in combination with changing perturbation direction and non zero initial CoM kinematics.

We predicted several muscles simultaneously with a simple simulation model. Of the above authors, Lockhart, He and Jo were the only ones to predict EMG traces. Lockhart's study was restricted to predicting only one muscle EMG at a time. Since changes in perturbation direction induce muscle activity in several muscles, we predicted two antagonistic muscle EMGs simultaneously. He's model predicted several muscles simultaneously, but used a controller model of large complexity and was not able to explain the effect of all his CNS parameters on the postural control process. Jo employed a model of the cerebellum using sliding modes to switch controller gains as a function of the sensed body kinematics. We wanted to keep the model simple in order to get an intuitive explanation for the controller gains.

We investigated the effect of higher order, linear muscle models on the EMG prediction, since none of the above studies took them into account. We looked at the physiology behind muscular contraction in order to identify the main dynamic

characteristics of a muscle. We were then able to identify a higher order muscle model and investigated its effect on the prediction compared to a muscle model of lower order.

With these investigations, we filled the gap between CoM and EMG prediction, simulating two antagonistic EMG traces with second order muscle models while still predicting the CoM kinematics. As we will alter the perturbation magnitude and direction, it is necessary to understand the effects of changes of the platform kinematics on the resulting EMG.

2.4 Dependency between platform kinematics and EMG shape

2.4.1 EMG scales with platform velocity and acceleration

EMG as a reaction to a perturbation is generally composed of an initial burst and a following plateau region. It follows a perturbation with a time delay, which is caused by the finite speed of nerve signal conduction. A muscle is considered active or “on” when its EMG exceeds a threshold which exceeds background noise. This time point is called onset. There exists strong evidence that the first burst is mainly dependent on the character of the platform acceleration (Siegmund et al. 2002), whereas the plateau region of an EMG shows a high correlation with the velocity and position profile of the platform motion.

Several researchers reported a dependency between platform acceleration and EMG onset and EMG magnitude. In 1997, Szturm observed that varying platform acceleration had no effect on time to peak displacement or peak magnitude of CoM displacement, but did have an effect on EMG magnitude (Szturm and Fallang 1998). Brown noted a dependency between the EMG platform acceleration and the time delay between perturbation and EMG onset (Brown et al. 2001). Siegmund observed in 2001 that different perturbations with the same velocity profile, but different accelerations showed a nonlinear scaling of the EMG amplitude and the time delay between perturbation and EMG onset (Siegmund et al. 2002). In experiments he was able to show that changes in the first burst of an EMG scaled with acceleration and that changes of the

plateau region scaled with the velocity of the perturbation. Jo and Massaquoi showed a simulated EMG profile, whose first bursts scaled with the magnitude of the acceleration driving the simulation (Jo and Massaquoi 2004).

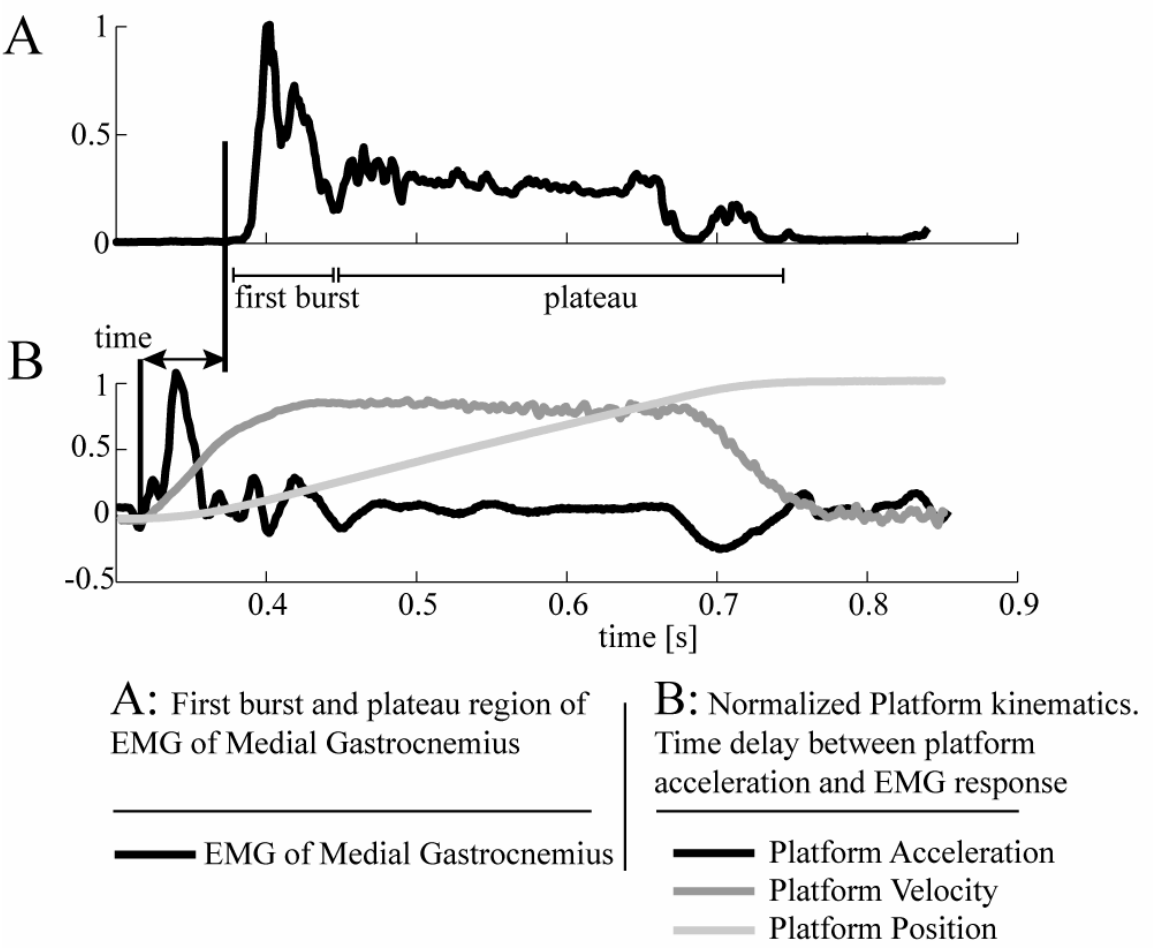

Figure 3: Dependency of EMG on the platform kinematics. A - EMG of muscle Gastrocnemius. B - Normalized platform kinematics. Observe that the acceleration is almost at its peak level when the velocity is not even at 30% of its peak and the position is still almost zero.

Though all these investigations were performed on muscular activity of humans, results on humans were comparable to the ones of cats. On the one side, cats have similar muscle structure as humans, using similar sensors. Signal conduction in nerves also results in a time delay, though this delay is shorter due to the shorter distance the signal has to travel. Figure 4 shows a direct comparison between a human and a cat EMG from a perturbation experiment both using a unidirectional perturbation. Both EMG traces show a first burst and a plateau. As mentioned in the model review chapter, Lockhart (2005) found that a cat EMG can be composed by the weighed sum of CoM kinematics.

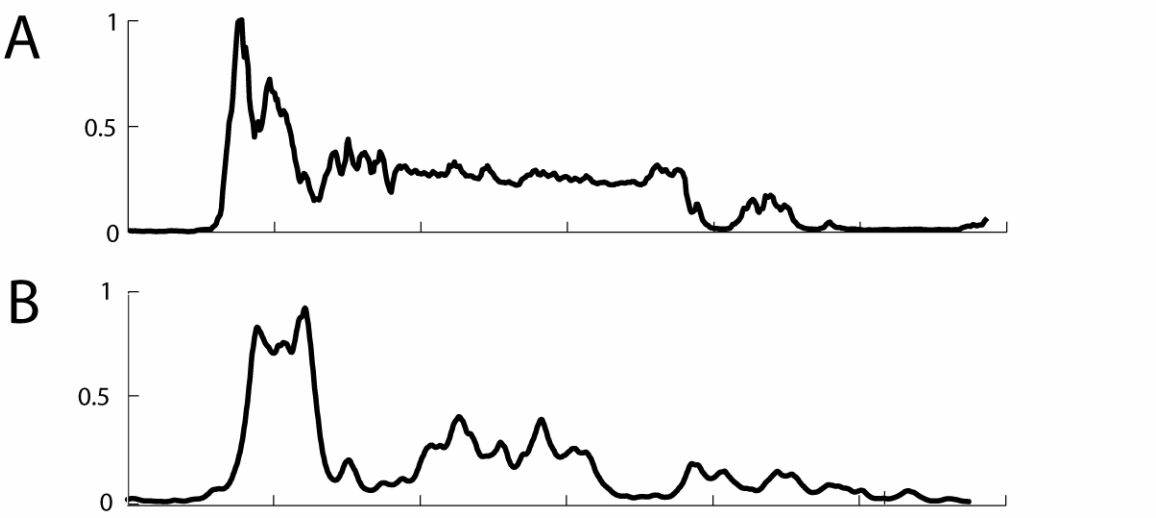

Figure 4: Comparison between human and cat EMG. A - cat EMG for muscle medial Gastrocnemius B - Human EMG for muscle Biceps Femoris Longhead

2.4.2 Our perturbation extensions

Until now, only unidirectional translations have been investigated. Lockhart showed that unidirectional perturbations resulted in EMG shapes that are dominated by an in initial burst and a plateau region. An obvious extension was to investigate the effect of bidirectional perturbations on the EMG composition and prediction. Bidirectional perturbations translate first the test subject in one direction for a certain amount of time and then reverse perturbation direction.

In order to investigate the effect of bidirectional perturbations on the EMG, we used two different kinds of perturbations: as short backward movement followed by an immediate, long forward displacement and a short forward movement followed by an immediate, long backward displacement. Consequences of changing the direction of perturbation will be discussed in the Methods section.

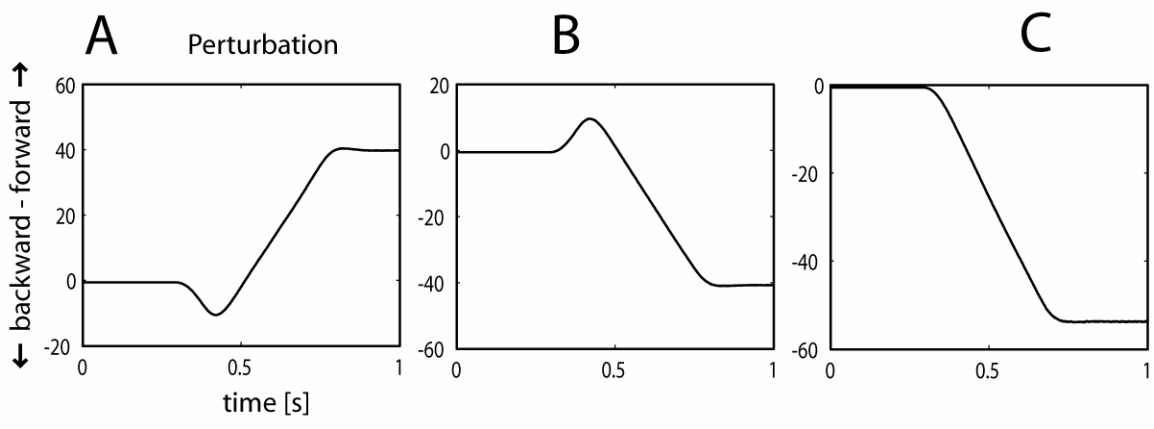

Figure 5: Perturbations. A - Bidirectional forward perturbation B - bidirectional backward perturbation C - unidirectional backward perturbation

2.5 Introduction to muscle models

In order to develop and justify a muscle model for our investigations, we also investigated muscle physiology. This was necessary in order to decide which simplifications were valid for our investigations and which muscle characteristics needed to be preserved in our model.

2.5.1 Muscle contraction

The process of producing active forces in skeletal muscle begins with the firing of a motor neuron that leads to the contraction of skeletal muscle. Motor neurons are located in the brainstem or the spinal cord and produce an action potential. This electrical signal travels down the nerve axons. The conduction is thereby achieved by Na++ and K- ions. On the junction of the axon with the muscle (neuromuscular junction), the axon braches and each branch connects to one muscle fiber. A motor neuron plus the muscle fiber it innervates is called a motor unit. One neuron can reach several muscle fibers via branching, but only one muscle fiber is innervated by one neuron branch. At this

junction, the electric action potential is converted to a chemical potential using the neurotransmitters acetylcholine (ACh).

"Excitation dynamics" is the conversion of an electrical stimulus into a chemical stimulus. The time frame for this lies typically in the region of 10ms. The ACh binds to the ACh receptors and causes a depolarization. This results in an action potential that travels down from the junction in the transverse tubular system in all directions of the fiber. The transverse tubular system signals the sarcoplasmic reticulum to release calcium close to the myofilaments. There, the calcium causes actin to combine with myosin in order to generate force. This is called calcium dynamics, or "activation dynamics". The time necessary for the activation dynamics lies in the range of around 40ms (Lieber 1992).

2.5.2 Mechanical properties of a muscle

The force output of a muscle is dependent on both its active and passive mechanical properties. The active mechanical properties are often summarized by the active-force-length and force-velocity relationship (Audu and Davy 1985); (Van der Helm and Rozendaal 2000). The optimal fiber length l_0 is defined as the muscle length in its active state, where the fibers produce maximal force output in an isometric contraction (Gordon et al. 1966). The force output at larger or smaller length then l_0 will be smaller then the maximal force.

The force velocity relationship indicates how much force a muscle produces depending on its contraction velocity. For positive velocities, i.e. a muscle shortening, the force will be smaller than the maximal force at optimal length. However, negative contraction velocities (i.e. an eccentric contraction) cause force to be produced greater than maximum isometric forces. This property is accredited to the dynamic interaction of the "actin myosin cross bridge" (Widmaier et al. 2006).

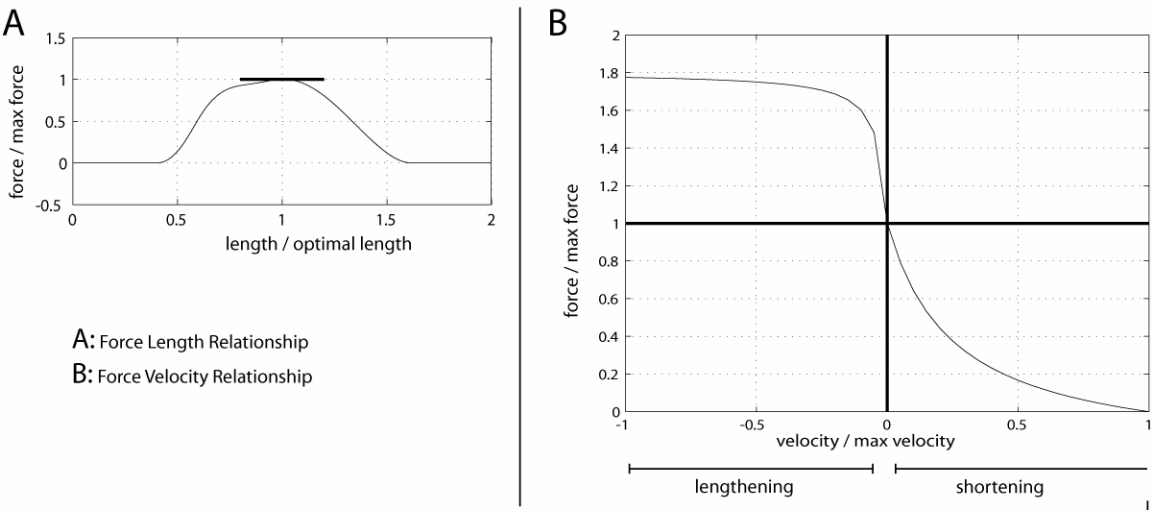

Figure 6: Force length and force velocity relationship. A - Operating point around optimal length allows for a linearization of the force-length-relationship B – Operation point around zero velocity allows for the force-velocity-relationship to reduce to the term F_{max}

2.5.3 Muscle models

Muscle models like the one of Winters (Winters and Stark 1985) model the nonlinear dynamical properties of the muscle as a composition of an active contractile element (CE) that depends on neural input and on two spring like passive elements arranged in series (SE) and parallel (PE) to the contractile element. The passive elements have no definitive structural basis but represent a combination of the elastic properties of the passive tissue in the musculoskeletal unit. The force generating properties of the contractile element depend on contraction velocity and muscle length as described by the force-velocity and force-length relationships.

The control for the model descends from the motor neurons (See Figure 7); the excitation dynamics translate the motor control signal $\vec{u}$ into an electric signal $\vec{e}$; the activation dynamics translate $\vec{e}$ into the chemical signal $\vec{a}$. Van der Helm and Roozendaal (Van der Helm and Rozendaal 2000) modeled excitation dynamics and activation dynamics as first order transfer functions.

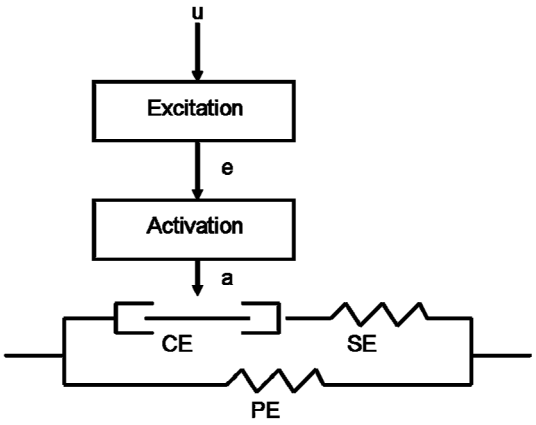

Figure 7: Nonlinear model of a muscle. The neural command u from the motor neurons is translated into the excitation e. The excitation e is then translated into the activation a via the Calcium dynamics. The Contractile Element (CE), the Series Elastic element (SE) and the Parallel Element (PE) model the mechanicsl nonlinearities of the muscle.

$$H_{act}(s) = \frac{1}{t_a \cdot s + 1}. \quad (1)$$

$$H_{exc}(s) = \frac{1}{t_e \cdot s + 1} \quad (2)$$

Where t_a and t_e are the time constants for the respective processes. They then improved the model of Winters and Stark by adding force feedback of the Golgi Tendon Organs (GTO) and sensory feedback on muscle length and velocity via the muscle spindles.

2.6 Somatosensory loss

We studied the effects of somatosensory loss in cats and compared EMG and CoM predictions of intact cats versus sensory loss cats. In order to better understand the reasons and consequences for somatosensory loss, a short review is given

Somatosensory loss is the loss of the sensory information that reaches the CNS via the afferent feedback pathways. The afferent nerves are the nerves that provide sensory input to the CNS. In contrast, efferent nerves conduct impulses from the CNS to the body

(Widmaier et al. 2006). Afferents are split into group I and group II afferents. Besides others, group I afferents report to the CNS muscle length and velocity information of the muscle spindles and the muscle force, which is measured by the GTOs. Amongst others, group II afferents provide information on pressure and temperature.

Somatosensory loss can be caused in humans by diabetes, in animal experiments with an overdose of Pyridoxine and can be simulated with ischemia. Pyridoxine, also known as B6 intoxication (Stapley et al. 2002) is permanent and can therefore not be used in humans. Diabetes also results in permanent somatosensory loss, called sensory poly-neuropathy (Horak et al. 2002). Somatosensory loss can be simulated via ischemia or surface movement (Horak et al. 2002; Mazzaro et al. 2005).

Simulated suppression of somatosensory feedback in used in order to avoid the high intervariability of the test subject, i.e. in order to not be forced to compare results of diabetic and non diabetic persons. This provides the possibility to measure a reaction to perturbation with and without somatosensory feedback. The body has to constantly withstand gravity during upright stance; the CNS is not able to perfectly stabilize the body upright, which causes the body to sway. Sensors in the ankle joint report flexion or extension of the ankle muscles. In rotational perturbation experiments around the ankle joint, Horak eliminated this sensory information by exactly matching the platform motion to the swaying of the body (Horak et al. 2002). This caused the ankle to include a 90 degree angle with the shank, independent of the tilt of the body. Since the ankle muscles were neither flexed nor extended, the sensors could not provide information on changes in angular position or velocity. This failure of sensory feedback information is comparable to somatosensory loss. A similar effect occurs, when the test subject stands on a soft surface, e.g. foam, and the feedback of the muscle spindles is not reliable anymore due to the character of surface. A further possibility to simulate somatosensory loss is temporal peripheral ischemia. The blood supply to the leg is interrupted by an air pressured cuff, as used during blood pressure measurement. Experimentally, this resulted in the sensor information being reduced down to 15 % of the original magnitude after 15 minutes of ischemia.

The loss of somatosensory feedback will result in higher excursion of the CoM during upright stance (Horak et al. 2002). Additionally, an increase in vestibulospinal

sensitivity in test subjects was reported (Horak and Hlavacka 2001). Another effect of somatosensory loss is an increased intensity of the EMG (Mazzaro et al. 2005). Furthermore, an increase in neural time delay was reported (Stapley et al. 2002).

CHAPTER III

METHODS

3.1 Overview

In order to develop better understanding of the postural stabilization process employed by the Central Nervous System (CNS), we studied the postural control signals of the CNS after a perturbation. Postural control experiments on a perturbation platform were performed on cats and muscle activity and kinematic data was recorded during their stabilization process. The cats experienced somatosensory loss after treatment with a B6 overdose after which further experiments were conducted (Macpherson et al. 1987). We then used system identification to develop a simple model of the physiology of the cat in order to reproduce the recorded data. By investigating the model parameters over several experiments, we gained insight into the postural control process of the CNS post-perturbation.

The dynamics of the cat body were simulated in Matlab and Simulink as an inverted pendulum plant (see Figure 1). We calculated the simulated dynamics, (i.e. CoM movements of the plant after perturbation) and accounted for the neural time delay inherent in every biological system. This information was fed back into a controller model of the CNS which generated the control signal. Muscle models closed the feedback loop. We called this model the CoM feedback model, as it used the CoM information of the plant to calculate corrective torques after perturbations (See Figure 12).

The feedback path composed the EMG as a response to a postural perturbation by a weighted sum of the CoM kinematics, i.e. the acceleration, velocity and position of the CoM (Lockhart 2005). Our CNS controller model weighed and summed the CoM kinematics to form the EMG response. We used the CoM feedback model to reconstruct the EMGs of two antagonistic muscles that were recorded during the postural

perturbation experiments. We developed two models and determined which one to use in order to obtain the best results.

We then investigated the influence of shape and direction of a perturbation on the control of the CNS before and after sensory loss, directing special attention to the change in weighting of the CoM kinematics in the composition of the EMG. The simulation was solely driven by the recorded platform acceleration, and it predicted the recorded kinematic and electromyographic data using the CoM feedback model. Free parameters in this model were the controller gains and a variable time delay representing the neural time delays caused by finite nerve conduction speed. We tuned the model parameters to get an optimal correlation of our predicted data with the recorded data. A gradient descent optimization adjusted the simulation parameters for the experiments before and after somatosensory loss.

3.2 Experimental Approach

For data collection, four cats were trained to stand still on a perturbation platform (Macpherson 1988). In order to measure maximal muscle activity of flexor and extensor muscles, the cats were perturbed in diagonal direction (see Figure 8) at 16m/s for 100ms in one direction followed by 400ms in the opposite direction. The first movement in one direction will be referred to as the *first phase*; the second, rotated part of the movement will be referred to as the *second phase.* The entire perturbations will be referred to as a *bidirectional perturbation.*

Over eight conditions, the duration of the initial platform movement was shortened from 100ms to 0ms. From condition nine through 16, the same experiment was performed, rotating the perturbations by 180 degrees. Perturbations with 0m/s movement in the initial direction (perturbation eight and 16 in Figure 9) will be referred to as *unidirectional perturbations*.

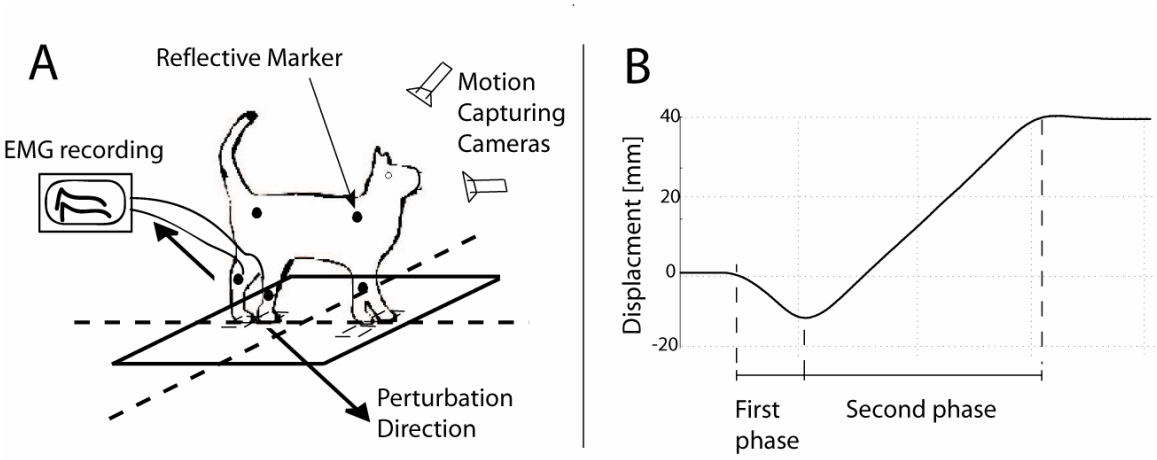

Figure 8: Experimental setup. A – The cat is perturbed in the diagonal direction to elicit the hind lim muscles maximally B - applied bidirectional perturbation

As the major movement of perturbations one to eight points forward, these perturbations will also be referred to as forward perturbations or forward trials. Perturbations nine through 16 will be referred to as backward perturbations or backward trials. During each perturbation, the EMG data of 16 muscles (see Table 1), the platform acceleration, position, and velocity, and the ground reaction forces of each paw were recorded. The data was sampled with 1000 Hz and the EMG data was bandpass filtered, demeaned and rectified. CoM kinematics were computed by integrating the summed ground reaction forces (Macpherson and Fung 1999).

Afferent neuropathy of Group I sensors was induced by an overdose of Pyridoxine (B6). Further experiments were conducted during the somatosensory loss and the following adaptation of the cat to the missing sensory information. In the following, non-poisoned cats will be referenced as intact cats, poisoned cats as B6 cats. Italic printed muscle names are forelimb muscles, other muscle names are hind limb muscles.

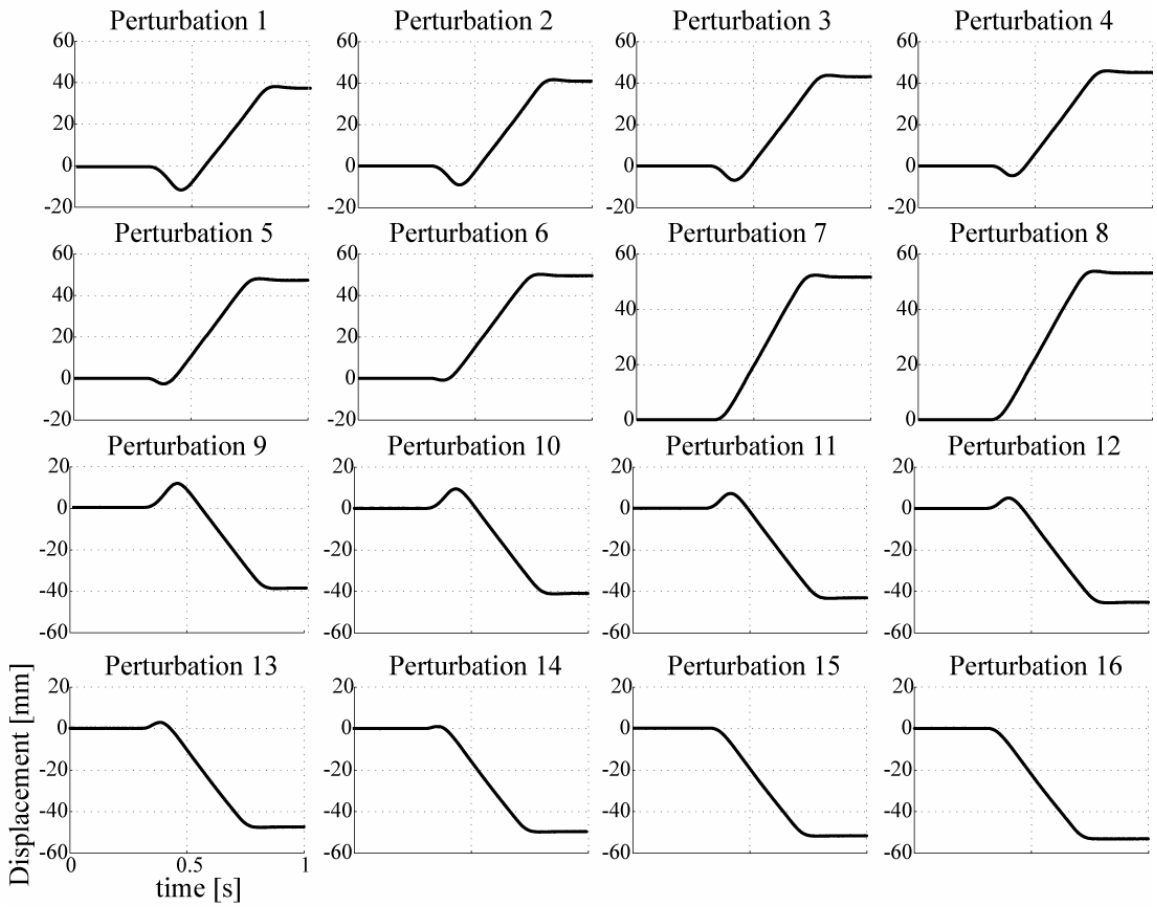

Figure 9: all 16 available perturbations. Perturbation one through eight are forward perturbations, nine through 16 are backward perturbations.

Table 1: Available recorded muscle EMGs for all cats

Cat	Knobi	Bear	Squrl	Sooty
1	Gluteus	Sartorius Anterior	Sartorius Anterior	Sartorius Anterior
2	Middle Biceps Femoris	Rectus Femoris	Rectus Femoris	Rectus Femoris
3	Semimembranosus	Vastus Medialis	Vastus Medialis	Vastus Medialis
4	Anterior Semimembranosus	Gracilis	Gracilis	Anterior Semimembranosus
5	Satorius Anterior	Adductor Femoris	Adductor Femoris	Adductor Femoris
6	Rectus Femoris	Semimembranosus	Semimembranosus	Semimembranosus
7	Vastus Lateralis	Medial Gastrocnemius	Medial Gastrocnemius	Lateral Gastrocnemius
8	Semitendinosus	Semitendinosus	Plantarus	Semitendinosus
9	Soleus	Anterior Biceps Femoris	Anterior Biceps Femoris	Anterior Biceps Femoris
10	Tibialis Anterior	Middle Biceps Femoris	Middle Biceps Femoris	Middle Biceps Femoris
11	Iliopsoas	Posterior Biceps Femoris Medial	Posterior Biceps Femoris Medial	Plantarus
12	*Acromiodeltiod*	Anterior Semimembranosus	Tibialis Anterior	Tibialis Anterior
13	*Teres Major*	Extensor Digitorum Longus	Extensor Digitorum Longus	Extensor Digitorum Longus
14	Triceps Brachii	Peroneus Brevis	Peroneus Brevis	Peroneus Brevis
15	*Triceps Lateralis*	Flexor Digitorum Longus	Flexor Digitorum Longus	Flexor Digitorum Longus
16	BicepsBrachii	Flexor Hallucis Longus	Flexor Hallucis Longus	Flexor Hallucis Longus

3.3 Simulated data

Similar trials of one cat on one day were averaged and saved together in one dataset. Each dataset included the averaged CoM kinematics, EMG recordings and platform movements of the whole day. We simulated the muscles Anterior Biceps Femoris (BFMA) and Sartorius Anterior (SRTA) of cats Bear, Squrl and Sooty; as these muscles data were not available for Knobi, we simulated Gluteus (GLUT) and Iliopsoas (ILPS) instead. We had the following number datasets available.

Table 2: Available number of intact and B6 datasets for each cat

Cat / Number of Datasets	Knobi	Bear	Squrl	Sooty
Intact datasets	3	4	4	3
B6 datasets	1	2	1	1

In only one out of the four available datasets for cat Knobi, the 16 perturbations were recorded as described in the chapter “Experimental Setup”. The other three datasets consisted of 14 perturbations.

3.4 Antagonistic muscle behavior through bidirectional perturbations

When the platform performed a bidirectional perturbation, antagonistic behavior was experimentally observed as two antagonistic muscles were involved in the stabilization process. The EMG corresponding to the first phase of the movement will be named agonist EMG, the EMG corresponding to the second phase of the platform movement will be referred to as antagonist EMG.

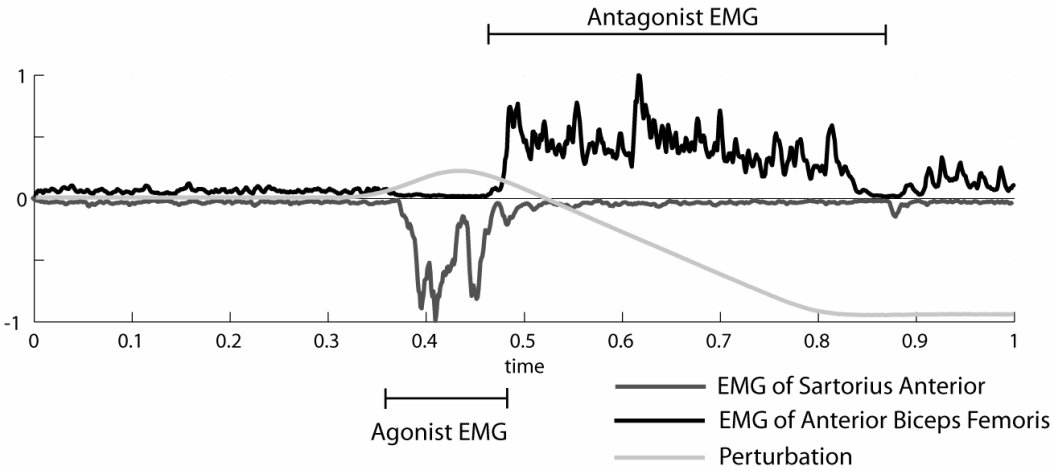

Figure 10: EMG activity of SRTA and BFMA for a bidirectional perturbation. The agonist SRTA is activated to counteract the short, initial movement of the platform; the antagonist BFMA is active during the longer, by 180 degrees rotated second phase of the platform movement

3.5 Increasing model complexity with two muscles

To the best of our knowledge, there exists no study that has attempted to reconstruct EMGs of antagonistic muscle in posture. We developed two simulation models for EMG prediction and compared their correlation coefficient between predicted and recorded EMG data.

On the one hand, we investigated a model with one first order push pull muscle. The muscle contracted at positive EMG values and stretched for negative EMG values. In the case of a unidirectional perturbation, the negative part of the EMG was set to zero. This had the advantage, that one controller could control the agonist and the antagonist EMG for bidirectional perturbation simultaneously.

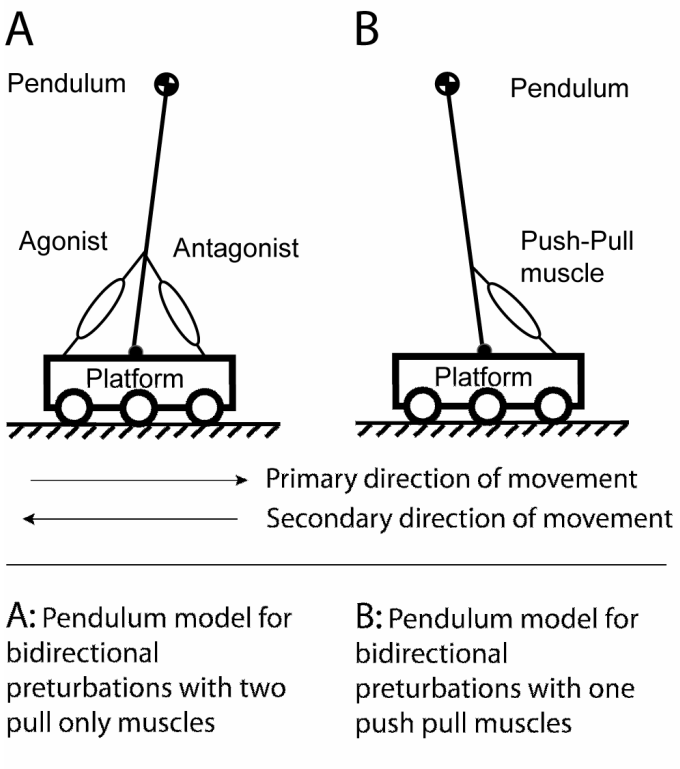

Figure 11: One link inverted pendulum models for simulation of postural control experiments. A – the pendulum is stabilized by two antagonistic muscles. B – one push pull muscle model stabilize the pendulum.

On the other hand, we used a model with two controllers, each controlling a pull only muscle. This opened the opportunity to individually control either muscles, but also resulted in higher complexity, since two controllers had to be tuned.

3.6 Predicting two EMGs with one PID controller

The cat and the platform were simulated as an inverted pendulum and cart model. To compute the input torque Γ around the pendulum pin, we subtracted the control torque employed by the feedback controller from the external perturbation torque Γ_{ext}:

$$\Gamma = \Gamma_{ext} - \Gamma_{feedback} . \quad (3)$$

Notably, the pin of the pendulum did not necessarily coincide with the ankle joint of the cat. The external disturbance torque was computed as

$$\Gamma_{ext} = F \cdot r = m \cdot a \cdot h \tag{4}$$

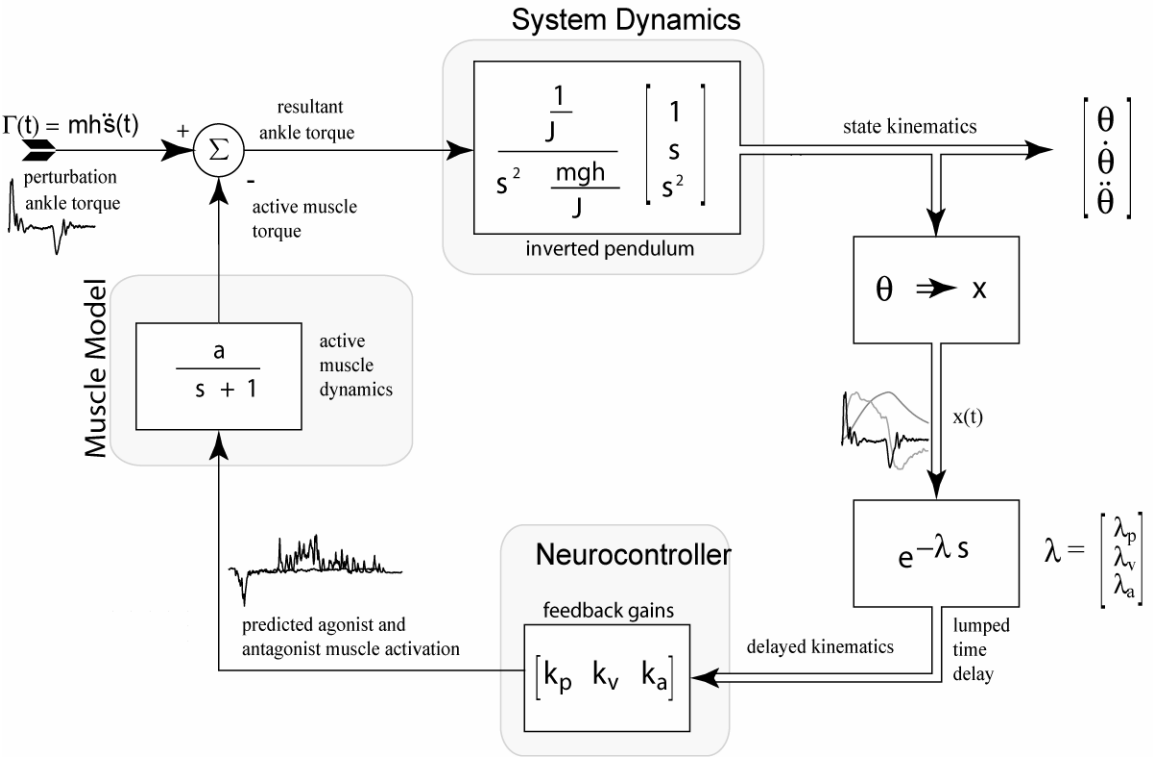

Figure 12: Block diagram of the simulation system of a postural control experiment with one controller. The cat was simulated as an inverted pendulum. The block diagram is composed by three subsystems: the system dynamics, the neural controller and the muscle model. The model is shown with a first order muscle model. Picture adapted from D. Lockhart

m=4kg being the mass of the cat measured on the force plates, a the recorded platform acceleration and h=0.2m the height of the CoM. This formed the input to the system dynamics. The output was the angular velocity of the pendulum's CoM, which was integrated to produce the angular position and was differentiated to produce the angular acceleration. Using the small angle approximation $\sin(q) \cong 0, \cos(q) \cong 1$, the system dynamics of the link inverted pendulum were linearized. Thus, the pendulum was simulated by the transfer function

$$\frac{\dot{q}}{\Gamma} = \frac{s/I}{s^2 - w^2}. \qquad (5)$$

The CoM kinematics were delayed in the feedback path to account for the physiological time delays inherent in biological systems. Though a cat has an ascending neural pathway for feedback and a descending neural pathway for the control signals, mathematically these can be combined into one time delay. We assumed full state feedback (van der Kooij et al. 2001) and simulated the delay in frequency domain as e^{-ls}.

The CNS was simulated as a PID controller, and the gains K_p, K_i and K_d functioned as the weighing factors for the delayed kinematics.

Position gain K_p ~ angular velocity

Integral gain K_i ~ angular position (integral of velocity)

Derivative gain K_d ~ angular acceleration (derivative of velocity)

The mathematical model for the CNS was developed as

$$\frac{EMG}{\dot{q}} = (s \cdot K_d + K_p + \frac{1}{s} K_i). \qquad (6).$$

A push-pull muscle transformed EMG into the feedback torque $\Gamma_{feedback}$ and closed the feedback loop.

We wanted to keep the muscle models simple, accounting for the dynamical behavior of a muscle while reducing complexity. (See Background: Introduction to muscle contraction). Since the test subjects only experienced small velocities and small deviations from upright stance, we set the force velocity and the force length relationship constant. The force velocity relationship reduced to a term F_{max}, as the muscles of the test subjects had a negligible contraction velocity when their muscles activated. The force length relationship was set to 1 because the deviations of the muscle length from the

optimal length l_0 were negligible due to the small magnitude of the perturbation. The nonlinear dynamical properties, i.e. the Contractile Element (CE), the Series Elastic Element (SE) and the Parallel Element (PE), were only significant for continuous contraction frequencies above 4 Hz. They were neglected, since our perturbations were not continuous and since the cats rested for several seconds between perturbations.. (Van der Helm and Rozendaal 2000). Left were the excitation dynamics H_{exc} which translate the motor control signal into an electric signal and the activation dynamics H_{act}, which translate the electrical signal into the chemical signal (see Figure 7).

We used a first order muscle model, to simulate only the excitation dynamics as a first order transfer function

$$H_{exc}(s) = \frac{A}{t_e \cdot s + 1}, \tag{7}$$

t_e = 25ms = 0.04s, A=1.5 and assumed that the activation dynamics were already combined in the time delay of the CNS (Hof and Van den Berg 1981), (Partridge 1965).

A second order model treated the activation dynamics separately from the neural time delay

$$H_{Muscle}(s) = F_{\max} \cdot H_{act}(s) \cdot H_{exc}(s) \tag{8}$$

$$H_{act}(s) = \frac{1}{t_a \cdot s + 1}. \tag{9}$$

$$H_{exc}(s) = \frac{1}{t_e \cdot s + 1} \tag{10}$$

t_e and t_a being time constants (Winters and Stark 1985), (Van der Helm and Rozendaal 2000). According to Fuglevand and Winter (Fuglevand et al. 1993), this led to the transfer function

$$H_{ad}(s) = \frac{r^2}{(s+r)^2}, r = 30\frac{rad}{s}. \tag{11}$$

Assuming that the product of the moment arm r with F_{max} could be combined into the controller gains, we neither included an F_{max} term nor the moment arm r in our model.

3.7 Moment arms and negative EMGs

As it can be seen in Figure 10, the agonist EMG was defined to be negative in order to produce negative torque in the muscle model. The antagonist EMG was defined positive to produce positive torque around the pendulum joint. This was implemented in the model by splitting the output of the CNS, i.e. the EMG, into positive and negative parts. The negative parts were treated as agonist EMG, and the positive ones as antagonist EMG. All recorded EMGs were demeaned and rectified (see chapter: Experimental Approach) and were therefore positive. We also disregarded the fact that the output of a muscle is force, not torque, and that force needed a moment arm r in order to produce torque around a joint.

A correct treatment of the moment arm would require a coordinate system around the ankle joint, defining one rotational direction as positive and the opposite direction as negative. This would result in positive and negative moment arms for flexing and extending muscle forces respectively.

We defined agonist EMGs as positive and antagonist EMGs as negative in order to regain the information about rotation direction. We combined F_{max} and the moment arm as one multiplying factor in the controller.

3.8 Predicting two EMGs with two PID controllers

Using one PID controller, the output of the controller was split into negative and positive parts, which were treated as agonist and antagonist EMG respectively. This had the advantage of only dealing with four free variables: three controller parameters and one time delay. But it restricted both muscles to be jointly controlled.

In order to be able to control each of the two antagonistic muscle EMGs individually, we split the delayed kinematics signal into two identical signals, delayed them individually and fed them into two PID controllers each having a different set of

gains. The number of PID controller parameters thereby increases from three to six: $K_{d1}, K_{p1}, K_{i1}, K_{d2}, K_{p2}$ and K_{i2}, the number of delays increased from one to two.

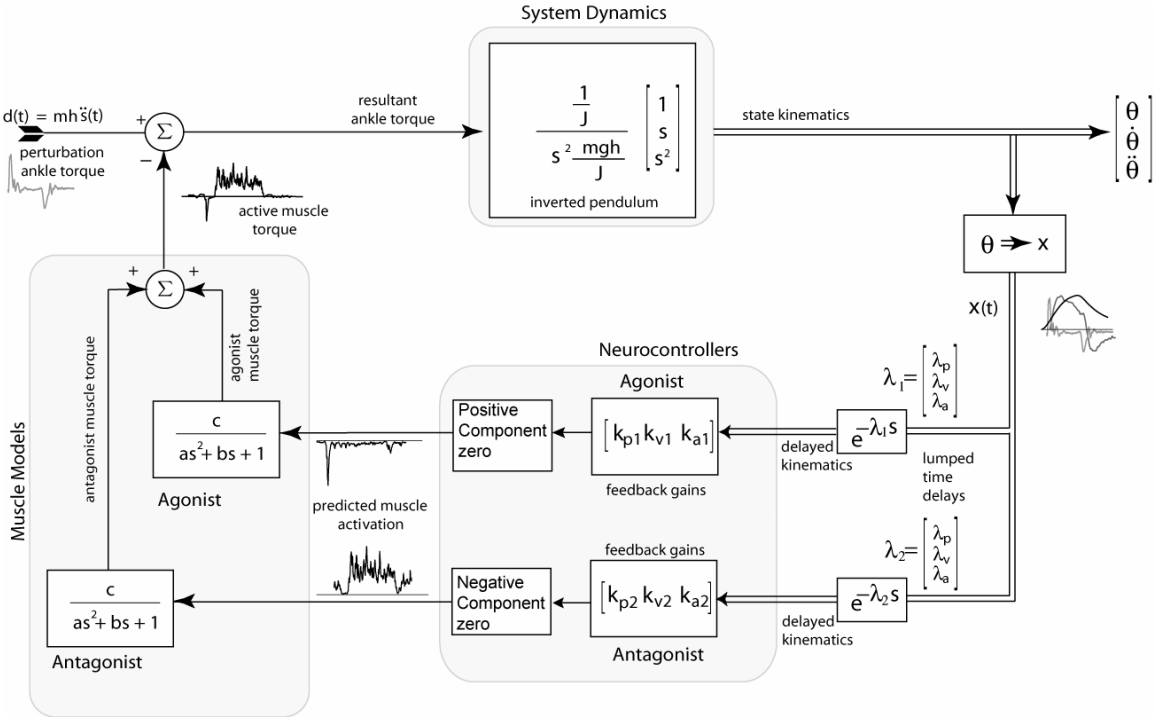

Figure 13: Block diagram of the simulation system of a postural control experiment with two controllers. The system dynamics are unchanged, the CoM kinematic signal is split into two equal signals, time delayed and fed through the agonist and antagonist neural controller. The agonist chops off the negative part of its output, the antagonist controller chops of the positive part. Both EMG signals are fed into muscle models. Note that the muscle models shown in the figure are of second order. The resulting torques are first added up and then subtracted from the external disturbance.

Negative EMG components were treated as agonist EMGs; the neural controller set all positive parts to zero. The antagonist controller acted inversely. Both neural control signals were fed into separate muscle models, and these models were not pull only muscle models: the agonist torque was exclusively negative, the antagonist EMG exclusively positive. Summed up, the resulted in the feedback torque $\Gamma_{feedback}$. This was possible, as the negative agonist EMG activity was nearly over when the positive EMG activity set in. The joint feedback torque was the subtracted from the disturbance torque.

3.9 Matlab procedures

3.9.1 Optimization

Using the constrained gradient descent optimization fmincon (Matlab), we minimize the error between recorded and predicted EMG. We measured the quality of the predictions using the correlation coefficient r^2 between the recorded and the predicted EMG and between the recorded and predicted CoM kinematics. In the model, an EMG is composed by the sum of the delayed kinematics which is weighed with K_p, K_i and K_d. Depending on the number of PID controllers, the parameters K_p, K_i and K_d of each PID controller and the time delay $l_j \mid j \in \{1,2\}$ were varied in order to find a close match of the predict EMG to the recorded EMG. The optimizer was thereby constraint to the following upper and lower bounds (Lockhart 2005):

$$\begin{aligned} 0 \le \mathrm{Kp} \le 9 \\ 0 \le \mathrm{Kd} \le 5.2 \\ 0 \le \mathrm{Ki} \le 0.5 \\ 20\mathrm{ms} \le l \le 55\mathrm{ms}. \end{aligned} \tag{12}$$

The EMG is the neural effort that is necessary to stabilize upright posture. EMG activity, which is the output of the PID controller, is therefore the control signal. CoM angular position, angular velocity and angular acceleration are the states of the system. The optimization process minimized the cost function (Lockhart 2005)

$$J_{\min} = \min\{J = \int_{t_1}^{t_2} \{\sum_{\forall i} (e_i^T m_i e_i) + \sum_{\forall i} \max(e_i^T m_i e_i)\} dt \mid i = (1,2,3,4,5)\}. \tag{13}$$

over the time interval [t1, t2], t1 = 0.3s, t2 = 0.925s. t1 was chosen, since the platform acceleration onset took place consistently at 0.31s. Latest 0.625 seconds after the onset of

the perturbation, the EMG CoM kinematics had returned to zero, i.e. the cat had returned to a stable, upright position.

In the cost function,

e1 = error 1: Agonist EMG recorded – Agonist EMG predicted
e2 = error 2: Antagonist EMG recorded – Antagonist EMG predicted
e3 = error 3: CoM position recorded – CoM position predicted
e4 = error 4: CoM velocity recorded – CoM velocity predicted
e5 = error 5: CoM acceleration recorded – CoM acceleration predicted
m_i = Weighting of error i

The max terms smoothed out the prediction so they would converge to zero. Model parameters were not adapted for each individual cat. The simulation parameters were: m = 4kg, h = 0.2m, g = 9.81 $\frac{kgm}{s^2}$, J = ml^2 = 0.16 kg m^2.

3.9.2 Normalization

Since the magnitude on an EMG was determined by the amplification factor of the recording device and the placing of the subcutaneous recording electrode on the muscle, it was not possible to compare magnitudes of different muscles within one dataset. Due to an increase in impedance, a magnitude comparison of one muscle over several datasets was not possible either. However, since the electrodes were not moved during the recording of the 16 trials and the amplification factor was not changed within one dataset, it was possible to compare EMG magnitudes of a muscle within its 16 trials. We therefore normalized the EMGs for each muscle to the maximum data value of this muscle within all 16 trials.

CHAPTER IV

RESULTS

4.1 Overview

We predicted antagonistic EMG and CoM kinematics of intact and sensory loss cats. We showed that the best approximations were possible using a simulation with a first order muscle model and two PID controllers. Investigations on the optimal controller gains provided insight into the limitations of the simulation model. Within each dataset, we found large variations for position and velocity gains.

EMG prediction was possible over all bidirectional perturbations, when the weights of the CoM kinematics remained constant, independent of the shape of the perturbation. We showed that gain variations were not the consequence of variations in perturbation magnitude or direction, but followed from our optimization method. This indicates that the CNS might not adapt weights on the CoM kinematics for small changes in perturbation.

Following the intact data, we repeated the investigations for the sensory loss cats. Our findings matched the ones of previous researchers, as we found reduced acceleration feedback.

4.2 Simultaneous prediction of antagonistic EMGs

4.2.1 Two PID controllers predict EMG better than one

Predicting two antagonistic EMG's simultaneously, the goal was to keep the number of free parameters as small as possible while still matching the recorded data accurately. Before starting to predict all datasets for all cats, we investigated which model

to use. We first tried to use the model with one PID controller and one time delay, since it represented the simpler solution, but were able to show that two controllers were necessary to correctly predict both, the agonist and the antagonistic muscle EMG.

In the simulation model with one PID controller, a mutual exclusive EMG prediction was possible of either the agonist or the antagonist EMG. It was possible to push the r^2 value of one muscle EMG over 65%, but always at the expense of the r^2 value of the other muscle. In Figure 14, panel A shows a simulation with stronger velocity gain and weaker acceleration gain than the simulation in panel B. This results in a poor fit of the agonist EMG in A compare to panel B and a better fit of the antagonist in A compared to B.

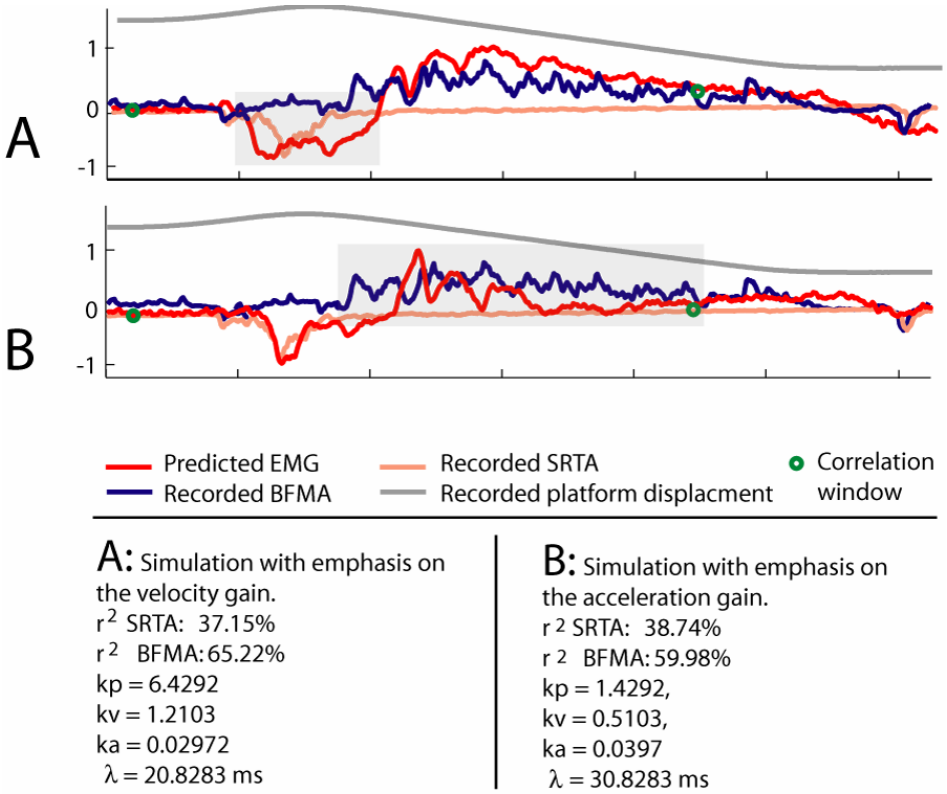

Figure 14: EMG prediction with one PID controller, cat Bear, dataset 10, perturbation 9. A - Simulation with emphasis on correctly predicting the antagonist BFMA. B - Simulation with emphasis on SRTA.

We therefore hypothesized that agonist and antagonist would have two different sets of gains and that we would need two PID controllers to predict both muscle EMGs simultaneously. The hypothesis was tested by gradually incrementing the acceleration

gain over nine simulations while holding the velocity and position gain constant. This resulted in significant increase of the SRTA correlation coefficient. Simultaneously, the correlation coefficient of BFMA decreased significantly. The same analysis was conducted for the velocity gain. For increasing velocity gain and constant position and acceleration gain, the correlation coefficient of SRTA decreased significantly, while the correlation coefficient of BFMA increased significantly (See Figure 15).

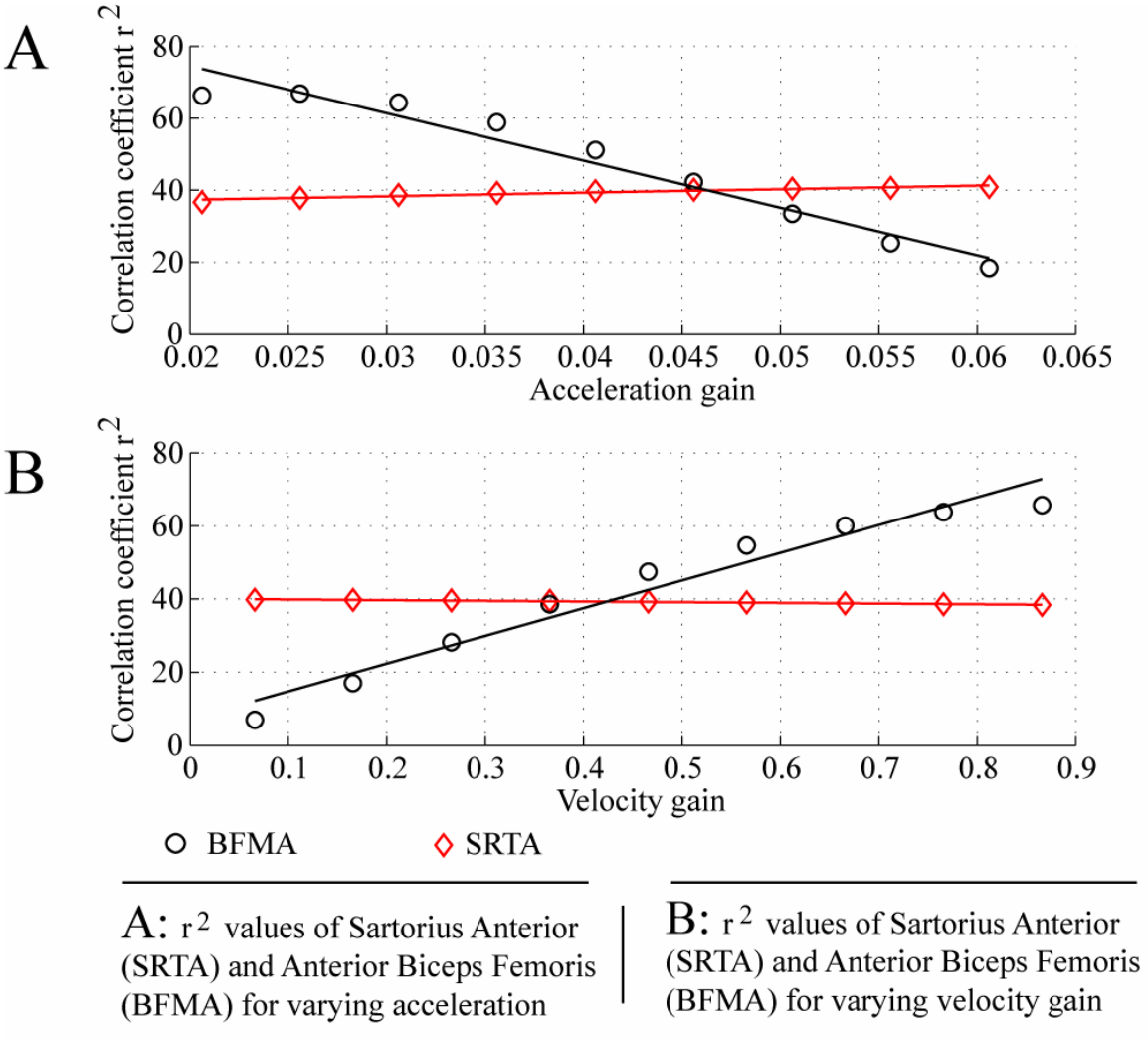

Figure 15: Linear regression analysis of EMG correlation coefficients for varying acceleration and velocity gain. A - SRTA regression slope 0.49133, BFMA regression slope -6.5698. The 95% confidence intervals for the slopes are: [0.3646, 0.6181] and [-7.8461, -5.2936]. B - SRTA regression slope: 0.1855, BFMA regression slope: 7.5807. The 95% confidence intervals for the slopes are: [-0.2134, -0.1576] and [6.1558, 9.0056].

The prediction of SRTA matched the recorded data increasingly, the stronger the output of the PID controller was dominated by the acceleration of the CoM; in contrast, the quality of the prediction of BFMA EMG activity increased with increasing weight on the velocity gain. We conclude from this observation that BFMA and SRTA have different sets of gains and antagonistic EMG's can only be predicted with two PID controllers that can account for these different sets.

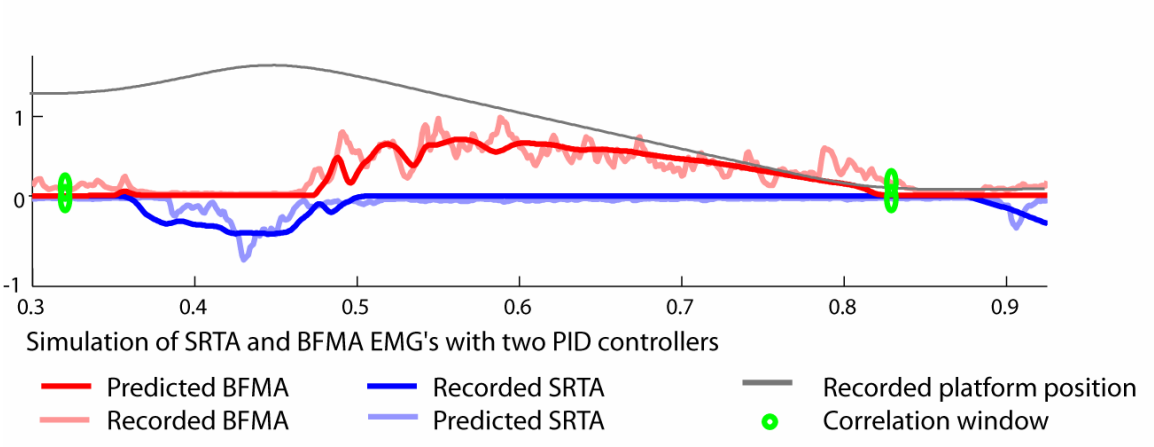

Figure 16: EMG Prediction with two independent PID controllers. Cat Bear, Dataset 10, perturbation 9, SRTA vs BFMA, r^2 BFMA = 80.22%, r^2 SRTA = 66.23%

By splitting the delayed kinematics signal into two identical signals, we fed two PID controllers with the same kinematic signals. Each controller had different gains and controlled one muscle independently. The controller of the agonist had set its emphasis of the acceleration component, the antagonist controller emphasized the velocity component. The simulation results in Figure 16 compared to the ones in Figure 14 show that we were able now predict both, the agonist and the antagonist, without decreasing one EMG prediction by improving the quality of the other one. As we were able to confirm the hypothesis, we used the model with two PID controllers for any further investigations. In order to establish the complete simulation system, we had to investigate which muscle model to use. We had simplified the muscle models in the Methods section and had chosen a first and a second order model for further investigation.

4.2.2 First order muscle models predict EMG better than second order models

After the investigations on muscle models (see chapter Background), we hypothesized that second order muscle models would allow for an improvement of our EMG predictions. In order to investigate this hypothesis, we compared the simulation results of our model using first and second order muscles. Optimizing the gains for BFMA and SRTA, we compared the quality of the prediction via comparison of the r^2 values and via visual inspection. We subtracted the r^2 values of the model with first order muscle models from the ones with second order muscle models. A negative median represented a better prediction with the second order model, a positive media a better prediction of the first order model. As the r^2 values are calculated in percent, the median gives the percentile improvement / weakening of the EMG simulation for the first against the second order muscle model.

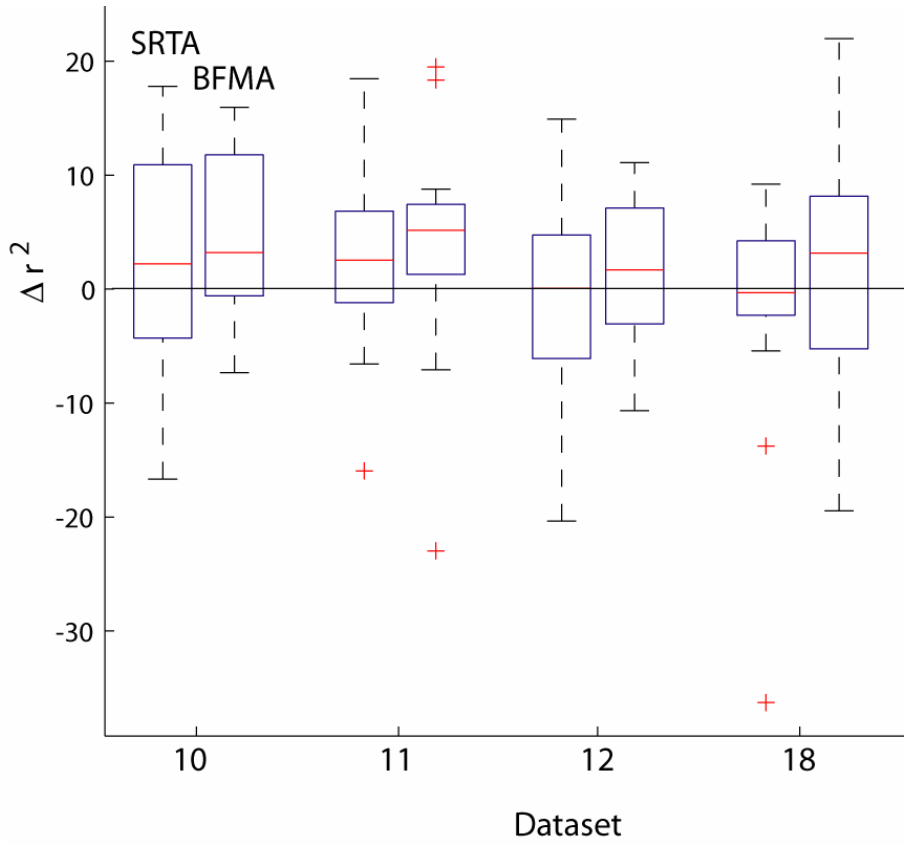

Figure 17: Box plot for delta r^2 values for SRTA and BFMA of cat Bear. A positive median translates to a better EMG approximation by the first order muscle, a negative median translates to a better

approximation by the second order muscle. Outliers can be the result of the sensitivity of r^2 to changes in EMG's with low activity. Overall, the first order muscle delivered the better approximations

However, the visual inspection revealed a better approximation with the first order model. This could be statistically supported: summarized for all datasets and all cats, the second order muscle model only improved the prediction for cat Bear, dataset 18, muscle SRTA. All other predictions had increased r^2 values using the first order muscle model.

Table 3: Comparison of prediction quality for first vs. second order muscle model. Except from cat Bear, all trials in all datasets showed better predictions for first order muscle models than for second order models. Only for cat Bear, the prediction of SRTA with a second order muscle model resulted in better predictions compared to first order models.

Cat / Muscles	Knobi First / Second	Bear First / Second	Squrl First / Second	Sooty First / Second
BFMA	2 / 0	4 / 0	4 / 0	4 / 0
SRTA	2 / 0	2 / 2	4 / 0	4 / 0

4.2.3 Muscular excitation dynamics appear to be lumped in neural time delay

Modeling the excitation and activation dynamics each as a first order transfer function appeared to be a physiologically meaningful model, for which Van der Helm and Roozendaal had provided justification (Van der Helm and Rozendaal 2000). But we found that the first order model yielded to more realistic predictions for our system.

As we obtained better solutions with a first order muscle model, we conclude that the excitation dynamics were already lumped into the neural time delay and therefore needed no extra consideration. This coincides with the model of Hof (Hof and Van den Berg 1981) and Partridge (Partridge 1965).

As for the visible inspection, weaker EMG prediction was observed in the accuracy of prediction of the first burst and a faster decrease of activation at the end of

the EMG trace (See Figure 18). This might be caused by the shorter settling time with which a second order transfer function responds to a perturbation.

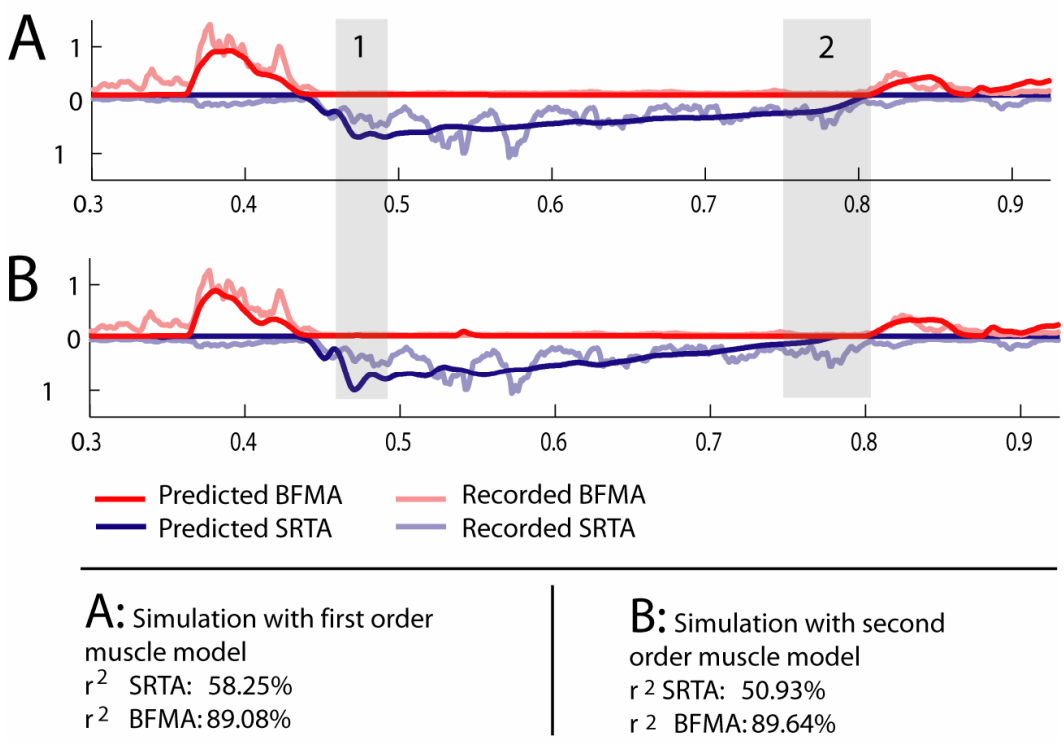

Figure 18: EMG prediction with first and second order muscle model. The first order model produced the better results. In the gray box 1, the first burst is approximated better by the first order model, the second order model's slope increased to fast. Though starting at a higher activation level, the second order model drops to zero faster than the first order model as seen in the gray box 2. This showed in an almost 8% higher r^2 value for the first order model.

4.2.4 Representative optimized prediction for uni- and bidirectional perturbations

Using a model with first order muscle models and two PID controllers, we successfully predicted EMG traces and CoM kinematics. The EMGs for all 16 perturbations for each datasets for muscles BFMA and SRTA of cats Bear, Sooty and Squrl were optimized individually. For cat Knobi, these muscles EMG had not been

recorded during the experiments. We therefore optimized the EMGs of GLUT and ILPS for cat Knobi.

Bidirectional trials included a short, agonist EMG burst and a long antagonist EMG with first burst and plateau region (see Chapter II: Dependency between perturbation kinematics and EMG shape). The decomposition of the agonist EMG into its CoM feedback components (see Figure 19 C) for a bidirectional perturbation showed a strong acceleration component (gray line), which was mainly composed by the first burst. While velocity feedback (black line) contributed to the last 40 ms of the burst, position feedback (green line) did almost not contribute to the burst. The second short burst at 0.8 seconds was induced by the platform de-acceleration and was also predicted by the simulation. We will investigate this feature later in this chapter. The breakdown of the antagonist EMG into its feedback components (see Figure 19 B) showed, that the first burst was also mainly acceleration dependent (gray line), while the plateau region was composed by velocity and position feedback (black and green line respectively). These findings confirmed the hypothesis of Lockhart that EMG was composed by a weighed sum of CoM feedback components. The CoM predictions showed good matches, especially in the CoM acceleration (see Figure 19 D).

The unidirectional perturbation resulted, as expected, in almost zero agonist EMG activity. The breakdown into feedback components showed a small acceleration dependent behavior, which can probably be accounted to noise on. (see Figure 20 C). The first burst of the unidirectional antagonist EMG was again acceleration dependent (see Figure 20 B). The CoM kinematics were predicted with high accuracy (r^2 >91 %).

When regarding all 16 perturbations and the according EMG predictions at once, it stands out that the first initial burst of the agonist decreased as the magnitude of the first perturbation phase decreased (see Figure 21). The feedback gains and time delays for the predictions in Figure 22 were found via optimization and are summarized in Table 4.

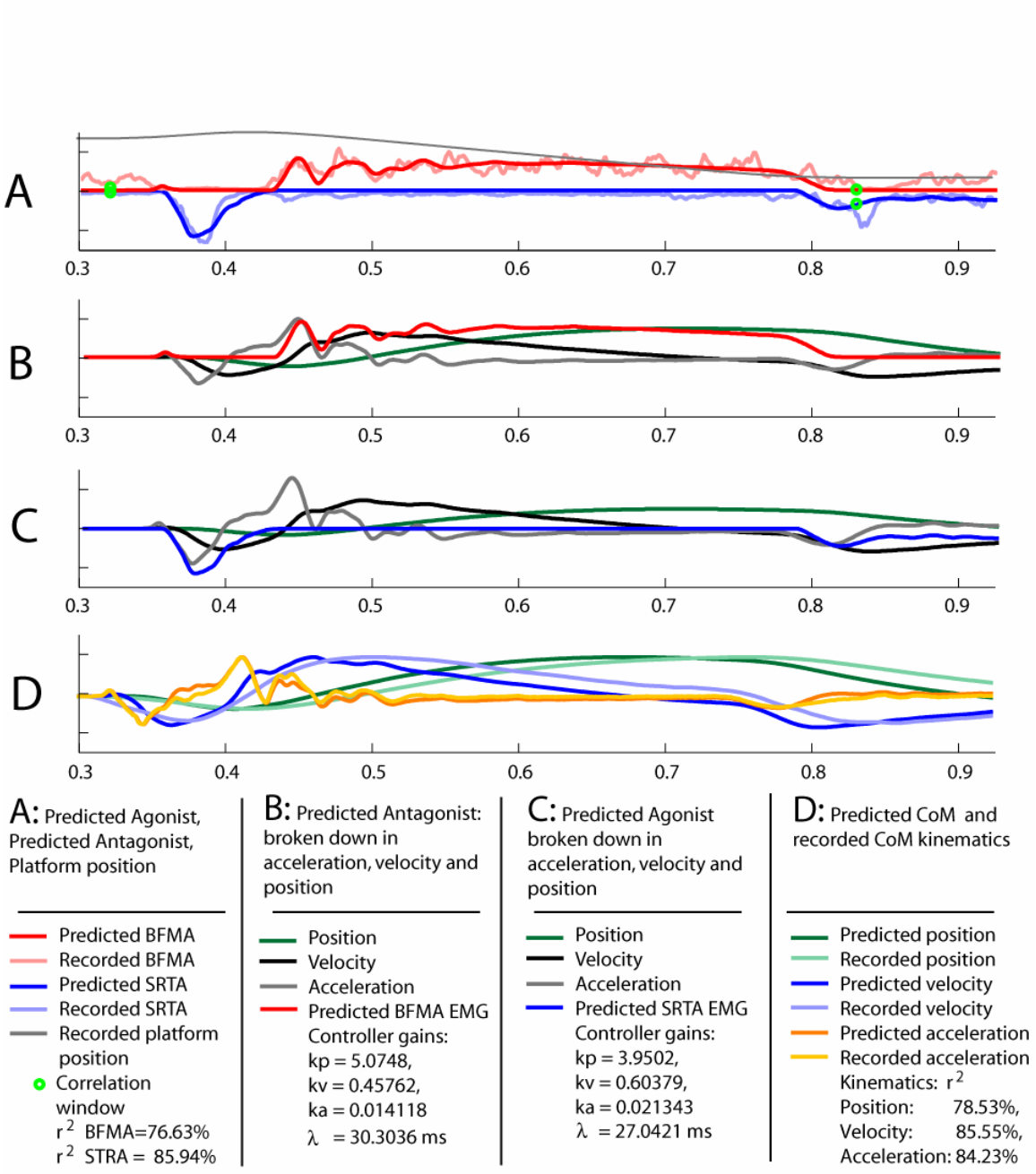

Figure 19: Predicted antagonistic EMGs for bidirectional perturbation. Breakdown into feedback components and CoM predictions. A -Optimized EMG and CoM predictions for backward bidirectional perturbation number 11, muscles BFMA and SRTA. r^2 of BFMA=76.63%, r^2 of SRTA = 85.94%. B – decomposition of BFMA EMG into acceleration, velocity and position components. The acceleration component mainly determines the first burst and drops to almost zero at 0.5s. The plateau is composed by the weighed sum of velocity and position of the CoM kinematics. . C – decomposition of SRTA EMG into CoM feedback components. . D – predicted and recorded CoM kinematics.

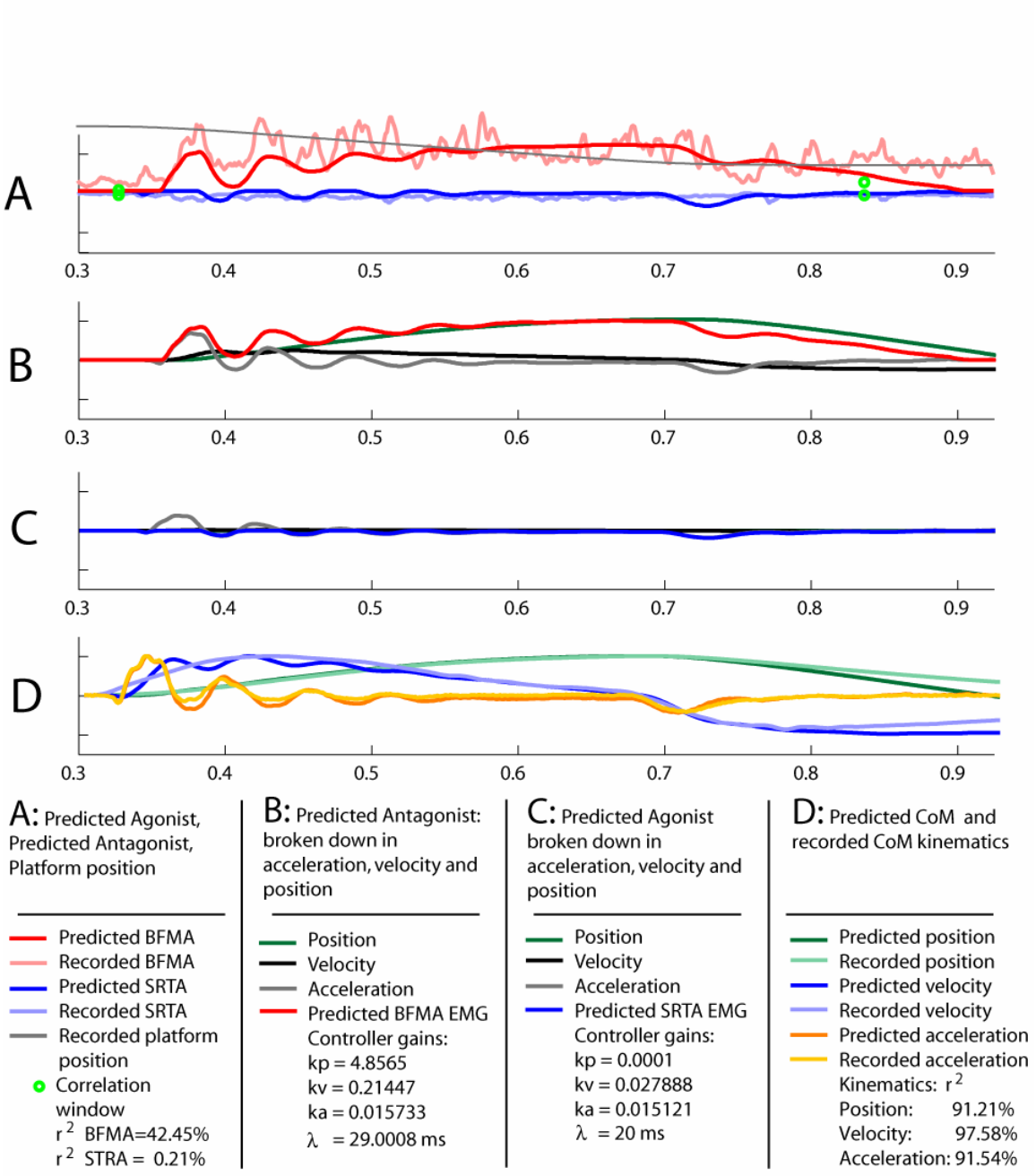

Figure 20: Predicted antagonistic EMGs for unidirectional perturbation, breakdown into feedback components and CoM predictions. A - Optimized EMG and CoM predictions for backward unidirectional perturbation number 11, muscles BFMA and SRTA. r^2 of BFMA=42.45%, r^2 of SRTA = 0.21%. The agonist SRTA's magnitude is almost zero besides some noise. B – decomposition of BFMA EMG into acceleration, velocity and position components. The acceleration component mainly determines the first burst and drops to almost zero at 0.5s. The plateau is composed by the weighed sum of velocity and position of the CoM kinematics. C – decomposition of SRTA EMG into CoM feedback components. D – predicted and recorded CoM kinematics.

The correlation coefficient r^2 appeared to be almost too sensitive to measure the quality of predictions of EMG's whose activation was very low. In the example, the r^2 value of SRTA dropped under 1%, though the prediction does not show significant deviations from the recorded data. But it provided a good measurement for the prediction quality on EMG's with high activation level.

Predictions of a second antagonist muscle pair, LGAS and TIBA failed due to high noise level a in the EMG recording of TIBA. The prediction resulted in the following gain values:

Table 4: Cat Bear, dataset 10: Controller gain values and time delays for both antagonistic muscles

	Controller 1: SRTA				Controller 2: BFMA			
Pert.	K_p	K_v	K_a	l_1	K_p	K_v	K_a	l_2
1	5.299	0.459	0.009216	38.3	2.2454	0.45777	0.020668	39.536
2	4.6705	0.4943	0.004505	41.888	2.0506	0.48754	0.017944	41.299
3	4.6566	0.49928	0.002809	29.558	2.4118	0.64023	0.013976	32
4	4.0151	0.68118	0.000638	55	0.82548	0.61964	0.010152	36.792
5	4.7407	0.28786	1.00E-05	20	0.58025	0.39198	0.009704	34.809
6	4.331	0.57682	1.00E-05	47.673	0.28585	0.39437	0.023231	41.364
7	3.7505	0.52633	1.00E-05	36.824	1.9099	0.53035	0.006684	26.074
8	3.8445	0.45319	1.00E-05	35.603	6.548	0.92579	0.023896	30.088
9	0.31118	0.73387	0.000972	38.743	5.1231	0.61137	0.006015	32.996
10	5.3265	0.60575	0.012078	41.3	4.7917	0.4482	0.002238	21.578
11	9	0.3209	0.002762	20	4.0468	0.4855	0.003028	29.977
12	9	0.37337	0.01126	33.793	3.3007	0.62182	0.004431	55
13	1.1027	0.18489	0.003192	33.724	3.3501	0.49428	1.00E-05	28.696
14	1.6523	0.23824	0.007807	21.3	3.3775	0.54599	1.08E-05	27.319
15	4.4804	0.51879	0.004665	52.569	3.0747	0.62289	0.009206	40.432
16	8.2336	0.6231	0.031868	51.005	3.1532	0.6193	0.022098	49.571

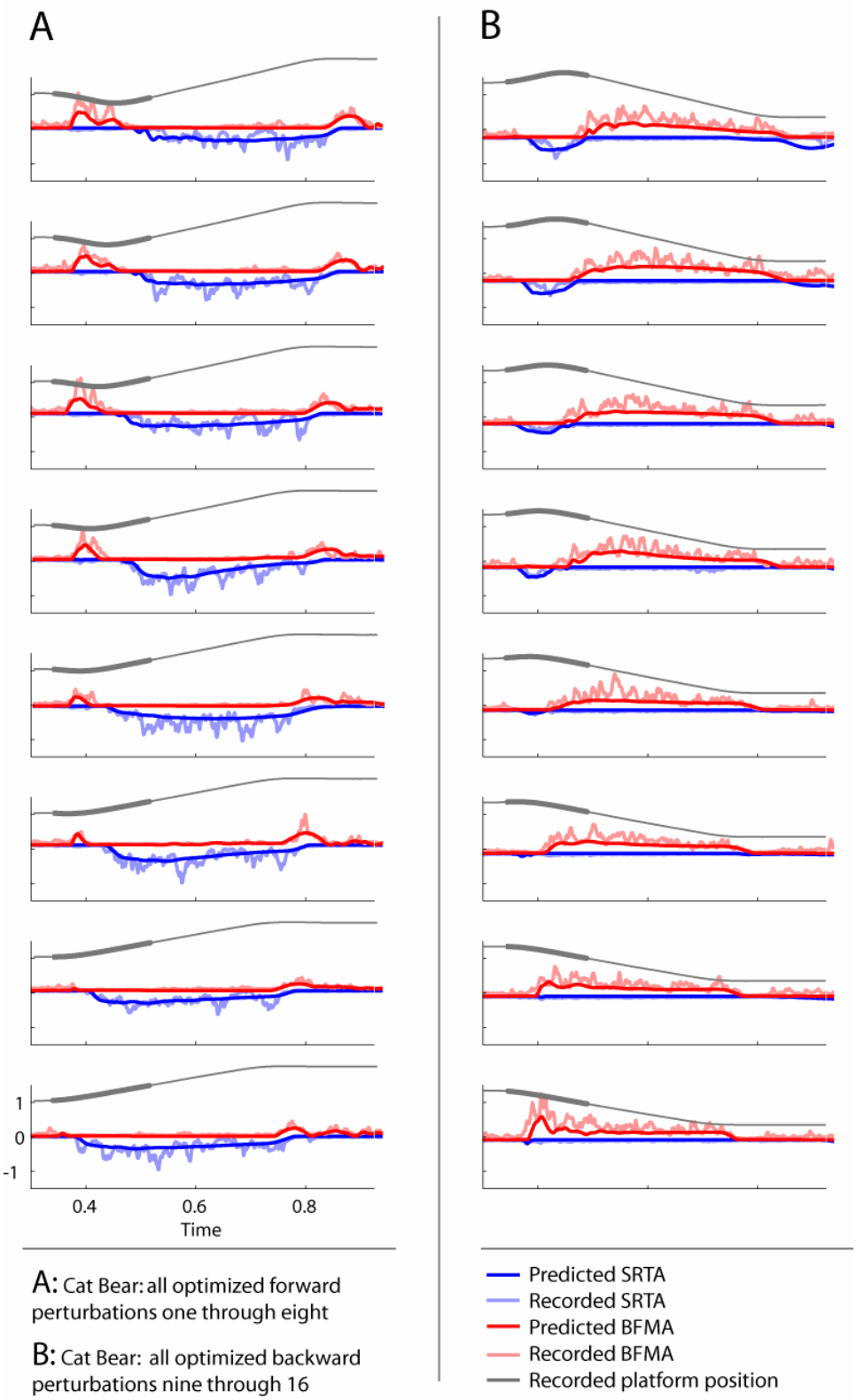

Figure 21: Cat Bear, dataset 10 - optimized EMG predictions for SRTA and BFMA for all 16 perturbations. Note the decreased first burst in bidirectional trials compared to the unidirectional trials

4.2.5 Further evidence for the correctness of our model

The de-acceleration of the platform led to a short EMG burst between 0.700 and 0.925 seconds for trials one through eight in BFMA (see Figure 21, panel A). We showed that this burst was almost exclusively composed by the CoM acceleration. This was another indication that the EMG was a weighed sum of the CoM kinematics. We found a close match between recorded and predicted EMG. Figure 22, panel A shows the overlay of predicted and recorded EMG, Table 5, column A, contains the correlation coefficients, which lie in the range of $46\% < r^2 < 86\%$ for this short time frame.

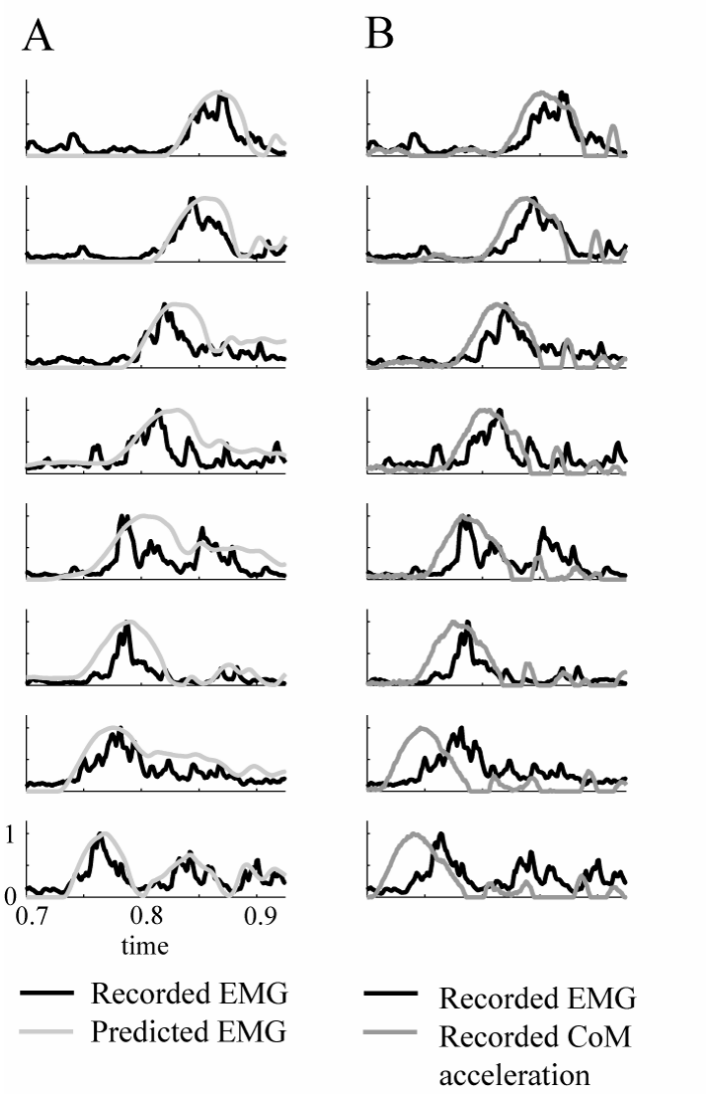

Figure 22: Correlation between recorded CoM acceleration and recorded EMG. A - Overlay of recorded and predicted EMG. The simulation gives good predictions for the EMG. B - Overlay of

recorded EMG and recorded, by l time delayed CoM acceleration. The traces of recorded EMG and CoM acceleration match very closely

In order to show that the bursts correlated with the CoM acceleration, we computed the correlation coefficient of the CoM acceleration with the recorded EMG. The EMG occurred time delayed after the perturbation due to the neural time delays. We used the optimal time delay which was identified in the optimization and time shifted the EMG. The resulting EMG overlaid the recorded CoM acceleration. The correlation coefficient was computed for the time window between t = [0.700;0.925] seconds.

Table 5: Correlation coefficients between recorded and predicted EMG in the time frame 0.700 – 0.925 seconds. Column 1 – trial number, column 2 – correlation coefficient of predicted and recorded EMG, column3: correlation coefficient of predicted and recorded CoM acceleration

Trial	r^2 recorded EMG predicted EMG [%]	r^2 recorded EMG recorded CoM acceleration [%]	Neural time delays between CoM movement and EMG reaction [ms]
1	84.33	74.82	39.536
2	86.85	77.38	41.299
3	71.56	71.47	32
4	46.82	65.05	36.792
5	52.32	38.12	34.809
6	77.88	63.08	41.364
7	80.81	2.13	26.074
8	84.04	2.55	30.088

The results in Figure 22, panel B, and Table 5, column 3, indicate that this burst is composed almost exclusively by the CoM acceleration. Though the r^2 values of EMG seven and eight are very low, the plots show a similar behavior as plots one through six. The time delay, which we identified in the optimization process (see Table 5, column 4), seemed too short in trials seven and eight. It is possible, that the optimizer was not able to identify the true time delay and that the correlation might improve significantly for these two trials with a 5ms longer time delay.

4.3 Shortening of a muscle prior to its contraction does not alter weighing of CoM kinematics

4.3.1 Overview

Our investigations on the *agonist* feedback gains showed that the variations of the gains for varying perturbation magnitude were an artifact of our optimization method. Since agonist EMG is composed almost exclusively by acceleration feedback, the optimizer did not find consistent position and velocity gains. The variations in *antagonist* K_a were found to be a result of varying signs of the CoM position, velocity and acceleration. However, the position and velocity feedback gains were consistent over the perturbations in which the muscle acted as an antagonist.

Based on the almost constant behavior of the antagonist position and velocity gains, we hypothesized that the controller gains remained constant over all 16 bidirectional perturbations, regardless of varying perturbation magnitude or reversal of perturbation direction. We simulated all 16 perturbations with constant gains without further optimizing. We obtained good EMG predictions for not optimized predictions, which indicate that the gains did remain constant for varying perturbation magnitude and direction.

4.3.2 Gain variations of agonist Kp and Kv are results of the optimization

During a bidirectional perturbation, the first phase of the platform movement caused agonist EMG activity, the second phase, rotated by 180 degrees, caused antagonistic EMG activity. Investigating the feedback gains for all datasets of one cat for all 16 perturbations, we found a pattern for controller gains that were connected to antagonist EMG activity, but a more random distribution of the feedback gains for agonist EMG activity.

Position and velocity feedback of antagonists were grouped narrowly around the median, showing a small standard deviation. When SRTA and BFMA acted as antagonists, the gains K_p and K_v showed consistency over the eight trials (see Figure 23). This finding was confirmed by the small standard deviation of antagonist gains around the median. Compared to antagonistic muscle feedback gains, all muscles showed large variations of controller gains when they acted as agonists. (see Figure 23, Figure 24). No pattern was identifiable in K_p and K_v for agonist trials. When SRTA and BFMA acted as agonists, the EMG was almost exclusively composed by a short first burst. This burst was mainly acceleration dependent, without a major CoM position or velocity component.

Our investigations revealed that the variations in agonist EMG prediction were not caused by true biological gain variation, but by a problem in our optimization method. CoM position and velocity played a minor role in the composition of the agonist EMG. The EMG activation was already over before the CoM underwent a significant displacement or reached its peak velocity. As position and velocity information were almost zero during the agonist EMG trace (See Figure 25 A and B), the optimizer could vary the multiplication factor K_p and K_v without a strong impact on the predicted EMG. This caused the large variations in K_p and K_v in the agonist trials.

The antagonistic EMGs, consisting of a first burst and a long plateau region, resulted in almost constant K_p and K_v (see Figure 23) over eight perturbations. An antagonistic EMG as response to a perturbation was composed by a first burst and a plateau region (See Figure 3, Figure 10). In antagonistic EMG predictions, the perturbation lasted long enough to allow the CoM position and velocity component to develop fully. A variation of weighing factors as in the agonist trials was therefore not possible anymore. This explained why the antagonist K_p and K_v showed high consistency.

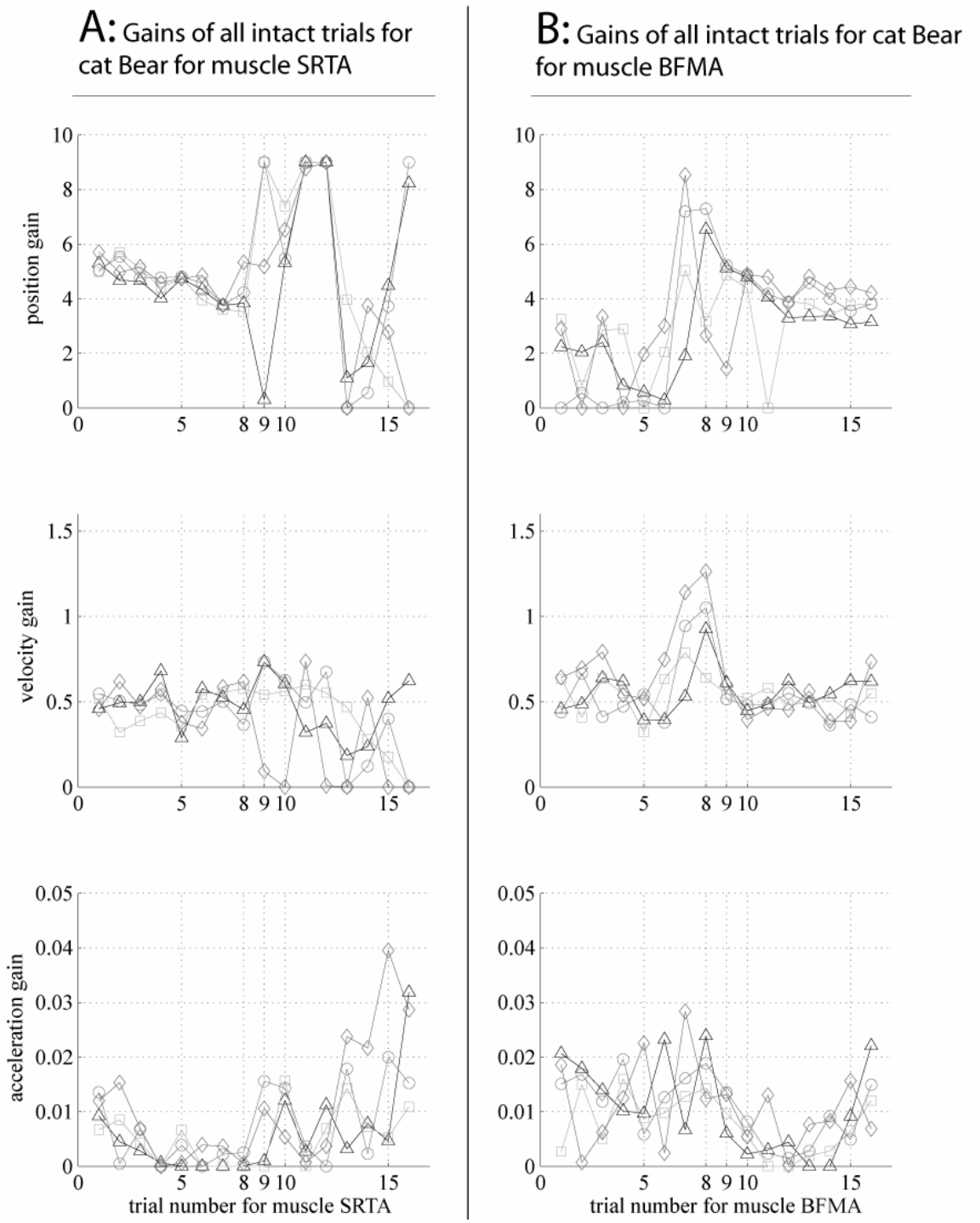

Figure 23: All gains for all datasets of cat Bear, grouped by position, velocity and acceleration gain, for muscles SRTA and BFMA. For SRTA, position and velocity gains show consistent values for trials one through eight, for BFMA position and velocity gain are consistent for trials 9 through 16.

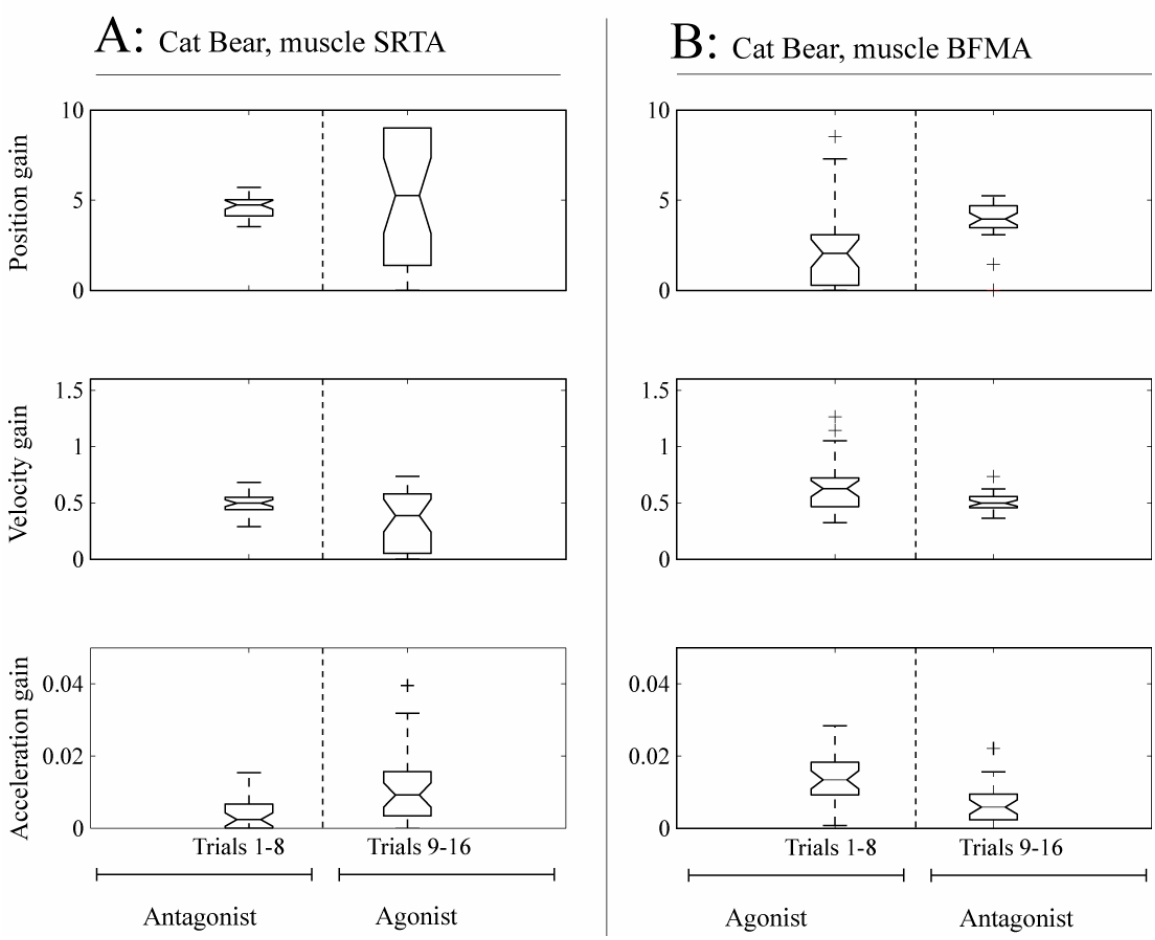

Figure 24: Box plots for all intact gains of cat Bear, grouped by position, velocity and acceleration. A - SRTA acted as antagonist for trials 1-8, as agonist for trials 9-16. B - BFMA for trials 1-8 acted as agonist, for trials 9 through 16 as antagonist. When the muscle was an antagonist, position and velocity gains grouped narrowly around the median, if the muscle was an agonist, the gains had a significantly larger deviation from the median. The acceleration gain shows a similar behavior, but not as prominent as position and velocity gain.

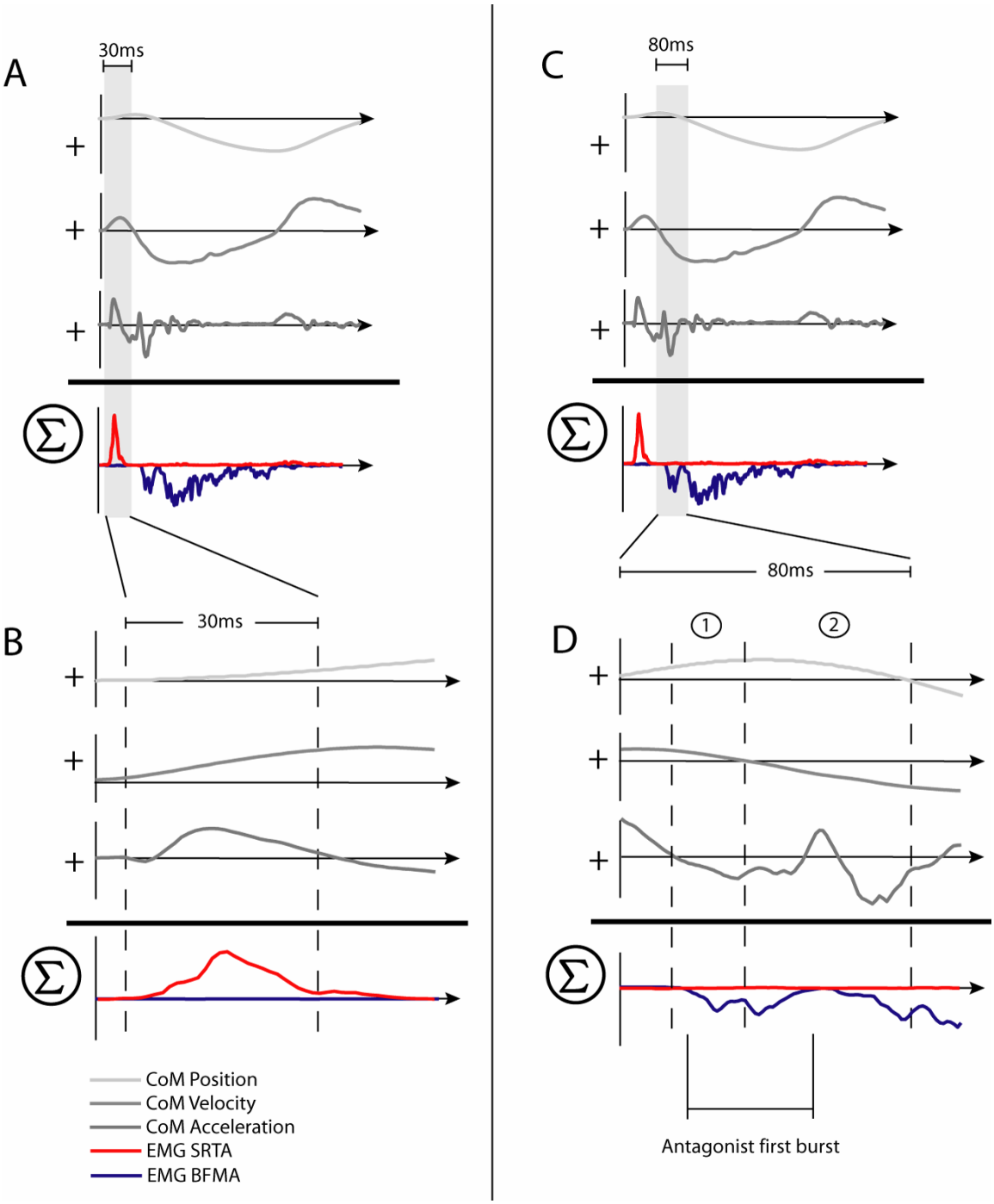

Figure 25: EMG composition via CoM kinematics. A - cat Bear bidirectional perturbation. B – zoom into burst of agonist EMG. Before position and velocity feedback component are fully developed, the EMG is already off again. C – cat Bear bidirectional perturbation. D – zoom into the first burst of the antagonist EMG. In the first phase, only the acceleration component is negative. Position and velocity are still positive and therefore weaken the EMG burst of the antagonist. In phase two, velocity becomes negative and only position weakens the first burst.

4.3.3 Large gain variations in antagonist acceleration feedback are a result of CoM position and velocity kinematics.

As we found that position and velocity gains of antagonist muscles were consistent over the range of perturbation magnitudes, we investigated the large gain variations of the acceleration gains for antagonist muscles in response to the second phase of the perturbation. We observed a decreased first burst in the recorded antagonistic EMGs for bidirectional compared to unidirectional perturbations (see Figure 21) and were able to show that this was the cause for the large deviations of acceleration gains. When a bidirectional perturbation was applied, the first phase of the platform displacement caused the antagonistic muscle to be shortened prior to its contraction. Over eight perturbations, the displacement of the initial first phase was reduced from 11mm to 0mm, resulting in a unidirectional trial for perturbation eight. As the first burst of the antagonistic was composed mainly by acceleration feedback, we investigated, if the reduction of the first burst was caused by the bidirectionality of the perturbation.

Due to the bidirectionality of our perturbations, the first burst of the antagonist EMG of a bidirectional perturbation was composed by the sum of positive acceleration and negative position and velocity information (see Figure 25 C and D). Since the EMG was composed as the sum of the weighed CoM feedback components, the positive CoM acceleration feedback of the antagonist first burst was weakened by summation with negative position and velocity feedback. This resulted in large acceleration gain variations, since the weight on the acceleration feedback compensated for the subtraction of position and velocity feedback. The optimization routine adapted the acceleration gain depending on the influence of position and velocity feedback; K_a was therefore not consistent over all eight antagonistic trials.

This indicated that the CoM weighs are independent of any prior muscle deformation or reversal of perturbation direction. The feedback gains of agonist and antagonist remained constant over the 16 perturbations – for uni- and bi-directional perturbations. The variations we found were caused by the optimization method.

4.3.4 Non optimized predictions with unidirectional feedback gains

We employed unidirectional gains for the simulation of for both, uni- and bidirectional perturbations. We hypothesized that feedback gains did not change over the 16 trials of one dataset and that we were therefore able to correctly predict EMG traces of all trials with the same gains. As the first phase of displacement for unidirectional perturbations was 0cm, the agonist EMG traces for unidirectional perturbations were almost zero except for noise on the channel. The antagonistic controller gains of the unidirectional forward / backward perturbations eight and 16 would therefore fully account for muscular activity of anterior / posterior muscles respectively without any influence of a prior shortening (see Figure 26).

In order to use gains that were not influenced by any prior muscular deformation, we used the gains of the antagonist muscles identified for *unidirectional* perturbations eight and 16, applied them in simulations to *bidirectional* perturbations and predicted the bidirectional agonist and antagonist EMG. For our investigations, we used the gains of SRTA, perturbation eight and the gains of BFMA of perturbation 16.

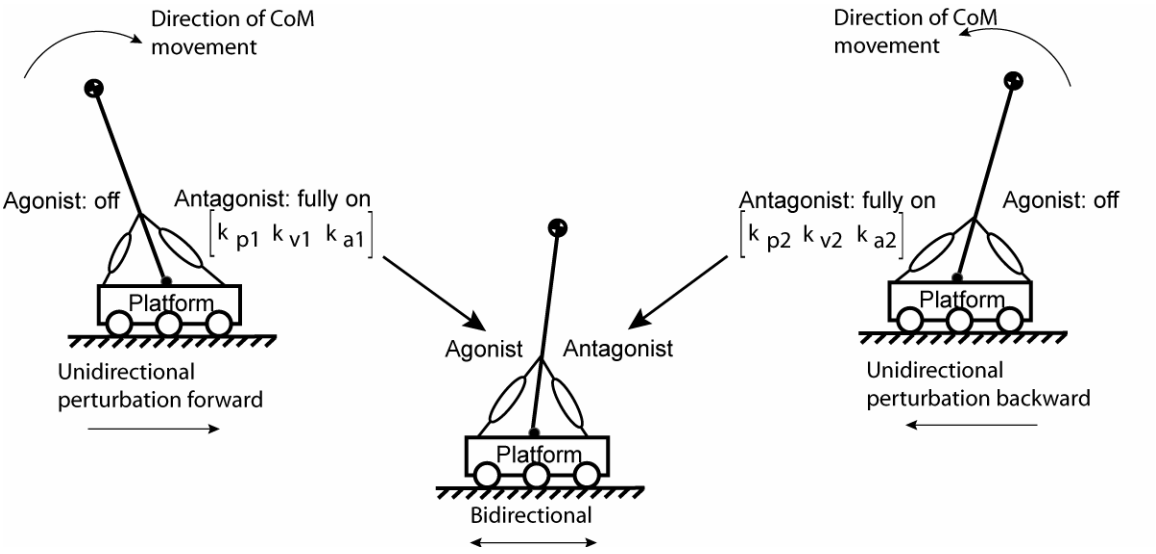

Figure 26: Unidirectional controller gains for bidirectional perturbation simulation. The gains of the antagonist EMG of the unidirectional forward perturbation are assigned to controller one, the gains of the antagonist EMG of the unidirectional backward perturbation are assigned to controller two. Bidirectional forward and backward perturbations are then simulated with these gains.

Using these gains identified via optimization, we predicted all EMG traces following uni- and bidirectional perturbations. Figure 27 shows the result plots for the EMG traces, Table 6 shows the resulting r^2 values for non-optimized and for optimized trials

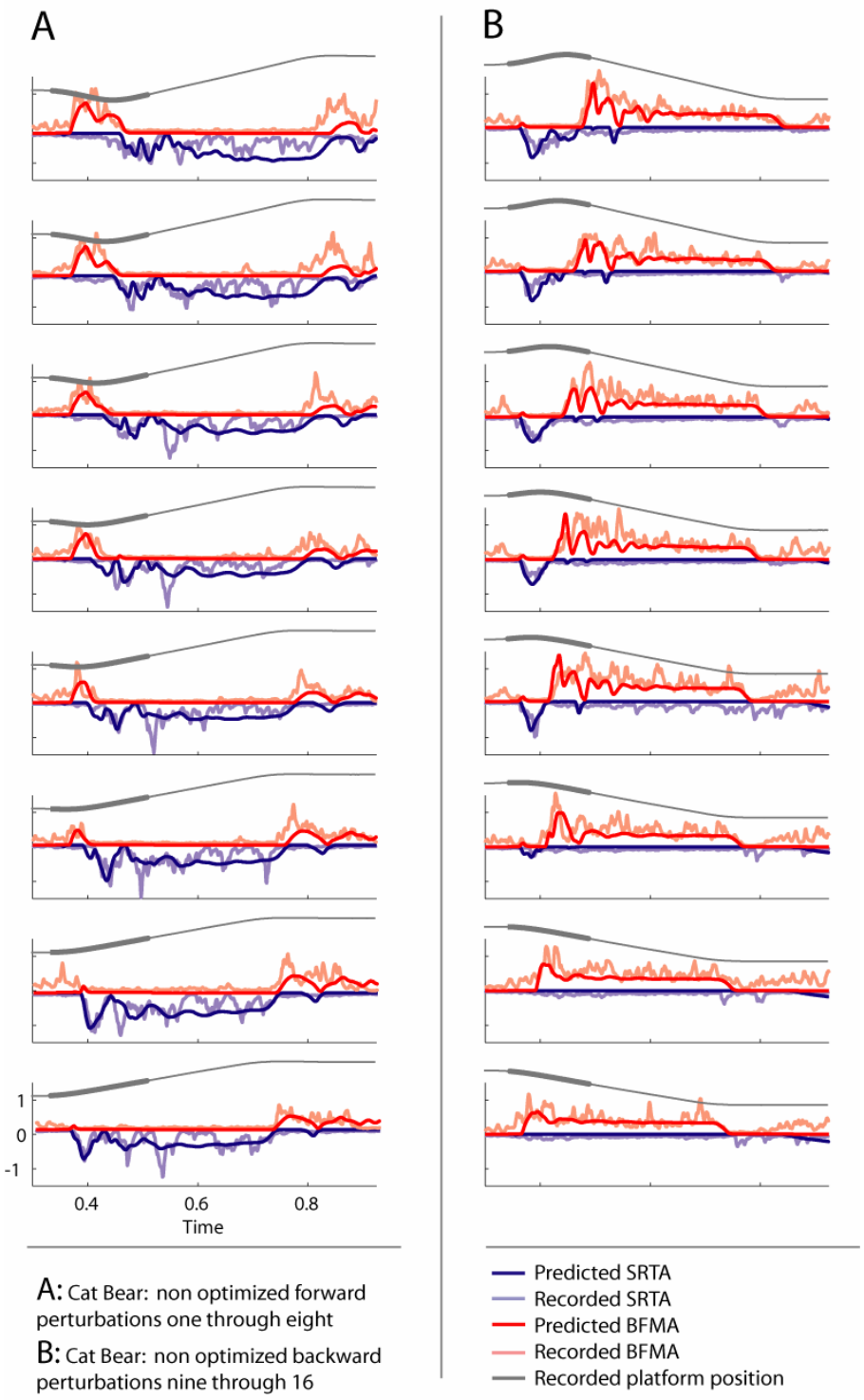

Figure 27: Cat Bear, dataset 10, all trials, not optimized. Simulated with the gains of the unidirectional perturbation gains of trial eight (k_{p1} = 3.8445, k_{v1} = 0.45319, $_{ka1}$ = 1e-5 l_1 = 35.603ms) and 16 (k_{p2} = 3.1532, k_{v2} = 0.6193, $_{ka2}$ = 0.022098 l_2 = 49.571ms) without further optimizing. A: Forward perturbation: the agonist BFMA EMG, has its highest magnitude in trial one. Over eight trials, the initial forward displacement becomes 0m/s, the agonist EMG only has a short on time when the platform stops. B: Backward perturbation: similar behavior for the trials nine through 16. The different EMG shapes are only due to the different platform acceleration

Table 6: Cat Bear: dataset 10. r^2 values for BFMA and SRTA for optimized and non optimized perturbations in % With decreasing activation level of the EMG, the significance of the r^2 value decreased. R^2 values of 0%, 0.44% or 0.58% in the non optimized trials 14 through 16 for SRTA did not reflect a bad prediction, but resulted from the low EMG level.

Perturbation No.	SRTA		BFMA	
	Optimized	Non optimized	Optimized	Non optimized
1	51.15	57.22	90.28	65.92
2	69.9	69.2	89.5	73.75
3	51.64	56.29	91.15	43.31
4	82.3	65.13	83.96	57.08
5	74.47	73.23	69.18	38.03
6	71.92	67.08	80.2	35.73
7	66.98	65.04	82.92	63.05
8	58.57	58.57	79.11	42.46
9	67.95	67.28	82.37	29.89
10	62.37	53.9	82.33	24.25
11	74.79	62.93	76.26	15.93
12	63.26	38.38	80.13	18.66
13	50.69	43.16	69.38	25.75
14	23.95	0.1	81.82	49.65
15	31.1	0.44	76	61.31
16	19.06	0.58	71.14	71.97

The high r^2 values for constant feedback gains indicate that the weights of the CoM kinematics did not change when the muscle was relaxed prior to its contraction and that the varying EMG shapes were induced by the variation of the CoM kinematics.

4.3.5 Gains remain constant for changes in displacement magnitude

Some of our findings contradict the previous findings in literature, some match previous research. We predicted antagonistic EMG using a simple model. Changing the magnitude of the perturbations and their direction, the feedback gains remained constant. The platform perturbations consisted of short initial backward platform displacements followed by a longer, 180 degree rotated forward movement. Within eight trials, the initial backward displacement was reduced from $\pm$ 11.4mm to 0mm in magnitude. The

initial movement resulted in short EMG bursts in the posterior muscles (perturbations on through eight) and the anterior muscles (perturbations nine through 16), which decreased in magnitude for decreasing initial platform displacement (See Figure 21). The same experiment was repeated, rotated by 180 degrees with the initial movement pointing forwards. We were able to predict the EMG bursts for all 16 trials without changing the feedback gains.

Park et al. used human data found increasing feedback gains for increasing perturbation magnitude during postural perturbation experiments (Park et al. 2004). Though our results indicate that the feedback gains are independent of perturbation displacement, these results are not necessarily be contradictory. Using a two link inverted pendulum, Park noted a shift from ankle to hip strategy for increasing perturbation velocity. It is possible that we were not able to see a linear scaling in feedback gains, since our model only employed a one link inverted pendulum. It is also probable that the linear feedback gain scaling reported by Park was rather caused by varying velocity and acceleration than by varying platform displacement; the plateau region of an EMG trace scales with velocity, the first burst with acceleration. Our perturbation used constant velocity profiles.

Horak and later Park et al. studied the effect of initial leaning on the stabilization process (Horak and Moore 1993; Park et al. 2005). Leaning initially forward subjects were perturbed backwards. This increased postural challenge resulted in increased feedback gains. From the perspective of the second phase of the platform movement, the initial platform movement induced a leaning in perturbation direction. This can be seen as a decreased postural challenge. Consequently, we would expect a gain decrease for initial displacement. The optimal acceleration gains, obtained from minimizing the error between recorded and predicted EMG, indeed showed an upward trend towards the unidirectional perturbations. (See Figure 23) As we were able to reconstruct all perturbation shapes with the same gains, we cannot say if this trend is significant or not.

4.4 Results of the investigations of effects of somatosensory loss

4.4.1 Representative predictions for uni and bidirectional perturbations for somatosensory loss cats

We investigated the results of B6 poisoning on the postural stabilization process in cats and conducted the same optimization and analyses as with the intact cats. We optimized controller gains for all 16 perturbations, investigated the behavior of the identified gains and simulated all trials with the unidirectional gains without further optimization.

The decomposition of the agonist EMG into its CoM feedback components (see Figure 28 C) for a bidirectional perturbation showed an acceleration component (gray line), which was almost non existent. The first burst of the agonist was composed mostly by velocity feedback (black line). Position feedback (green line) contributed to the last 40 ms of the burst. Except from Figure 30, panel A, perturbation 7, no second short burst at was identifiable 0.8 seconds, as we observed it in intact cats. The breakdown of the antagonist EMG into its feedback components (see Figure 28 B) showed, that the antagonist first burst was also mainly velocity dependent (black line), while the plateau region was composed by position feedback (green line). Acceleration gain was again almost non existent.

When comparing the EMG predictions for all 16 perturbations, it stands out that the first initial burst of the agonist shrank with decreasing magnitude of the first perturbation phase (see Figure 30). The feedback gains and time delays for the predictions in Figure 30 were found via optimization and are summarized in Table 7. The gains, which were identified using the cost function in chapter 3.9.1, showed similar variations in position and velocity gains as in the intact cats (see Figure 31, Figure 32). The acceleration gains were, as described in chapter 2.6 almost non existent. The statistical significance on investigations of patterns in the optimal gains was limited, since we only had one B6 dataset for cats Knobi, Sooty and Squrl and two B6 datasets for cat Bear available.

Predictions without optimization using the unidirectional gains of perturbation eight and 16 (see Chapter 4.3.4) predicted EMG without noteworthy acceleration gain (see Figure 33). We found the acceleration gains to be decreased or almost zero compared to the intact gains and were able to confirm Lockhart's results (Lockhart 2005). A correct prediction was sometimes not possible due to the high noise level in the B6 trials.

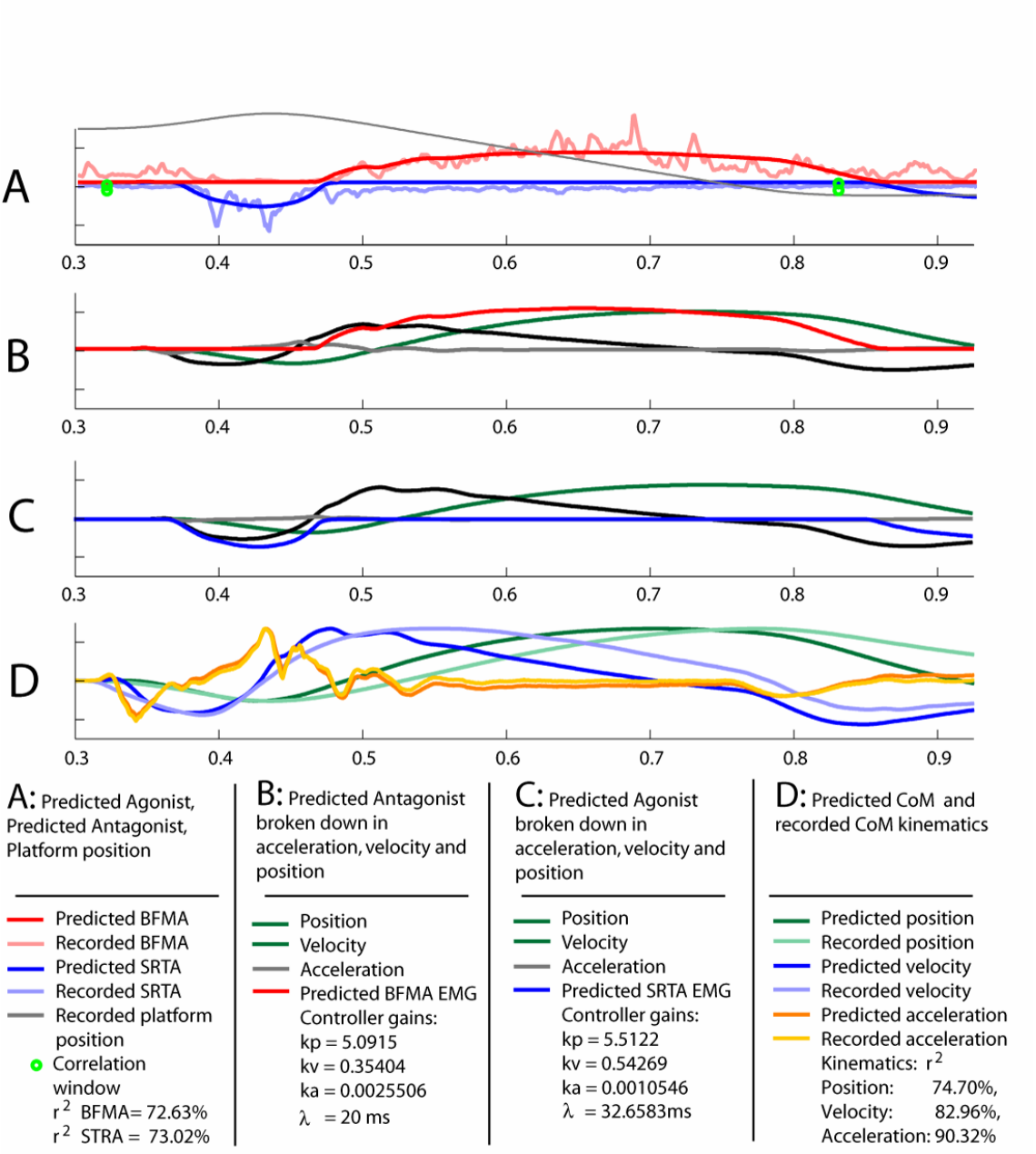

Figure 28: Predicted antagonistic EMGs for bidirectional perturbation. Breakdown into feedback components and CoM predictions for cat Bear, dataset 86, perturbation 10. A -Optimized EMG and CoM predictions for backward bidirectional perturbation number 10, BFMA and SRTA. r^2 of

BFMA=72.63%, r^2 of SRTA = 73.02%. B – decomposition of BFMA EMG into acceleration, velocity and position components. The acceleration dependent burst is almost non existing. The plateau is composed by the weighed sum of velocity and position CoM kinematics. C – decomposition of SRTA EMG into CoM feedback components. D – predicted and recorded CoM kinematics.

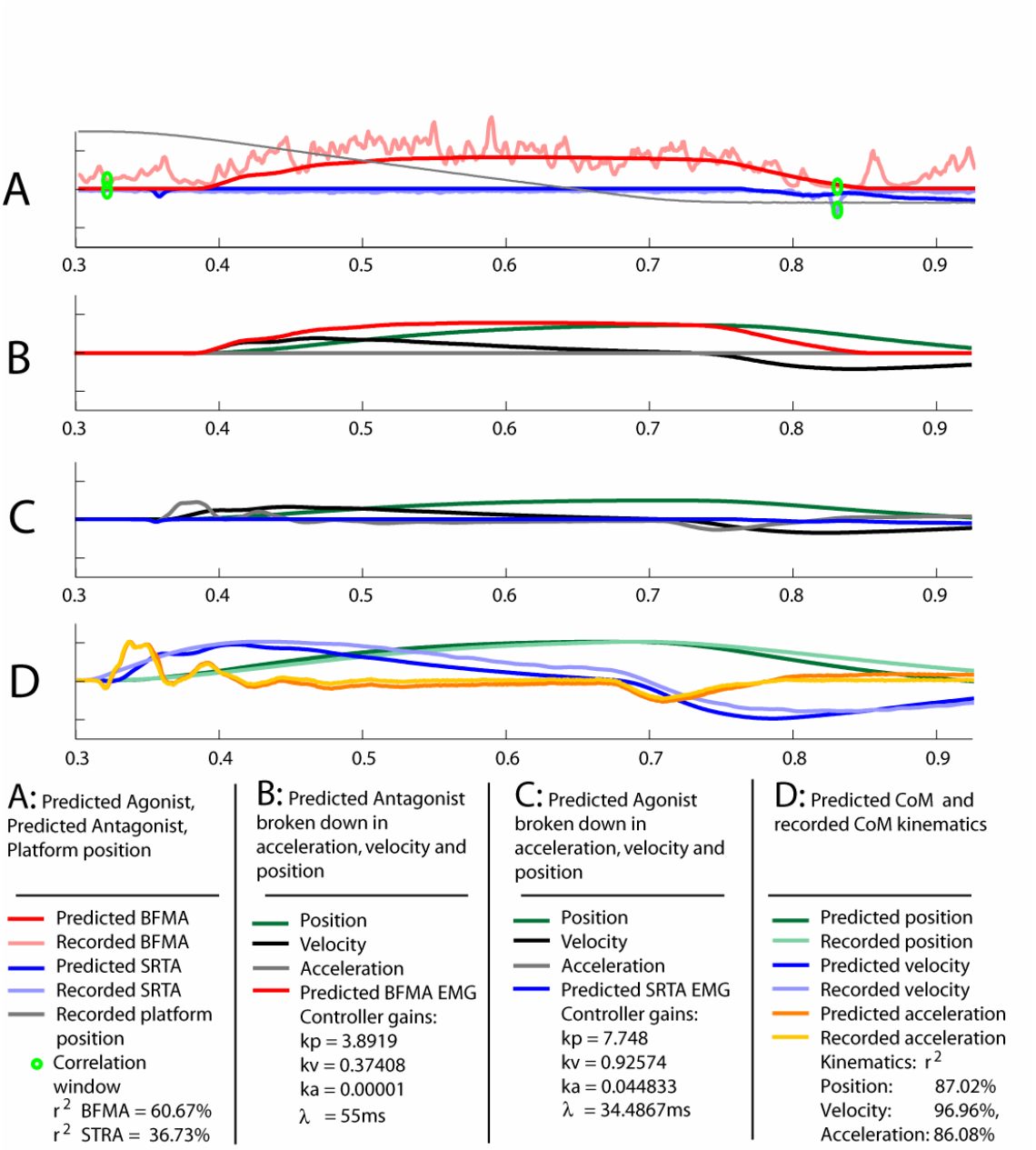

Figure 29: Predicted antagonistic EMGs for unidirectional perturbation, breakdown into feedback components and CoM predictions for cat Bear, dataset 86, perturbation 16. A - Optimized EMG and CoM predictions for backward unidirectional perturbation number 11, muscles BFMA and SRTA. r^2 of BFMA=60.67%, r^2 of SRTA = 36.73%. The agonist SRTA's magnitude is almost zero besides noise. B – decomposition of BFMA EMG into acceleration, velocity and position components. Again, the first burst is almost not existing. The plateau is composed by the weighed sum of velocity and position CoM kinematics. C – decomposition of SRTA EMG into CoM feedback components. D – predicted and recorded CoM kinematics.

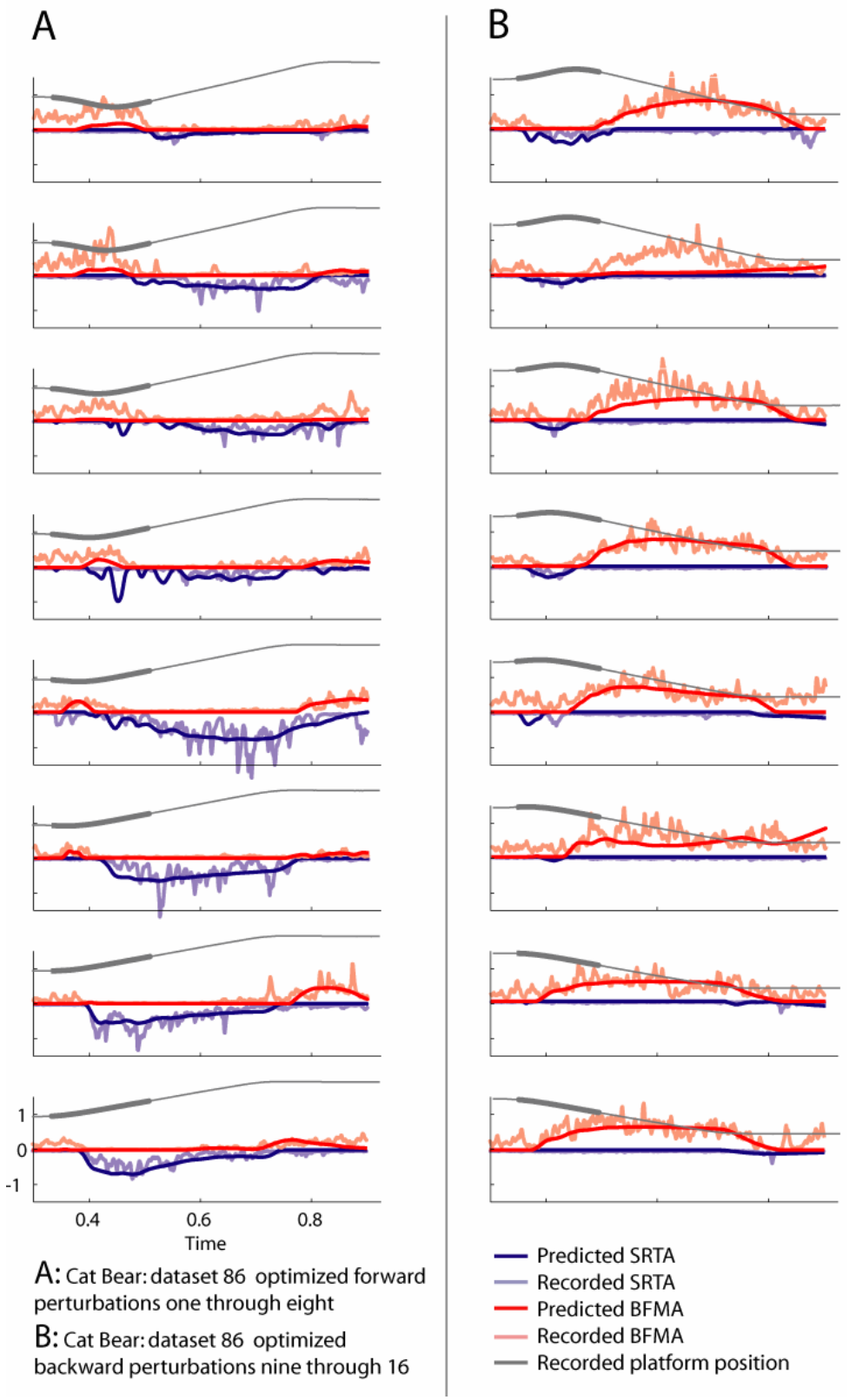

Figure 30: Cat Bear, dataset 86, B6, all optimized EMGs of trials one through 16. Note the noise of BFMA in trials one through four, which is almost as strong as the EMG. A: all forward perturbations, B: all backward perturbations

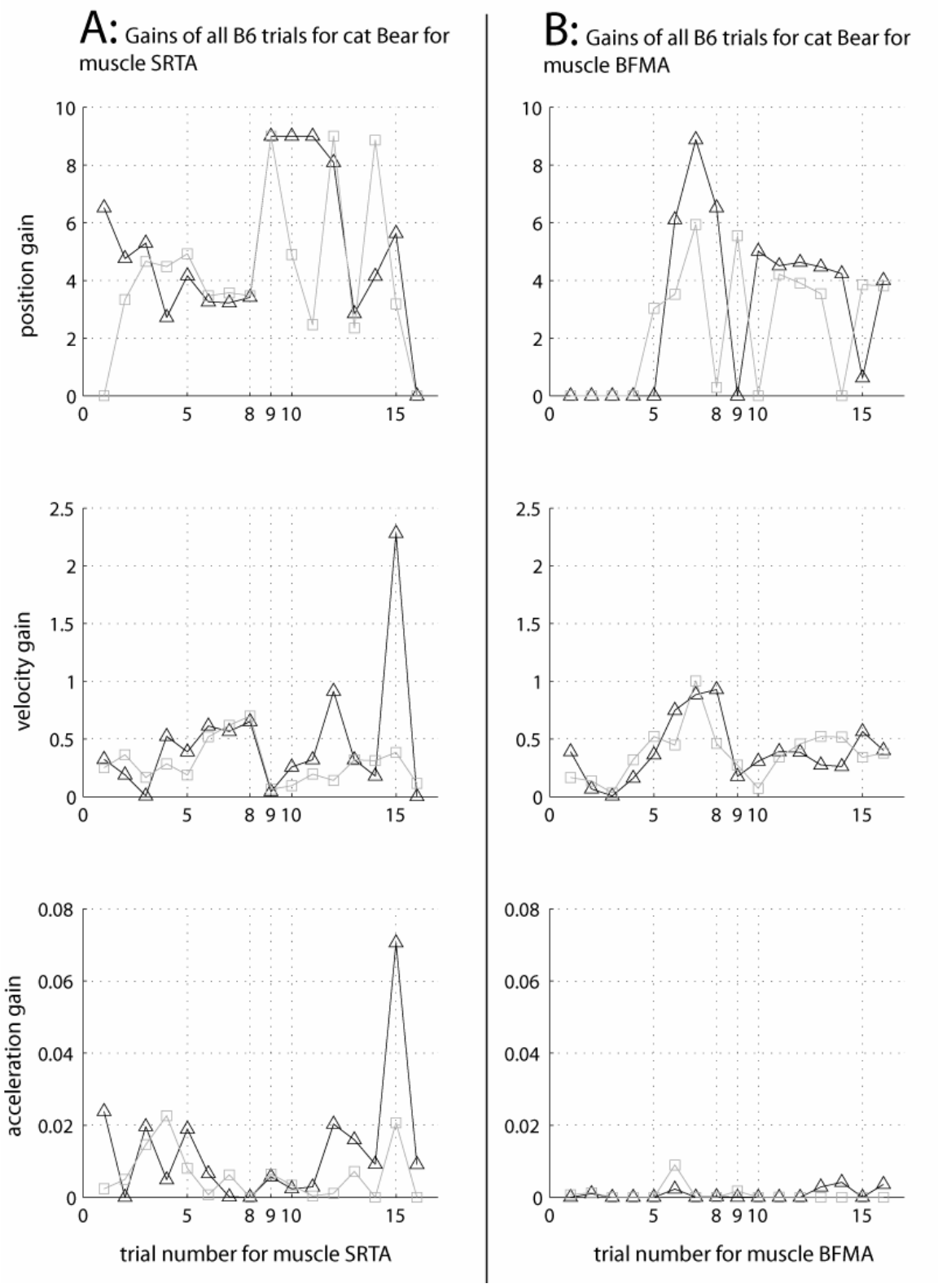

Figure 31: All gains cat bear, datasets 80 and 86, grouped by position, velocity and acceleration gain for muscles SRTA and BFMA.

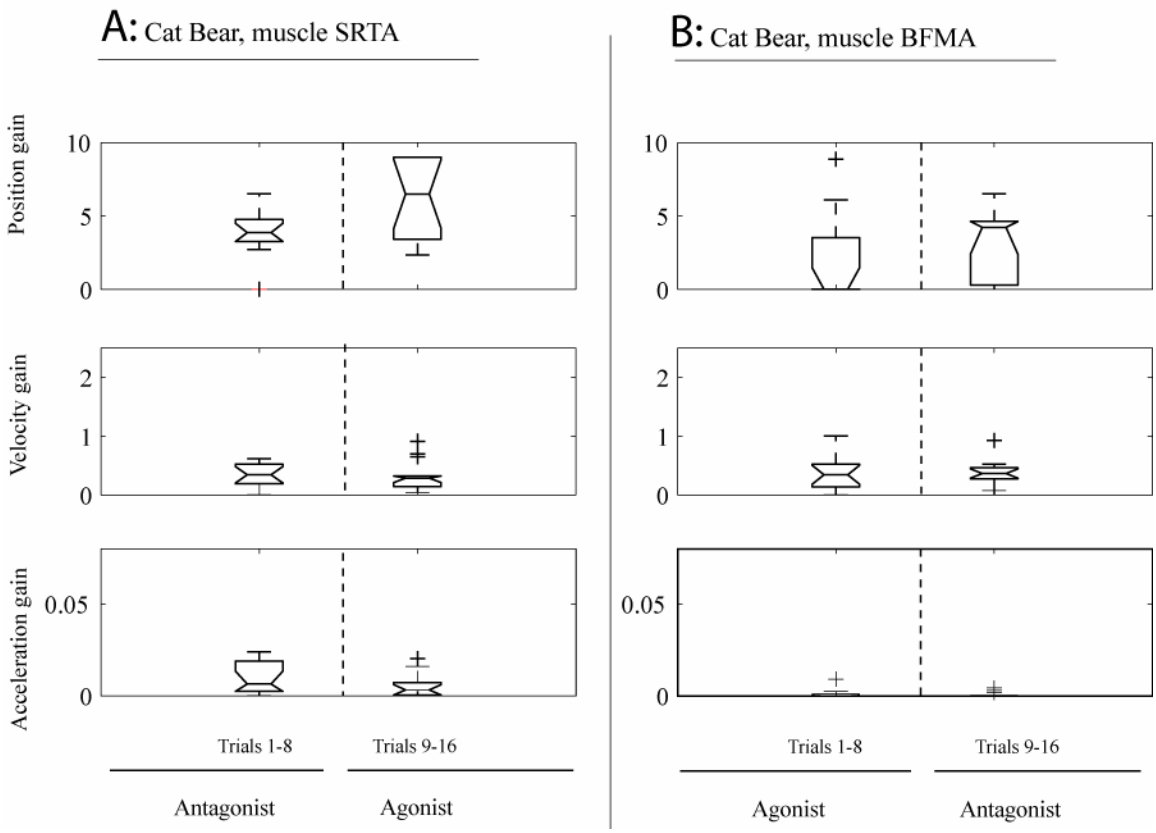

Figure 32: Box plots for all intact gains of cat Bear, grouped by position, velocity and acceleration. A - SRTA acted as antagonist for trials 1-8, as agonist for trials 9-16. B - BFMA for trials 1-8 acted as agonist, for trials 9 through 16 as antagonist. For both muscles, the same patterns as for the intact trials were observed. The drop in acceleration gain was not as significant as expected.

Table 7: All controller gains and time delays for the optimized B6 trials

Bear - 86	**Controller 1: SRTA**				**Controller 2: BFMA**			
Pert.	Kp	Kv	Ka	l_1	Kp	Kv	Ka	l_2
1	0.0001	0.25114	0.002378	53.808	0.0001	0.16591	0.000746	55
2	3.334	0.36276	0.004958	28.294	0.0001	0.13649	0.001276	48
3	4.6661	0.16659	0.014607	20.297	0.0001	0.033759	1.00E-05	30.211
4	4.4828	0.28509	0.022615	20	0.0001	0.32075	1.00E-05	55
5	4.9258	0.18809	0.008064	29.31	3.0283	0.52137	1.00E-05	24.6
6	3.4674	0.51819	0.000745	41.801	3.5169	0.44796	0.008982	27.001
7	3.5719	0.61775	0.006235	42.998	5.9389	1.003	1.00E-05	55
8	3.4734	0.69739	1.00E-05	47.658	0.28952	0.46034	1.00E-05	31.25
9	9	0.063407	0.006471	20	5.5504	0.2741	0.00178	20
10	4.8952	0.095061	0.00342	22.665	0.0001	0.07345	1.00E-05	55
11	2.4641	0.19494	0.000395	28.357	4.2174	0.34144	7.39E-05	37.017
12	9	0.14116	0.001118	20	3.9085	0.45576	1.00E-05	55
13	2.3496	0.31934	0.007181	21.12	3.5401	0.52083	1.00E-05	55
14	8.8668	0.31191	1.00E-05	49.583	0.0001	0.51705	1.00E-05	55
15	3.1891	0.38345	0.020678	20	3.8577	0.34189	1.00E-05	32.591
16	0.0001	0.11565	1.00E-05	45.422	3.8108	0.37608	1.00E-05	48.119

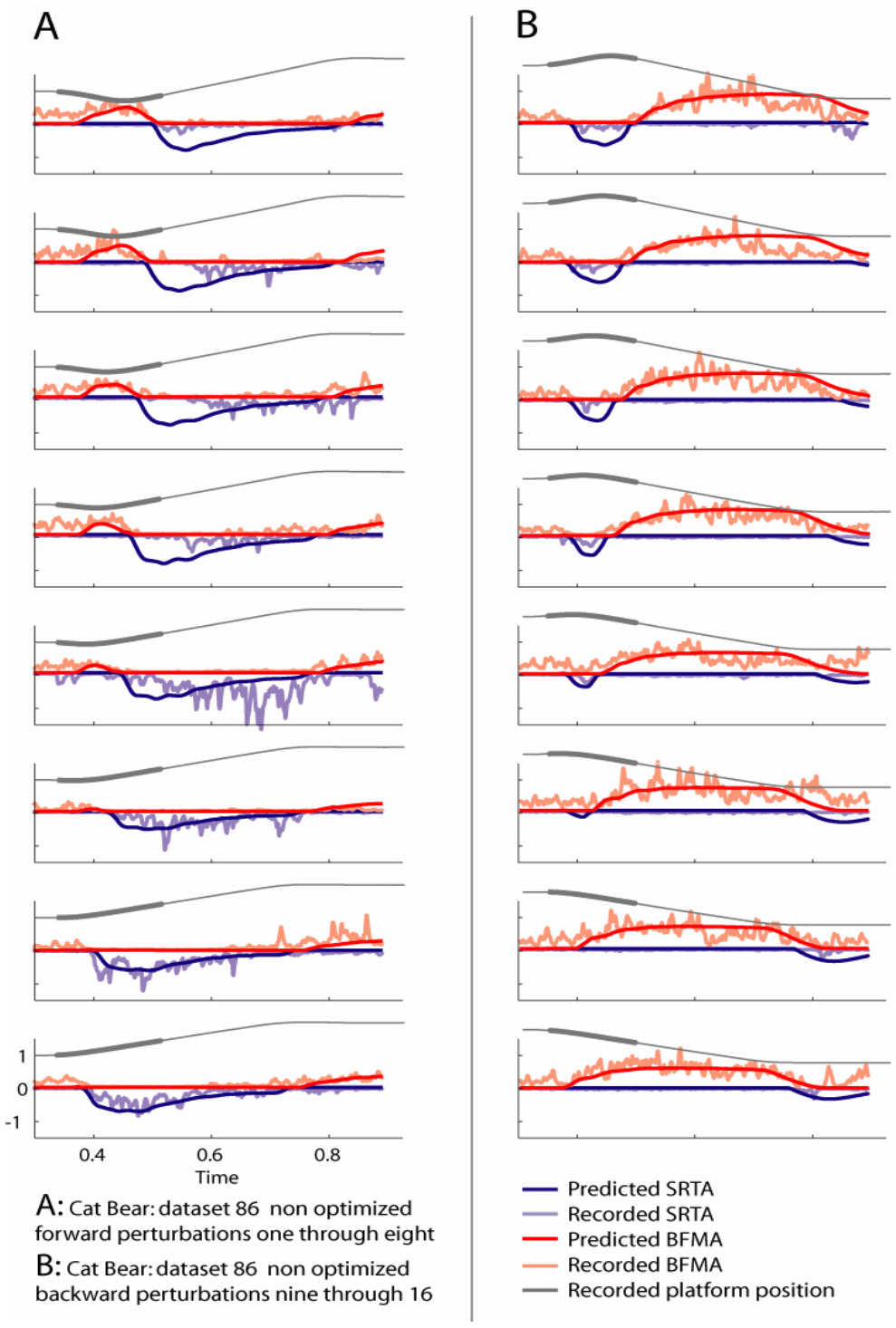

Figure 33: Cat Bear, dataset 86 (B6), all trials simulated with the gains of the unidirectional perturbation gains. Trial eight (kp1 = 3.9760, kv1 = 0.6471, ka1 = 1.00E-05, l_1 = 55ms) and 16 (kp2 = 3.8919, kv2 0.3741, ka2 = 1.00E-05, l_2 = 55ms) without further optimizing. A: Forward perturbation: the agonist BFMA EMG, has its highest magnitude in trial one. Over eight trials, the initial forward displacement becomes 0m/s, the agonist EMG only has a short on time when the platform stops. B: Backward perturbation: similar behavior for the trials nine through 16. The different EMG shapes are only due to the different platform acceleration

4.4.2 Comparison of intact vs. somatosensory cats

Comparing the results of the intact and the somatosensory cats, we found a reduction in acceleration feedback in muscle BFMA, but not a complete knockout of the acceleration gain as we had expected it. As in Figure 34, the EMG prediction showed similar behavior in the plateau region, missing the first acceleration dependent burst for the same perturbation shape.

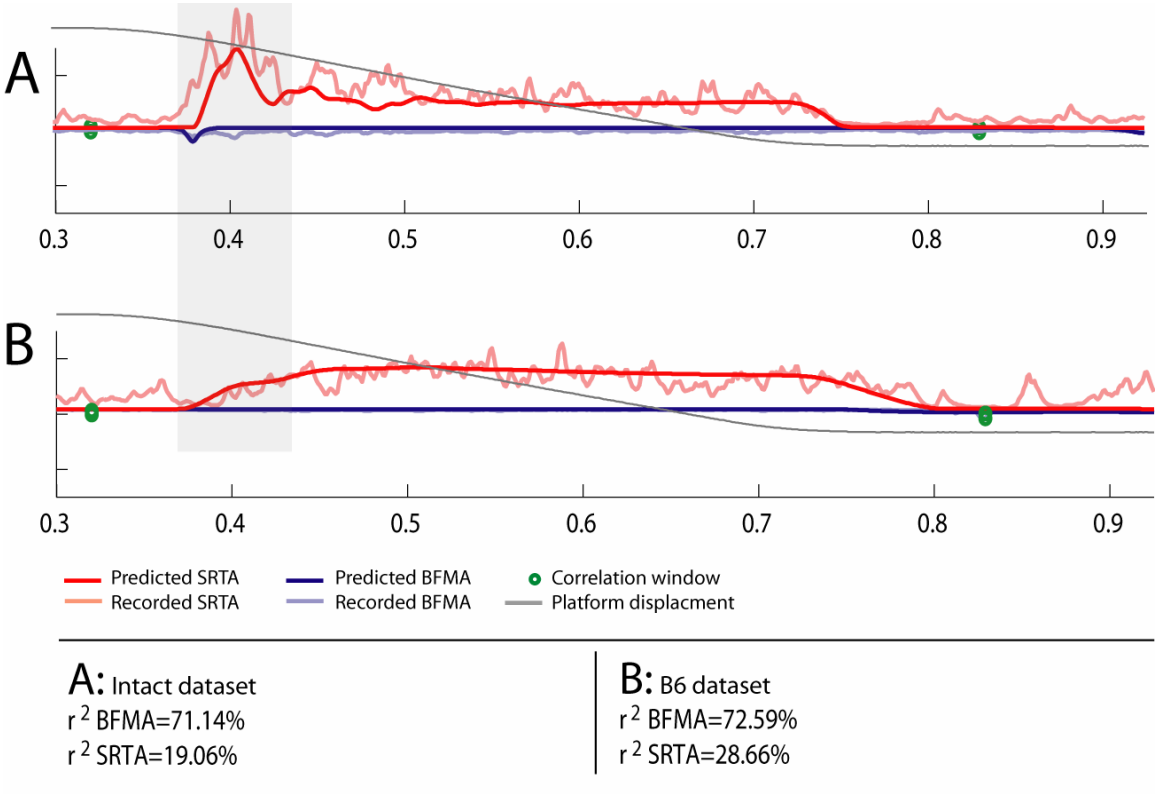

Figure 34: Comparison intact vs. B6 EMG prediction. A - EMG prediction for intact cat, perturbation 16. B - EMG prediction for B6 cat, perturbation 16. The first burst in the B6 dataset is missing.

Though the optimal acceleration gains of the B6 trials in Table 7 showed some large deviations from zero in k_a, we showed that this was caused by the optimization method. The non optimized simulations in Figure 33 used $k_{a1}=k_{a2}=0.00001$ and still showed close matches of recorded and predicted data for all trials.

Stapley et al. reported increased neural time delays for somatosensory loss cats than for intact ones (Stapley et al. 2002). As the acceleration bursts rise quicker in magnitude, a missing first burst would make the EMG rise later over the level, from which on it is considered “on”. So Stapley’s observation could rather be interpreted being a result of to missing acceleration feedback than being a true increase in time delay. An interesting observation is that the B6 EMG takes about 50ms longer to return to non active. As the first EMG burst is missing in the stabilization process, a longer delay until returning to a stable upright position might be the result.

The non-optimized predictions showed good results for the backwards perturbations (See Figure 33). The SRTA gains predicted the backward perturbations reasonably well. However, the forward perturbations for SRTA were not well predicted, though the gains were capable of predicting the backward trials. Unfortunately, this study can not answer, if this prediction discrepancy is caused by not identifying the correct unidirectional gains during the optimization, or by a gain change due to somatosensory loss. A prediction of all B6 trials was not possible. Some EMGs were buried in noise and could therefore not be reconstructed.

CHAPTER V

DISCUSSION

We studied the effects of varying perturbation magnitude and direction on the postural control process of the central nervous system (CNS) caused by perturbation, before and after sensory loss. Modeling the CNS as two delayed feedback controllers, we reconstructed the EMGs of two antagonistic muscles simultaneously that were recorded during postural perturbation experiments on cats. Minimizing the error between predicted and recorded EMG and CoM kinematics, we were able to identify controller gains that would result in the best prediction of the recorded EMGs. We showed that two controllers were necessary to predict two EMGs. We also showed that first order muscle models predicted EMGs better than second order models.

The results indicate that feedback gains of a one link inverted pendulum model employed for postural perturbation remain constant over varying perturbation magnitude. As mentioned in Chapter 4.3.5, this does not necessarily stand in contrast to the results of Park (Park et al. 2004), who found a gradual scaling in feedback gains for a two link inverted pendulum model. Park's subjects were exposed to a magnitude range of 3-15cm, tuning the velocity and acceleration such that subjects increasingly bend their hip for increasing perturbation magnitude. It is possible that the CNS shifted the responsibility for stabilization from the ankles to the hip for increasing perturbation magnitudes, leaving the overall sum of feedback on the CoM constant. The one link inverted pendulum used for simulation in our experiments was not able to capture any hip strategy. It is also possible that the linear feedback gain scaling reported by Park was rather caused by varying velocity and acceleration than by varying platform displacement, because the plateau region of an EMG trace scales with velocity and the first burst with acceleration. We used perturbations with constant velocity profiles which would therefore not scale the EMG.

While varying perturbation magnitudes were investigated by earlier researchers, another enhancement of this study compared to previous research was the investigation of bi-directional perturbations. Park et al. (Park et al. 2005) had shown increased feedback

gains for initial forward lean, which they interpreted as an increased postural challenge. From the perspective of the second phase of the bi-directional perturbation, the cats were facing a decreased postural challenge, since second phase of the perturbation pushed the feet back underneath the CoM and facilitated stabilization. We were able to reconstruct EMGs with constant feedback gains regardless of prior movement, though we observed a weakened first burst in the antagonist EMG, which could be interpreted as scaling but occurs without changing feedback gains. (see Figure 21).

He et al. (He et al. 1991) had predicted the EMGs of 10 muscles simultaneously, using three link inverted pendulum model. He caught far more physiological details, since he increased the number of muscles, the number of joints and by modeling the sensory systems. His feedback gain matrices gave insight into the weighing of the sensory information for each muscle. Though our model was far simpler, we were able to predict EMG and CoM kinematics for biceps femoris and sartorius anterior (cats Bear, Sooty and Squrl) as well as for Gluteus and Iliopsoas (cat Knobi) with only eight parameters.

The good approximation of EMG using CoM feedback indicates that the CNS can extract the CoM information out of the sensory information given, but calculation of the CoM requires an internal model of the body. We provided further evidence for an internal model, which was also assumed by van der Kooij for his investigations on the effect of varying the weight of sensory information.

Summarized, our work extended Lockhart's and Park's work by predicting two antagonistic muscle EMGs simultaneously. We employed previously used concepts like a one link inverted pendulum model after Peterka, an optimization method with a cost function similar to the on of Kuo, a PID controller like Lockhart and muscle models like He or Partridge. Our work bridged the gap from EMG and kinematic prediction with a difficult model to simpler models predicting kinematics only. By reducing the model complexity of e.g. the model of He et al. to a simulation system similar to the one of Peterka, we made the problem or EMG prediction easier accessible.

5.1 Limitations and further annotations

This study was limited to the prediction of sartorius anterior (SRTA) versus biceps Femoris (BFMA). Predictions of tibialis anterior (TIBA) versus SRTA failed due to too high noise level in the EMG of TIBA. The limited amount of data made statistically significant conclusions on loss of the somatosensory system difficult.

Besides implementing an individual time delay in each controller, resulting in eight free parameters, we also predicted EMGs using an individual neural time delay for each kinematic feedback component. For two controllers each having position, velocity and acceleration feedback, this summed up to six controller gains and six neural time delays, equal 12 free parameters. We did not investigate this data further, since the jump from eight to 12 free parameters did not result in significantly better simulation results.

5.2 Future work

The most important improvement of the model could be the transition to a human subject. When modeling a human, future investigations could increase the degree of reality of the model. Though the simulation results predicted recorded data well, the model remains a very simple approximation of the real physiology of a cat during postural perturbation experiments. If applied to humans, the model would need to be extended to a two or three link inverted pendulum (Kuo and Zajac 1993; Roy 2004). Alexandrov showed that the hip and knees in humans contribute to the stabilization process even for small perturbations (Alexandrov et al. 2001). Besides the fact that our muscle models neglected force length and force velocity relationship, we also assumed full state feedback. More elaborate muscle models could simulate the dynamical properties like the ones of Winters and Stark (Winters and Stark 1985), and at the same time included sensory feedback models like Golgi Tendon Organs and muscle spindles (Van der Helm and Rozendaal 2000) in the muscle model. This would increase the difficulty in stabilizing the model, but simulate the physiology more accurately. He et al.

provided an overview over a complex model of the body dynamics and a comprehensive overview over sensory system and higher order brain centers. (He et al. 1991)

In the real world, perturbations are not limited to diagonal displacements. If EMG prediction shall one day help to build controllers that make paraplegic patients overcome their injury, a wide variety of disturbances will need investigation in order to account for the variety of disturbances a human is exposed to in every day life.

As a multitude of muscles are involved in stabilizing posture after perturbation, the extension of this study would have to predict a far greater amount of muscles in order to be of use for patients with spinal cord injuries. Predicting more than two muscles, it would be interesting to implement synergies by allowing direct influence of the controller of one muscle onto another muscle.

To prevent falls of diabetic patients in the future, further investigations on temporal progression of feedback gains after B6 poisoning could be of great value. Investigations on the duration of EMG trace of B6 and intact cats could give insight into the consequences of the missing acceleration burst. A larger dataset with intermediate trials during the poisoning process would be helpful for these investigations.

With the future goal of improving the quality of life for spinal cord injury patients and the elderly, all these investigations are just first steps on a long journey - revealing the incredible complexity of the neural system.

APPENDIX A

UNIDIRECTIONAL GAINS OF ALL CATS

Cat Bear

Table 8: Cat Bear, unidirectional gains of perturbation eight for muscles SRTA (controller 1) and unidirectional gains of perturbation 16 for muscle MGAS (controller 2).

Dataset	Kp1	Kv1	Ka1	l_1	Kp2	Kv2	Ka2	l_2
10	5.2956	0.68825	1.00E-05	55	4.0112	0.35701	0.01838	54.307
11	5.7898	0.40348	0.002057	33.383	4.2083	0.33613	0.012017	38.651
12	5.8073	0.29733	0.006444	30.706	3.9676	0.3704	0.010641	38.073
18	6.2217	0.6041	0.000955	21.207	4.2345	0.6858	0.01867	37.303

Table 9: Cat Bear, unidirectional gains of perturbation eight for muscles STEN (controller 1) and unidirectional gains of perturbation 16 for muscle FDL (controller 2).

Dataset	Kp1	Kv1	Ka1	l_1	Kp2	Kv2	Ka2	l_2
10	1.2753	1.1114	1.29E-02	37	2.5678	0.87065	0.00596	35.948
11	2.3338	0.88573	0.016663	41.014	4.159	0.36075	0.014745	38.316
12	2.5098	0.79228	0.014809	42.077	3.2586	0.539	0.009078	28.94
18	1.4395	1.1357	0.01438	38.52	1.9021	1.0224	0.009908	28.295

Table 10: Cat Bear, unidirectional gains of perturbation eight for muscles SRTA (controller 1) and unidirectional gains of perturbation 16 for muscle BFMA (controller 2).

Dataset	Kp1	Kv1	Ka1	l_1	Kp2	Kv2	Ka2	l_2
10	3.8445	0.45319	1.00E-05	35.603	3.1532	0.6193	0.022098	49.571
11	3.5265	0.57665	1.00E-05	50.501	3.813	0.54851	0.012034	48.33
12	4.2317	0.36513	0.002539	28.006	3.8026	0.40988	0.014931	47.227
18	5.3373	0.61835	0.000555	20	4.2194	0.73477	0.006863	34.611

Cat Sooty

Table 11: Cat Sooty, unidirectional gains of perturbation eight for muscles SRTA (controller 1) and unidirectional gains of perturbation 16 for muscle BFMA (controller 2).

Dataset	Kp1	Kv1	Ka1	l_1	Kp2	Kv2	Ka2	l_2
12	5.1542	0.31549	1.94E-02	33.002	3.6644	0.55545	0.019273	41.299
14	5.0632	0.53968	1.94E-02	32.187	4.8892	0.28566	0.018917	25
15	4.9723	0.65198	0.021147	33.788	4.0147	0.30753	0.015951	33.3

Cat Squrl

Table 12: Cat Squrl, unidirectional gains of perturbation eight for muscles SRTA (controller 1) and unidirectional gains of perturbation 16 for muscle BFMA (controller 2).

Dataset	Kp1	Kv1	Ka1	l_1	Kp2	Kv2	Ka2	l_2
10	3.867	0.46303	1.17E-02	34.972	4.3498	0.29842	0.019281	37.799
11	3.1157	0.69526	9.49E-03	20.305	3.8529	0.42885	0.012246	33.736
12	3.045	0.7602	0.017435	20.491	0.0001	0.74975	0.000139	30.999
18	3.6441	0.54205	0.015282	26.448	4.8565	0.21447	0.015733	29.001

Cat Knobi

Table 13: Cat Knobi, unidirectional gains of perturbation eight for muscles ILPS(controller 1) and unidirectional gains of perturbation 16 for muscle GLUT (controller 2).

Dataset	Kp1	Kv1	Ka1	l_1	Kp2	Kv2	Ka2	l_2
12	2.6343	0.72872	0.034175	37.058	4.1064	0.38307	0.018086	28.3
14	3.4029	0.53255	3.23E-02	39	4.1367	0.43389	0.021959	28.638
15	3.3186	0.5564	0.028299	41.777	0.64606	1.5992	0.014042	20.144

APPENDIX B

EMG PREDICTIONS WITH CONSTANT GAINS

Cat Bear

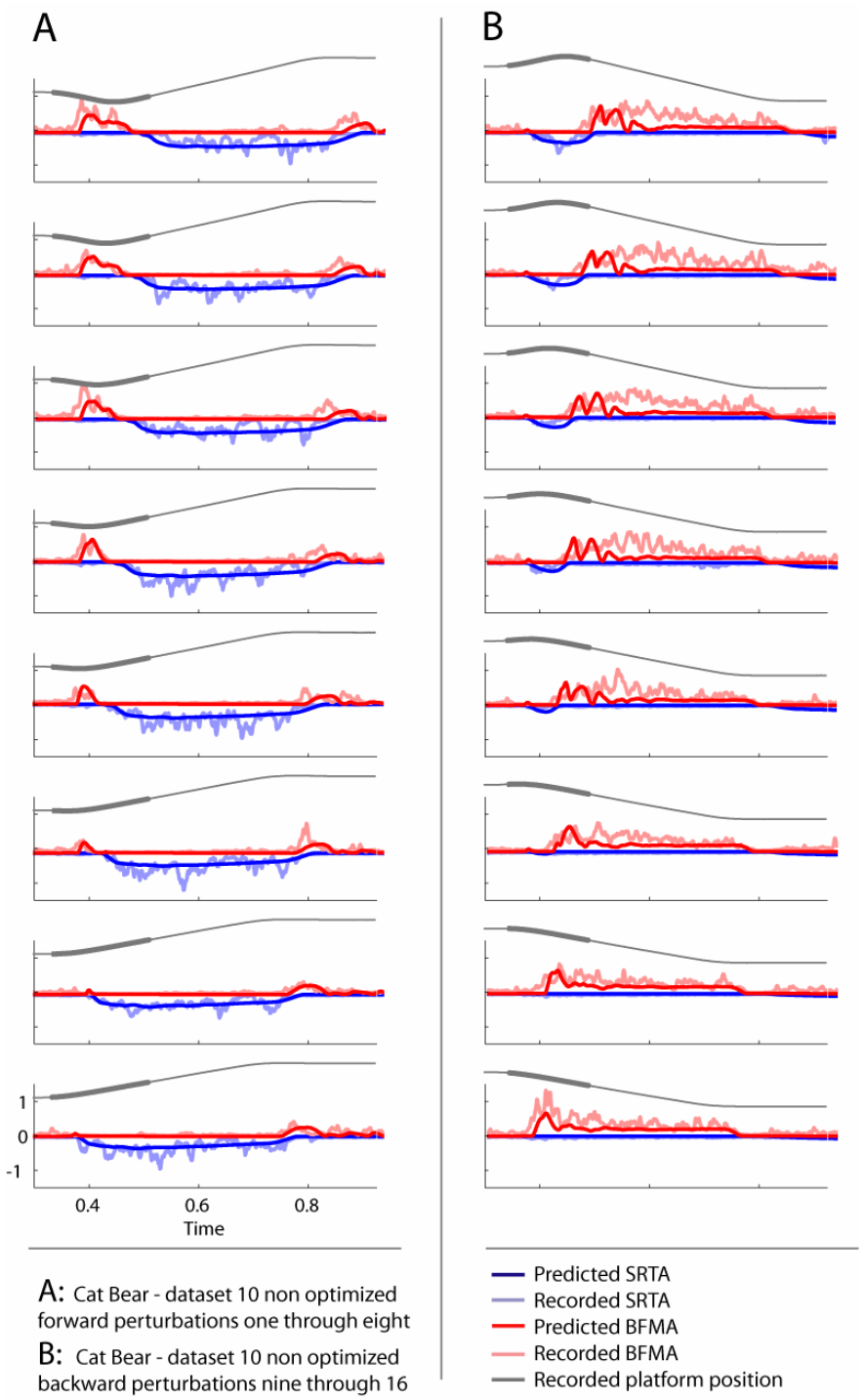

Figure 35: Cat Bear, dataset 10, muscles SRTA vs. BFMA without further optimization: simulated with the gains of the unidirectional perturbations of trial eight and 16.

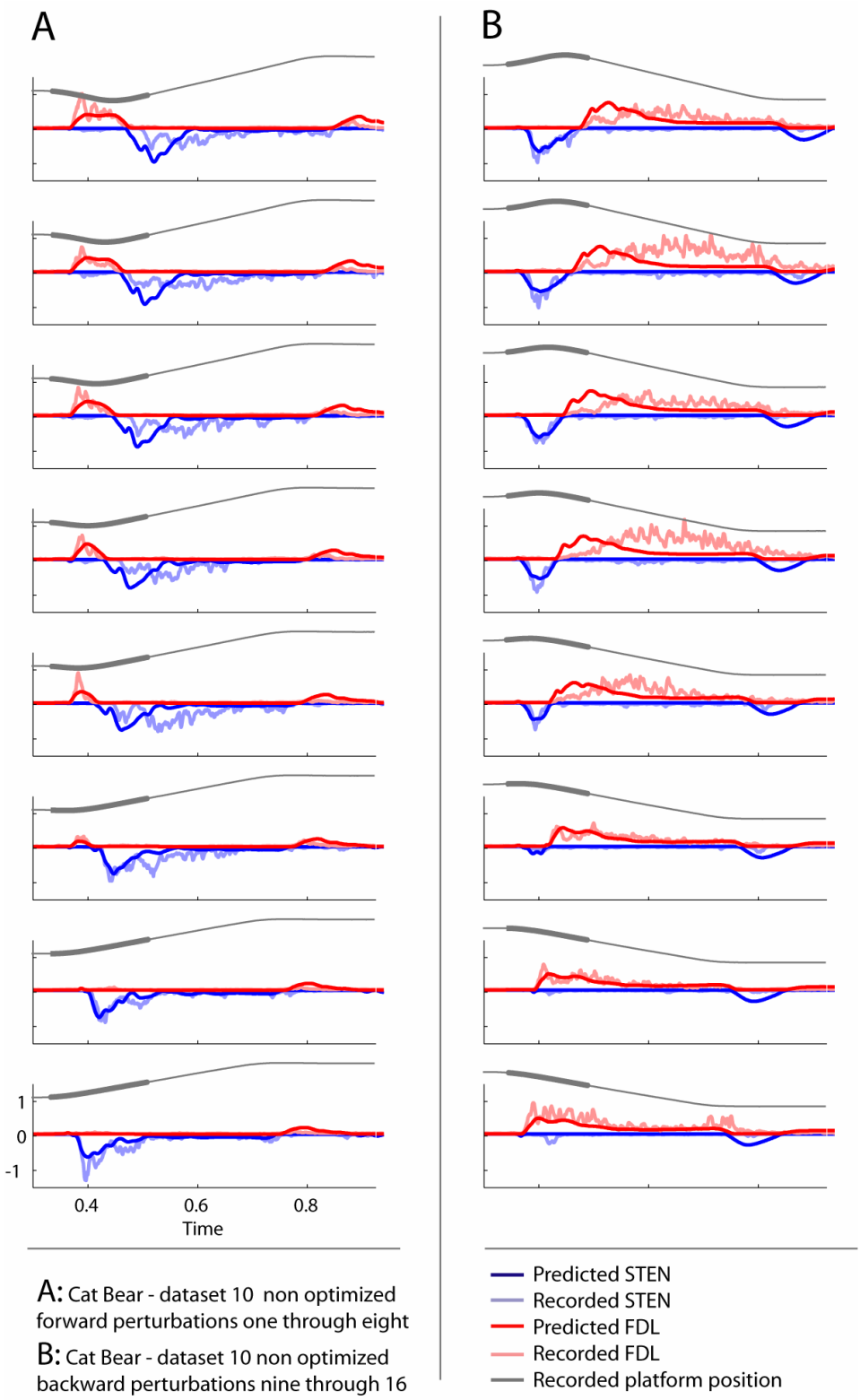

Figure 36: Cat Bear, dataset 10, muscles STEN vs. FDL without further optimization: simulated with the gains of the unidirectional perturbations of trial eight and 16.

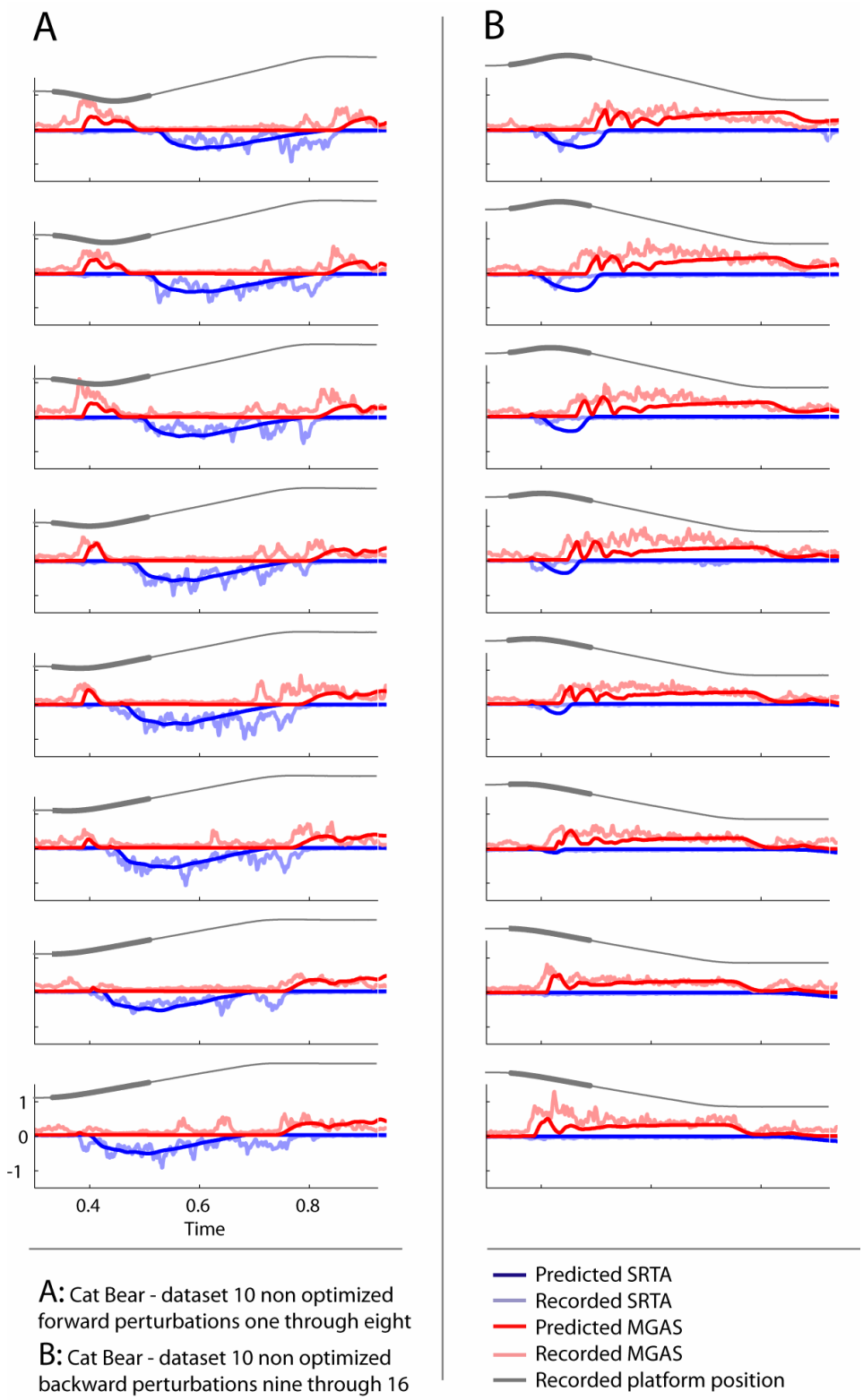

Figure 37: Cat Bear, dataset 10, muscles SRTA vs. MGAS without further optimization: simulated with the gains of the unidirectional perturbations of trial eight and 16.

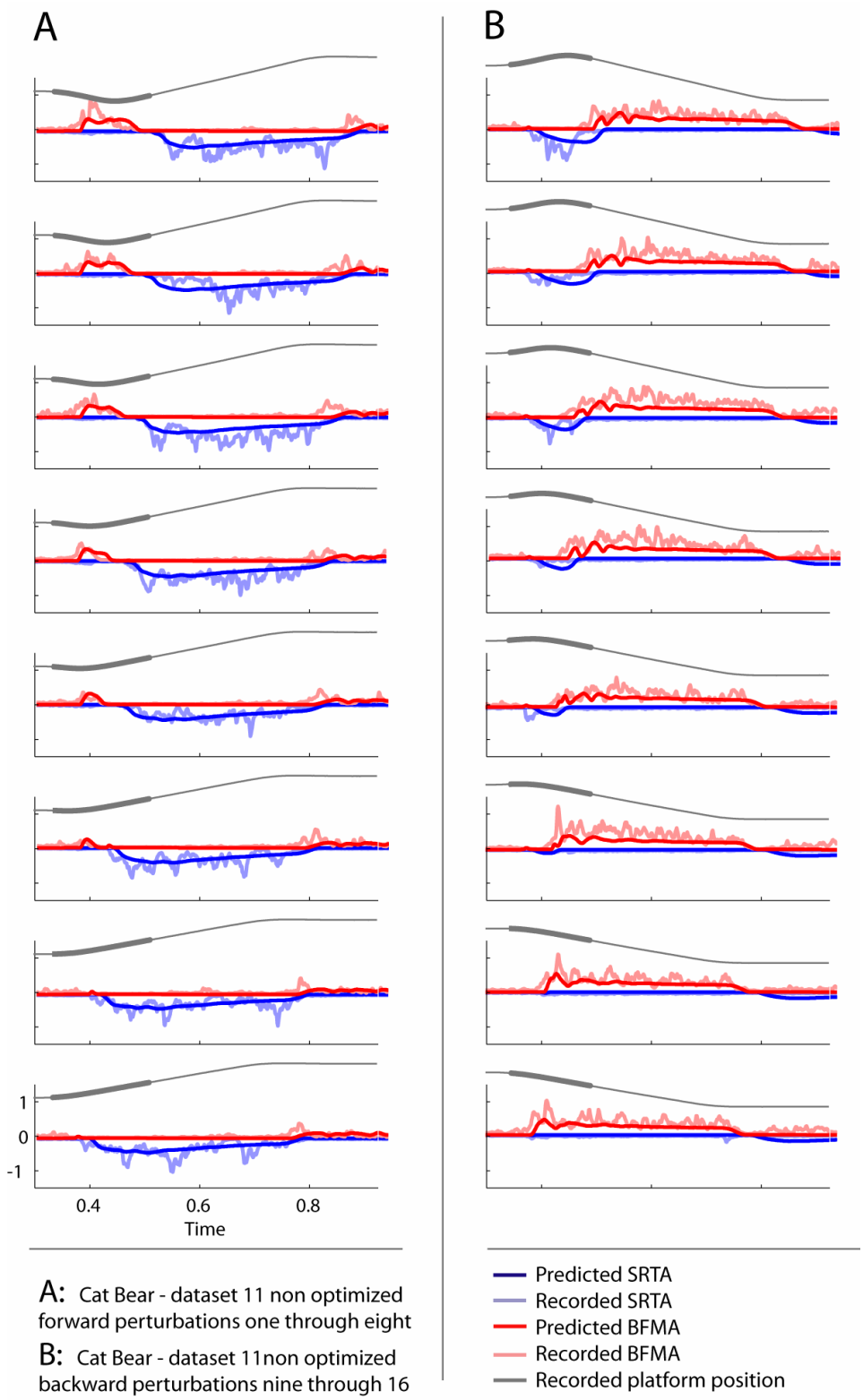

Figure 38: Cat Bear, dataset 11, muscles SRTA vs. BFMA without further optimization: simulated with the gains of the unidirectional perturbations of trial eight and 16.

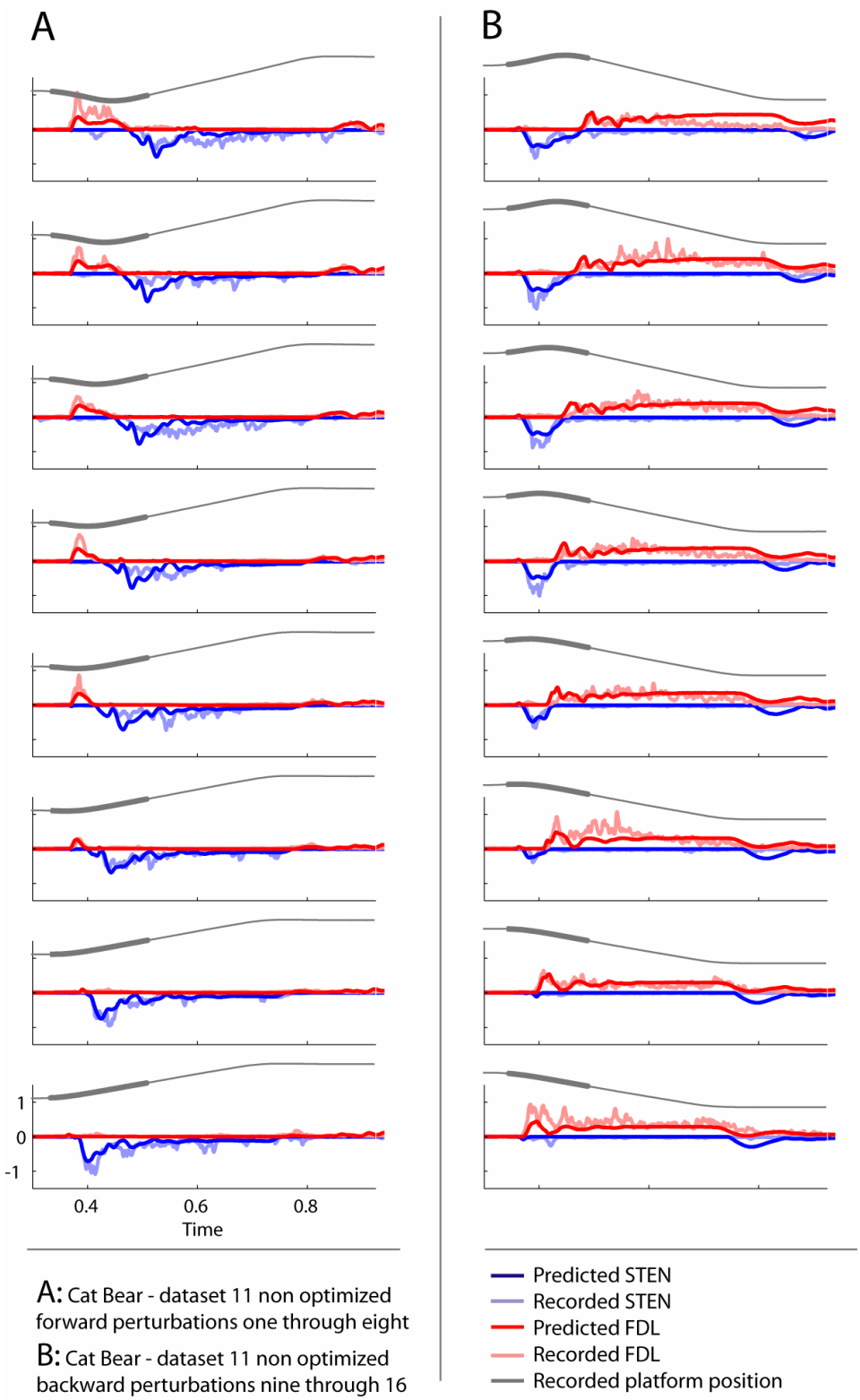

Figure 39: Cat Bear, dataset 11, muscles STEN vs. FDL without further optimization: simulated with the gains of the unidirectional perturbations of trial eight and 16.

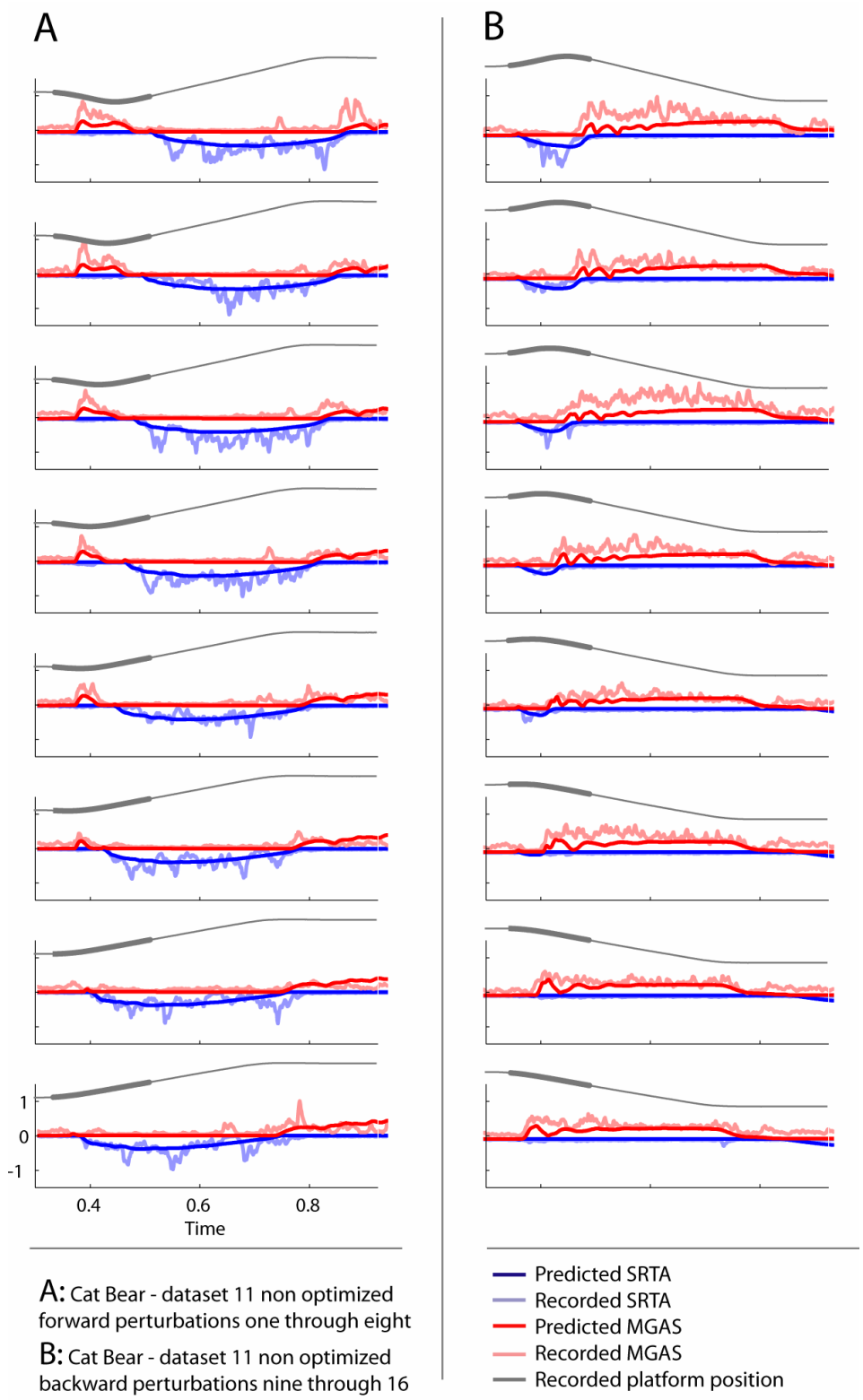

Figure 40: Cat Bear, dataset 11, muscles SRTA vs. MGAS without further optimization: simulated with the gains of the unidirectional perturbations of trial eight and 16.

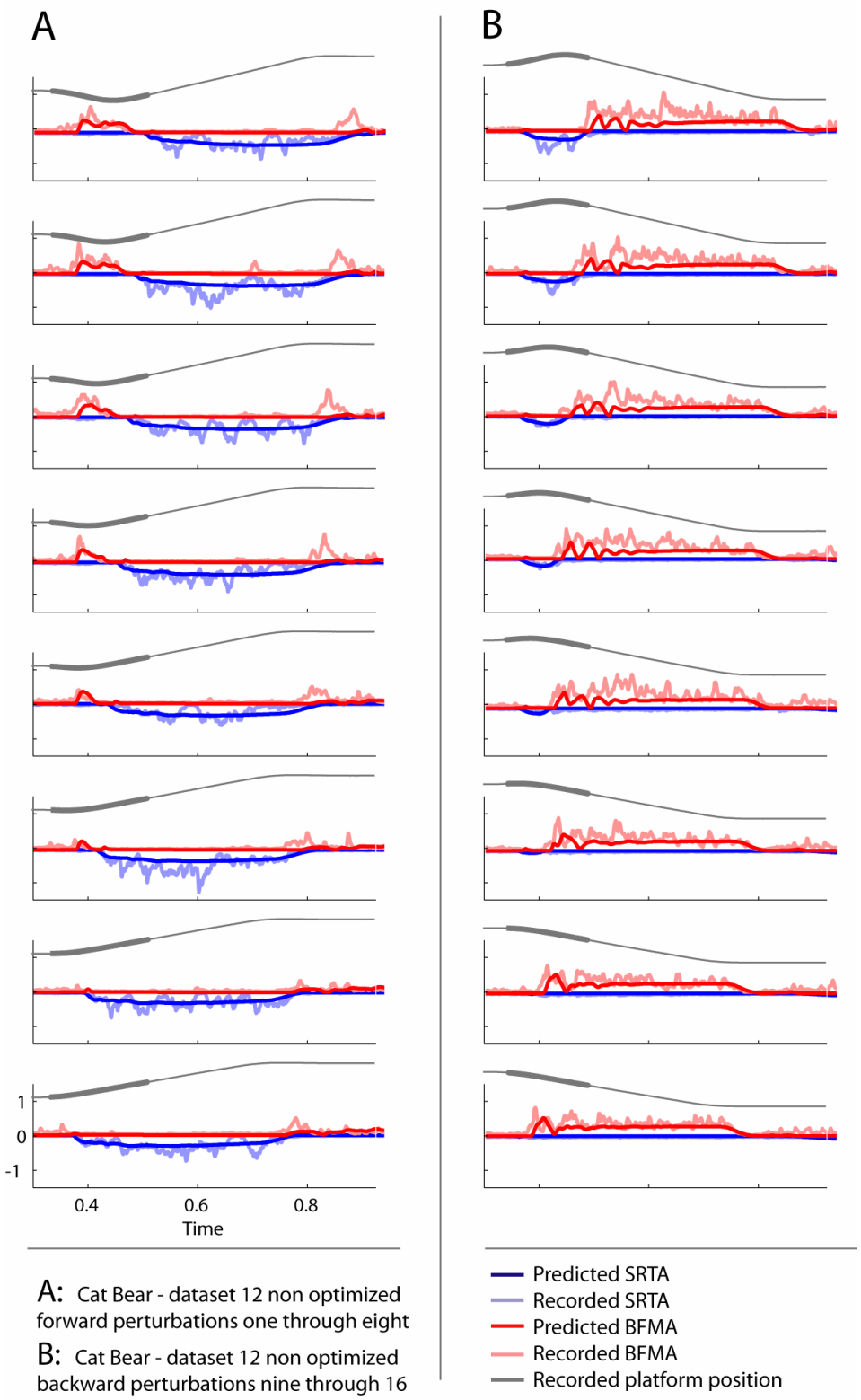

Figure 41: Cat Bear, dataset 12, muscles SRTA vs. BFMA without further optimization: simulated with the gains of the unidirectional perturbations of trial eight and 16.

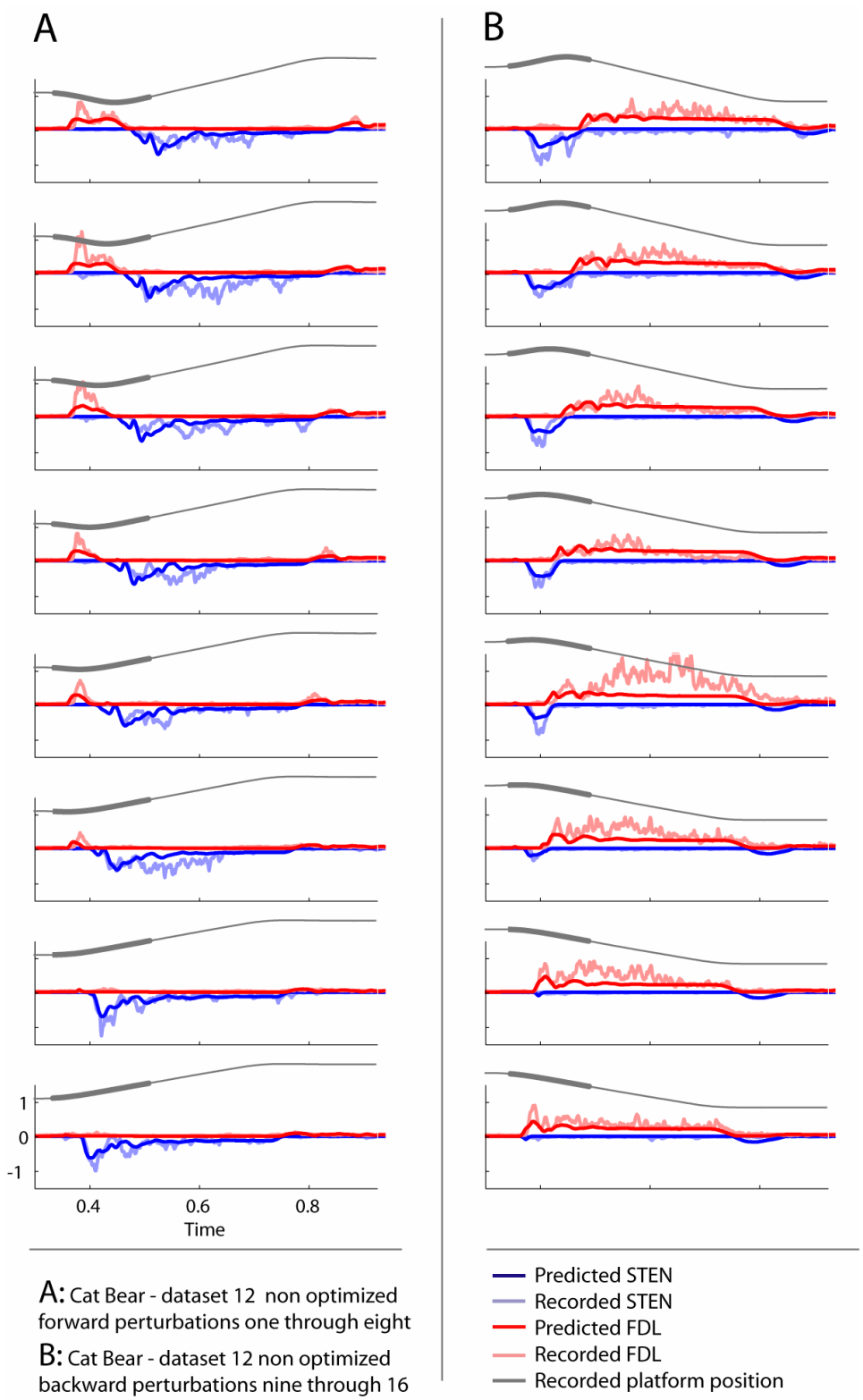

Figure 42: Cat Bear, dataset 12, muscles STEN vs. FDL without further optimization: simulated with the gains of the unidirectional perturbations of trial eight and 16.

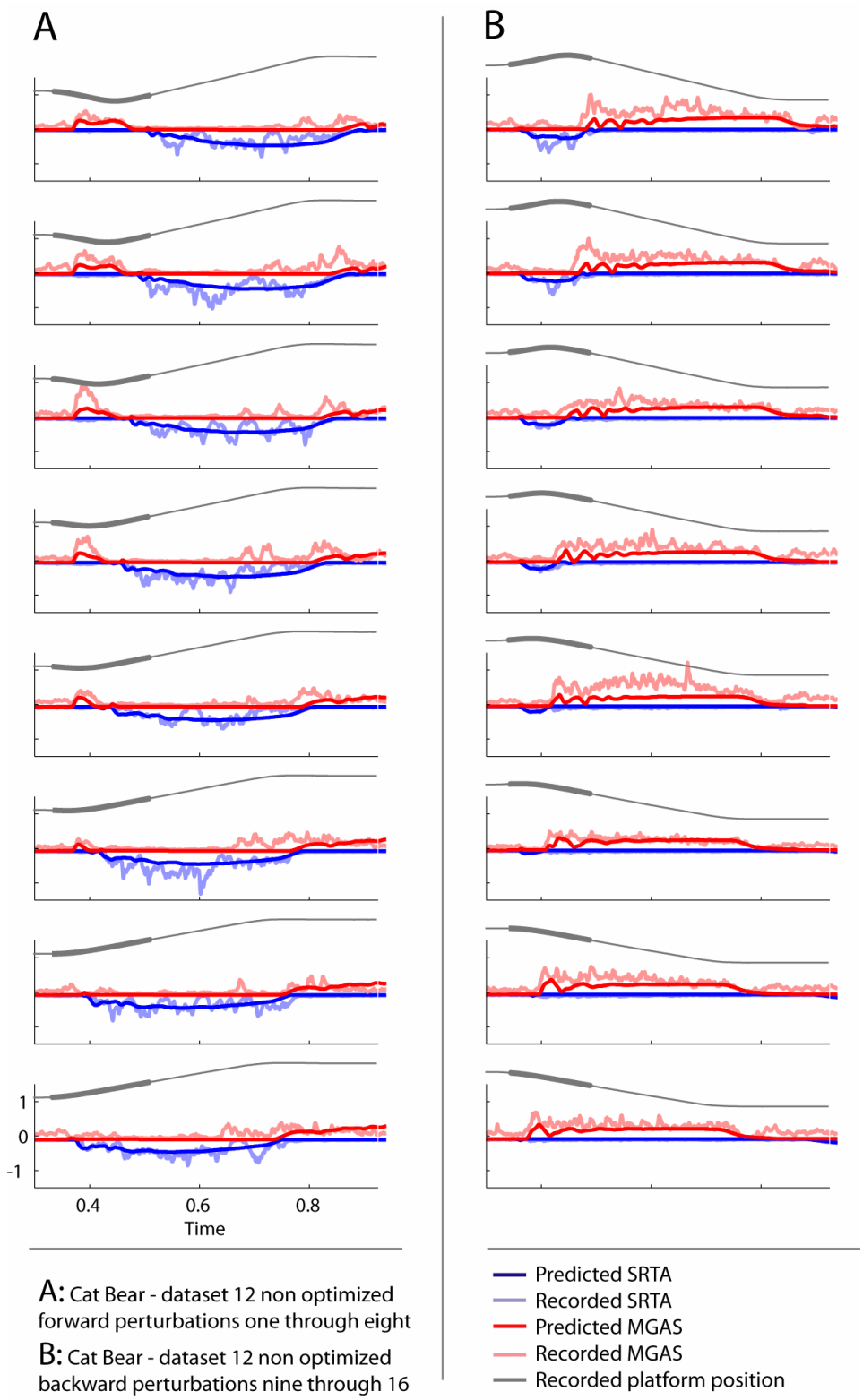

Figure 43: Cat Bear, dataset 12, muscles SRTA vs. MGAS without further optimization: simulated with the gains of the unidirectional perturbations of trial eight and 16.

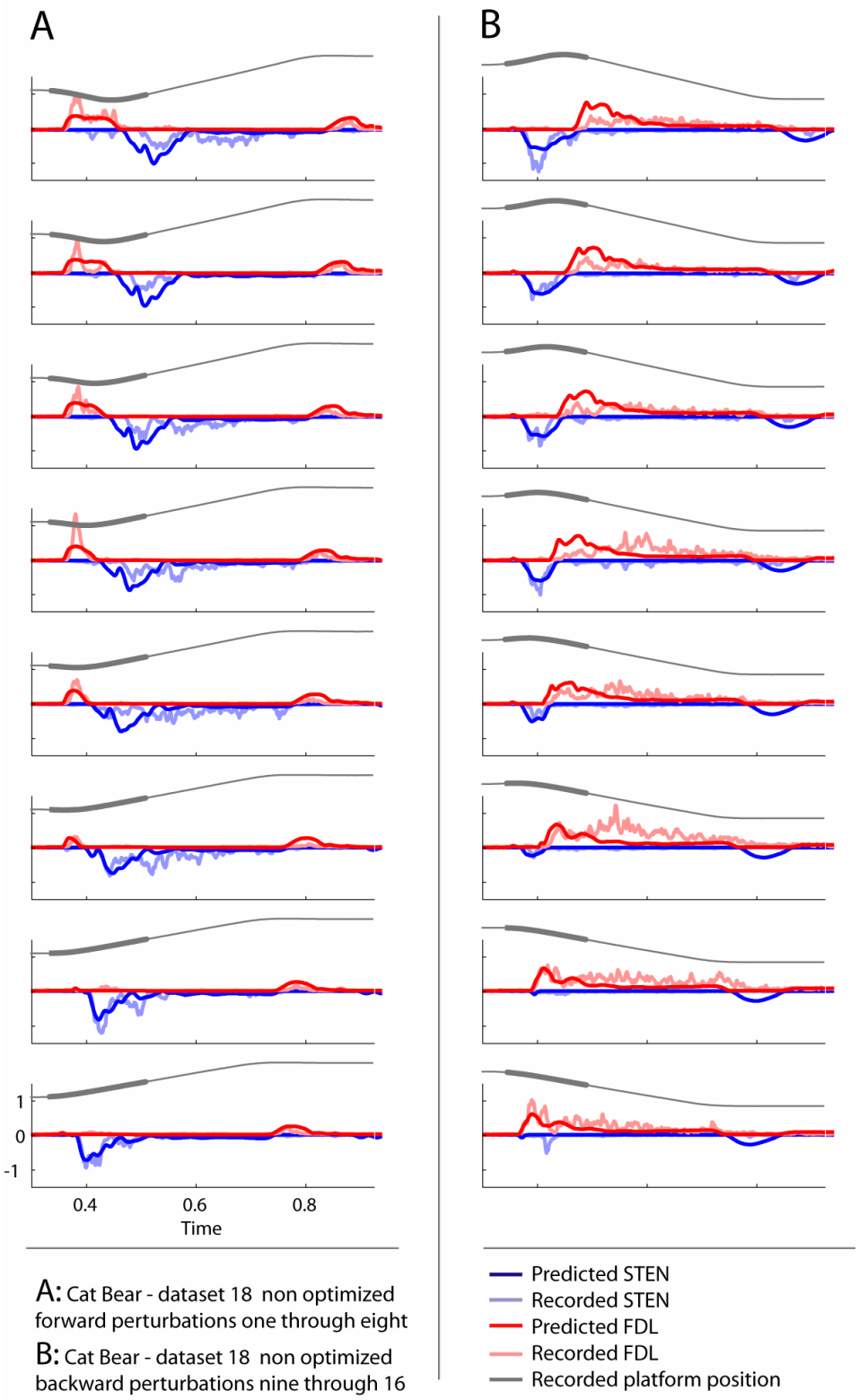

Figure 44: Cat Bear, dataset 18, muscles STEN vs. FDL without further optimization: simulated with the gains of the unidirectional perturbations of trial eight and 16.

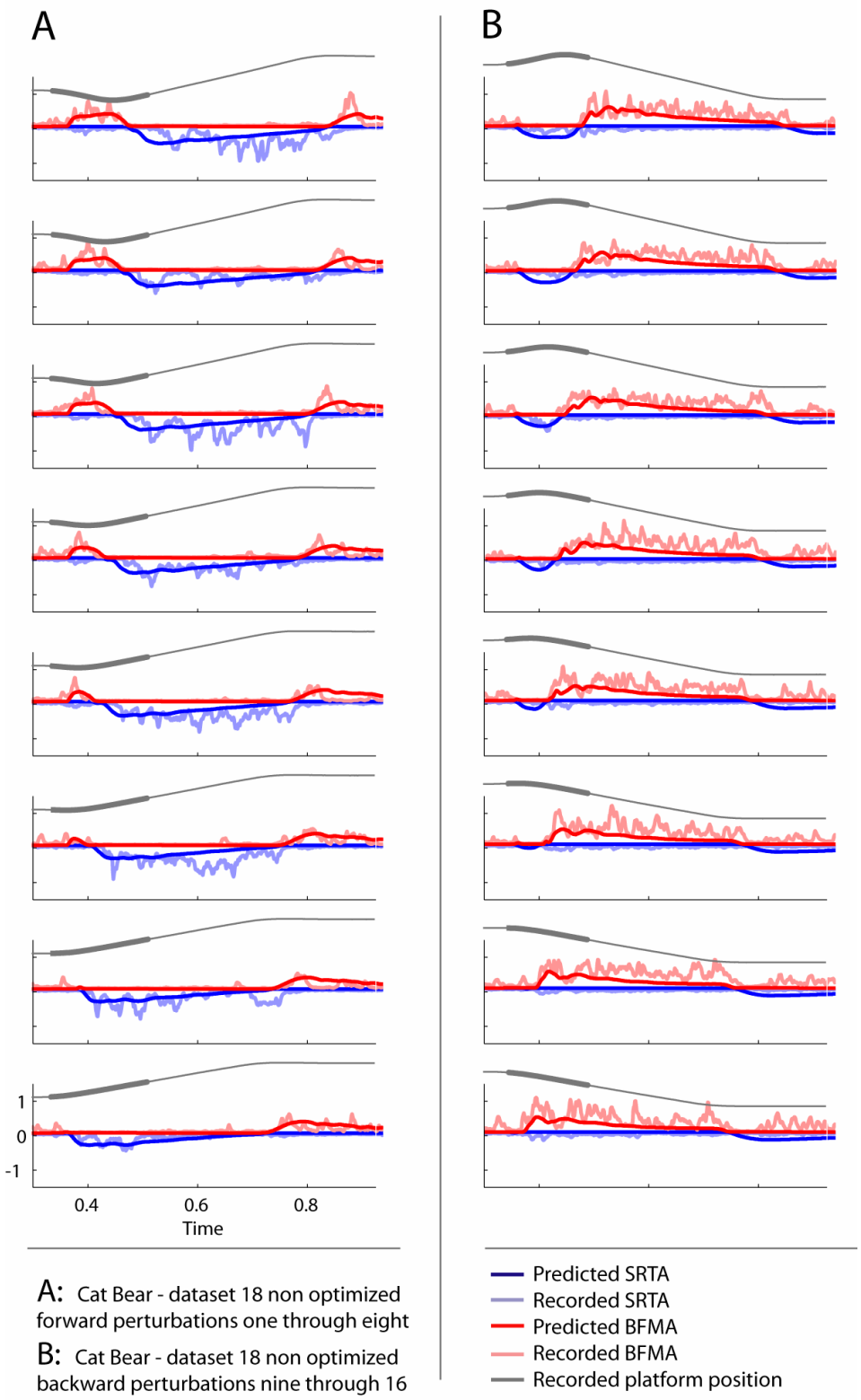

Figure 45: Cat Bear, dataset 18, muscles SRTA vs. BFMA without further optimization: simulated with the gains of the unidirectional perturbations of trial eight and 16.

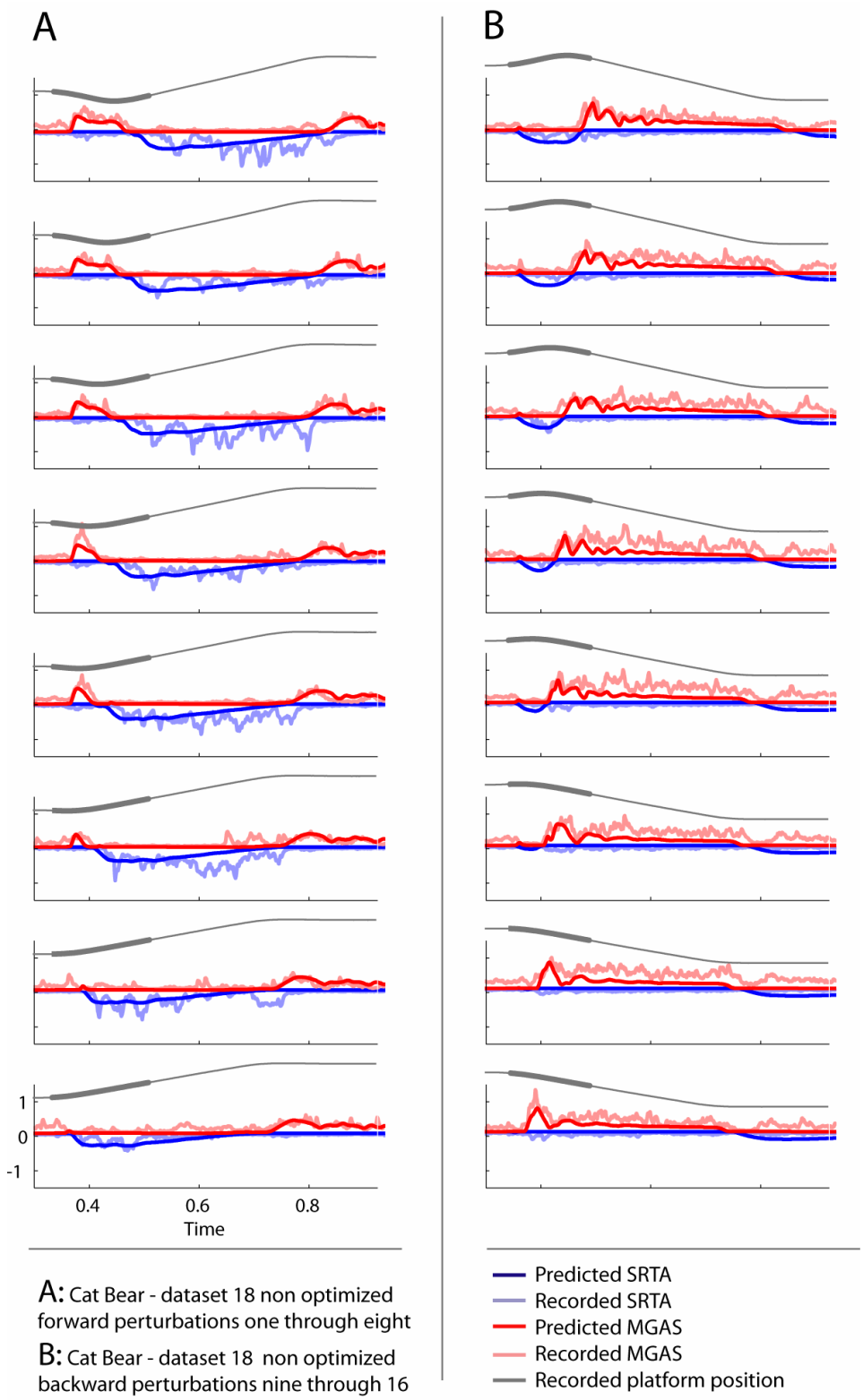

Figure 46: Cat Bear, dataset 18, muscles SRTA vs. MGAS without further optimization: simulated with the gains of the unidirectional perturbations of trial eight and 16.

Cat Sooty

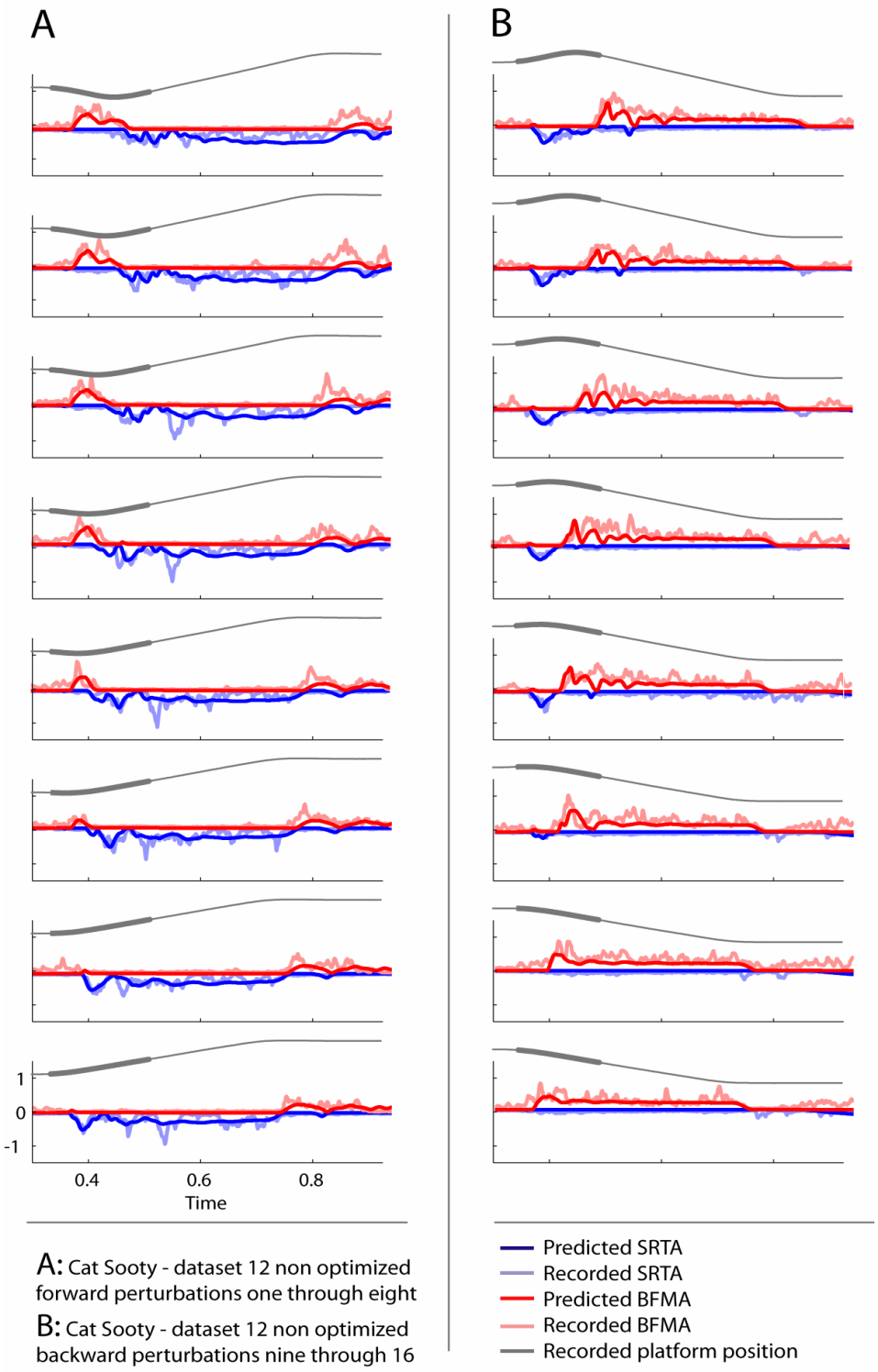

Figure 47: Cat Sooty, dataset 12, muscles SRTA vs. BFMA without further optimization: simulated with the gains of the unidirectional perturbations of trial eight and 16.

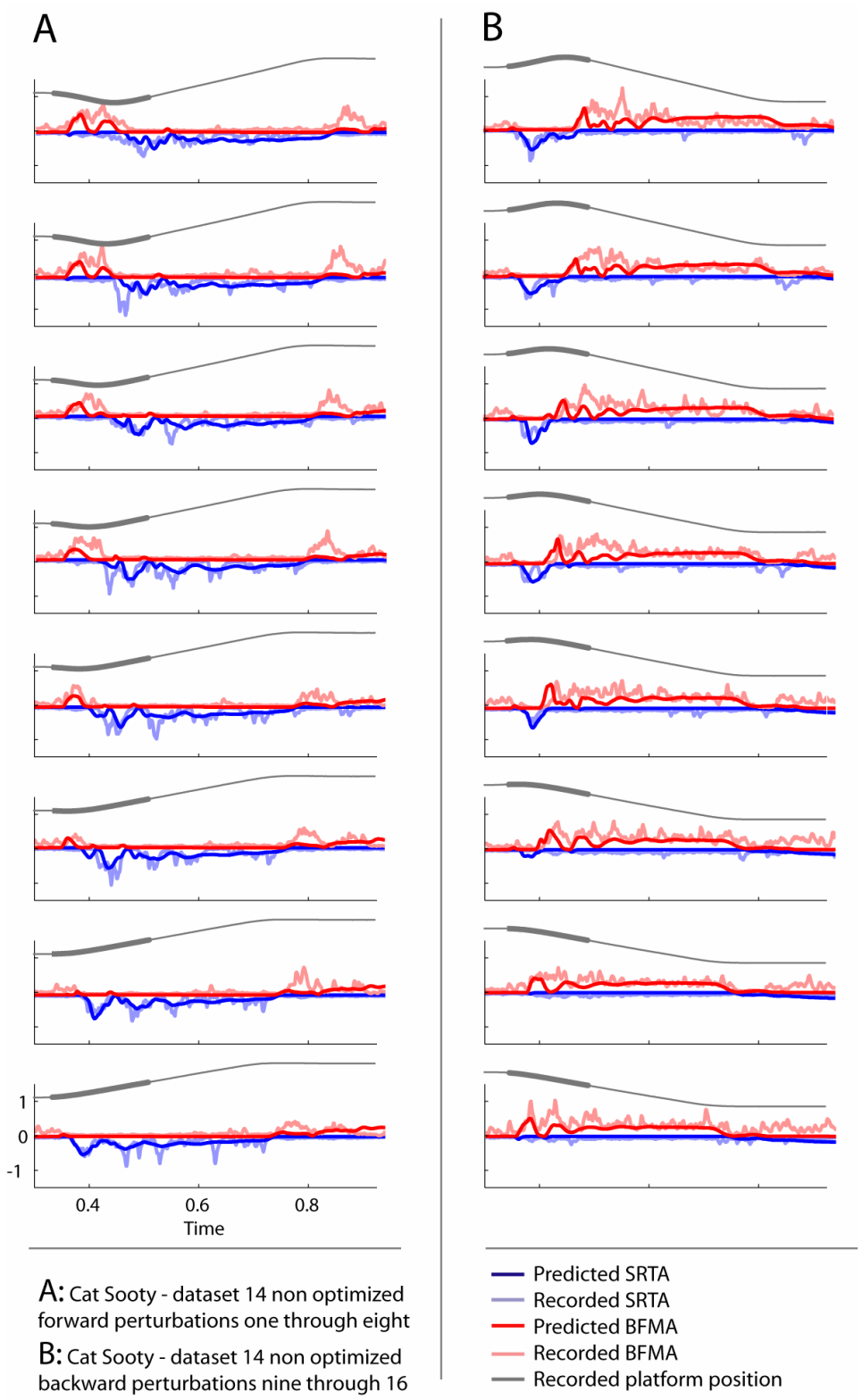

Figure 48: Cat Sooty, dataset 14, muscles SRTA vs. BFMA without further optimization: simulated with the gains of the unidirectional perturbations of trial eight and 16.

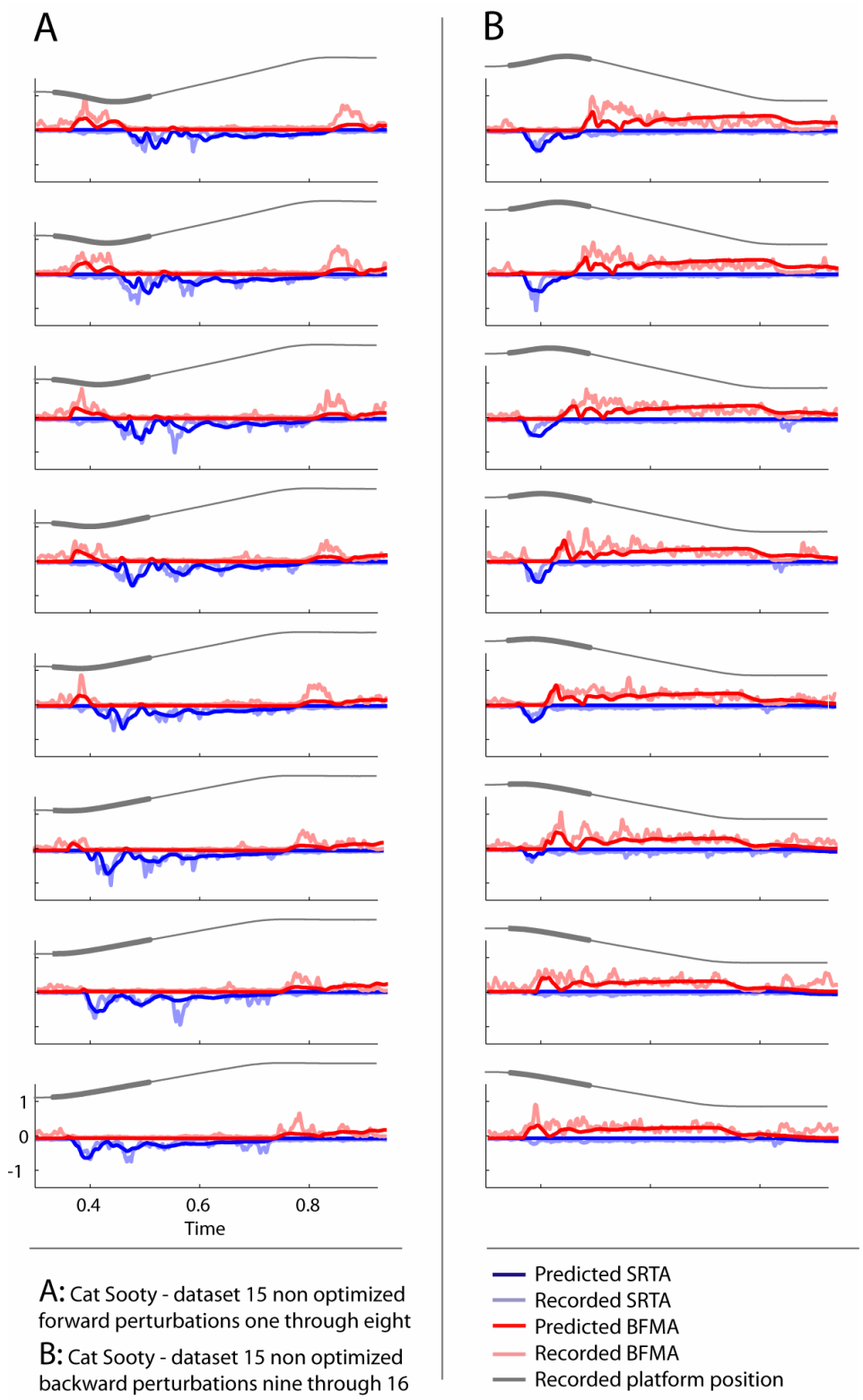

Figure 49: Cat Sooty, dataset 15, muscles SRTA vs. BFMA without further optimization: simulated with the gains of the unidirectional perturbations of trial eight and 16.

Cat Squrl

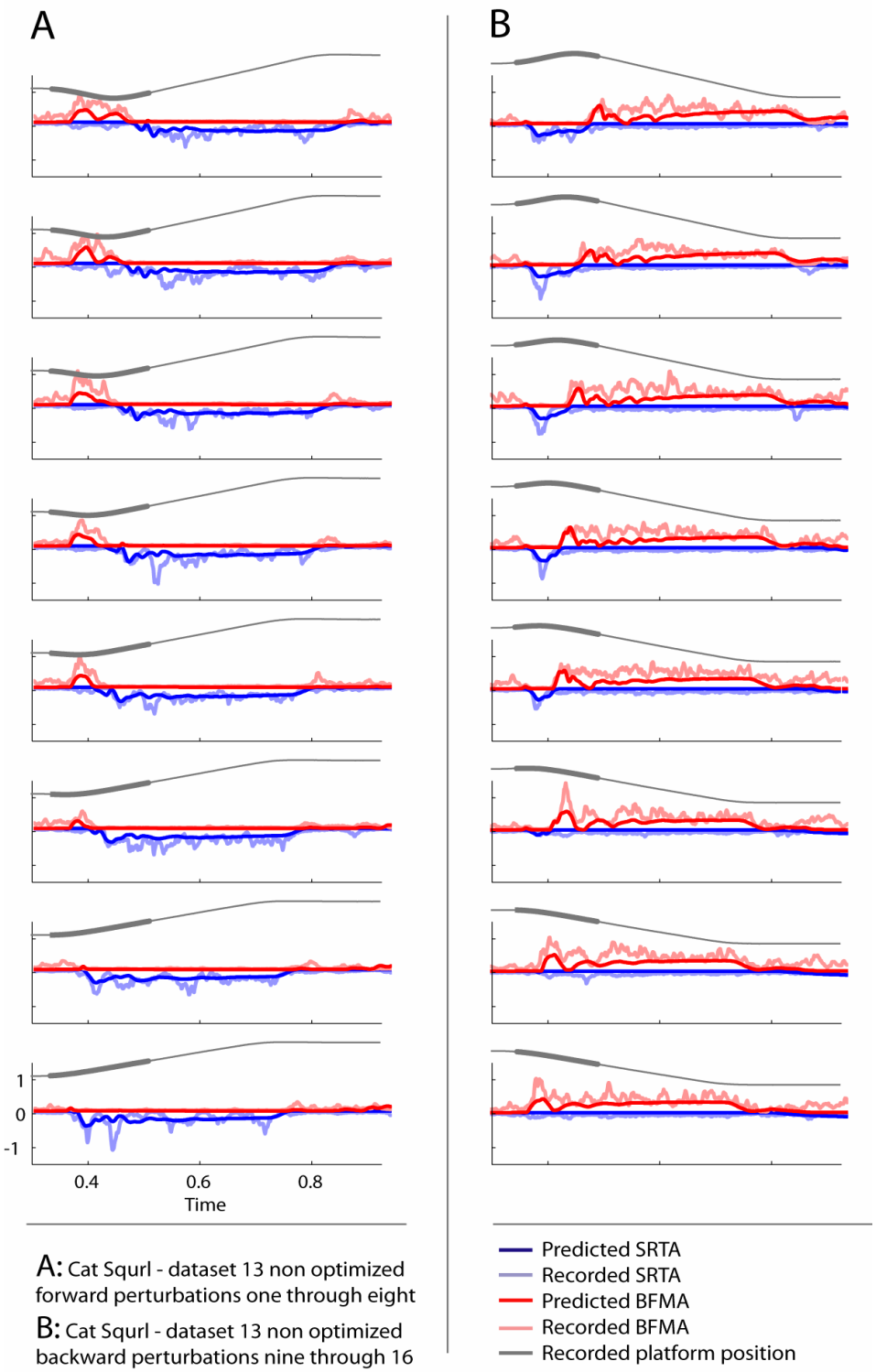

Figure 50: Cat Squrl, dataset 13, muscles SRTA vs. BFMA without further optimization: simulated with the gains of the unidirectional perturbations of trial eight and 16.

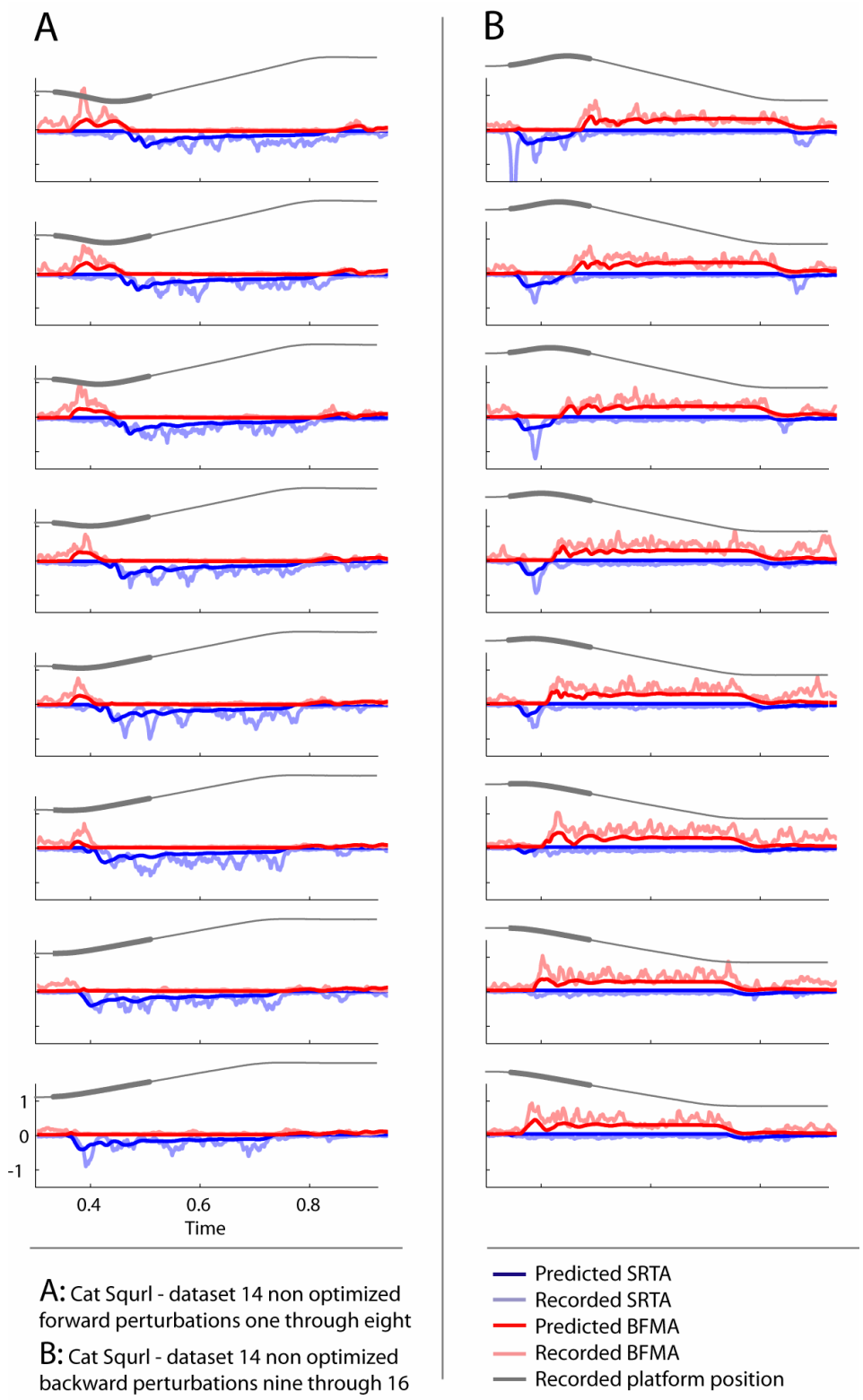

Figure 51: Cat Squrl, dataset 14, muscles SRTA vs. BFMA without further optimization: simulated with the gains of the unidirectional perturbations of trial eight and 16.

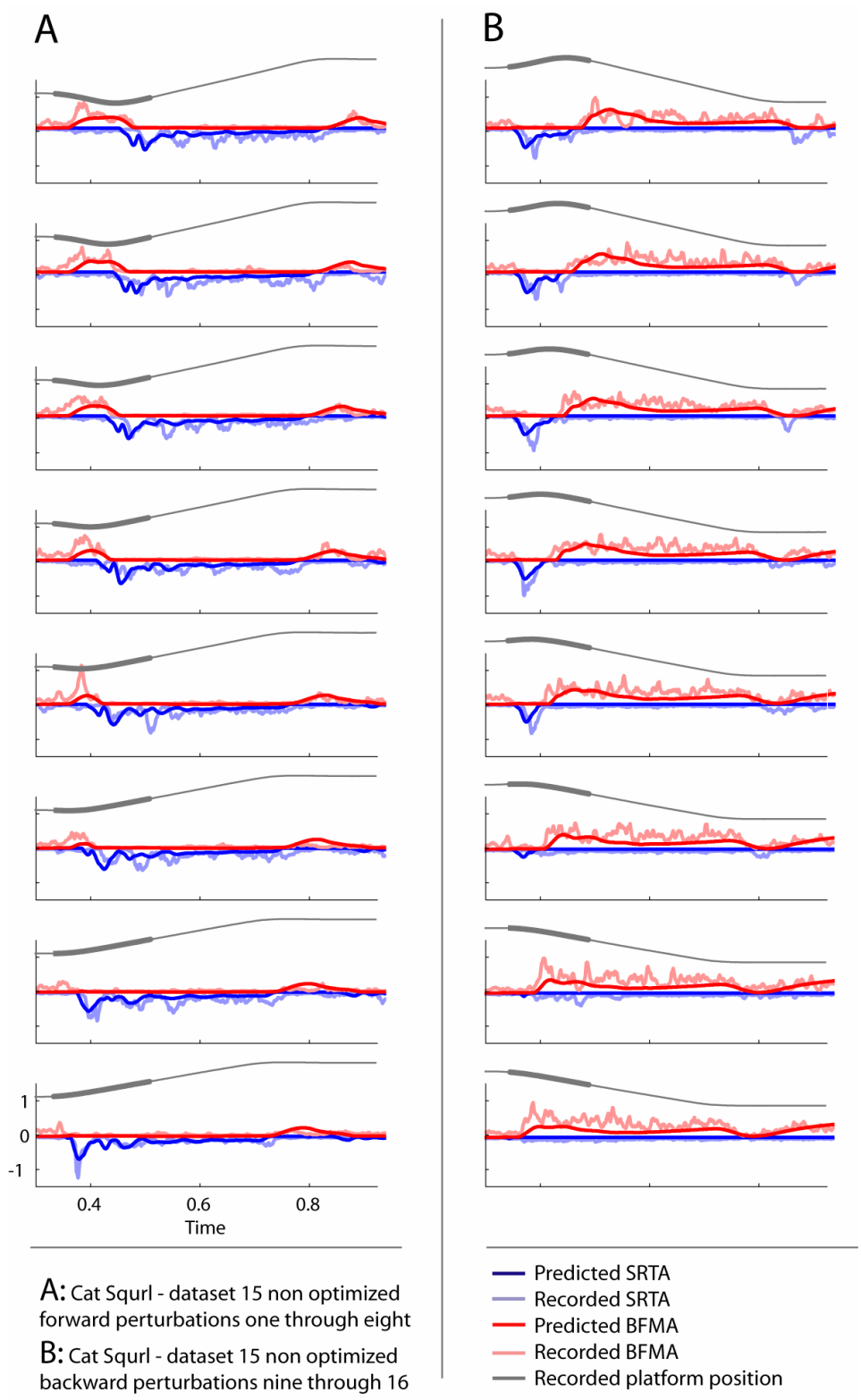

Figure 52: Cat Squrl, dataset 15, muscles SRTA vs. BFMA without further optimization: simulated with the gains of the unidirectional perturbations of trial eight and 16.

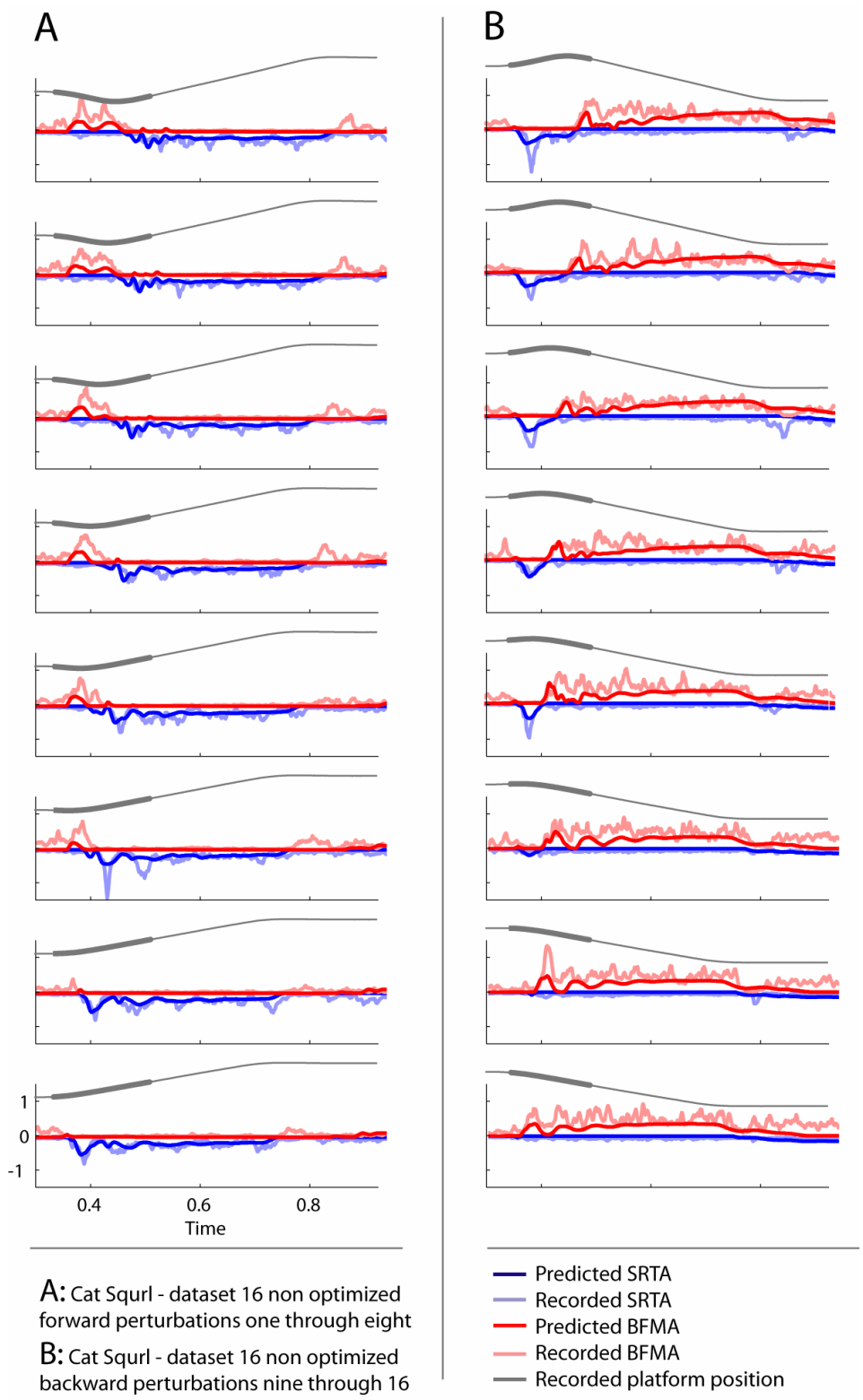

Figure 53: Cat Squrl, dataset 16, muscles SRTA vs. BFMA without further optimization: simulated with the gains of the unidirectional perturbations of trial eight and 16.

Cat Knobi

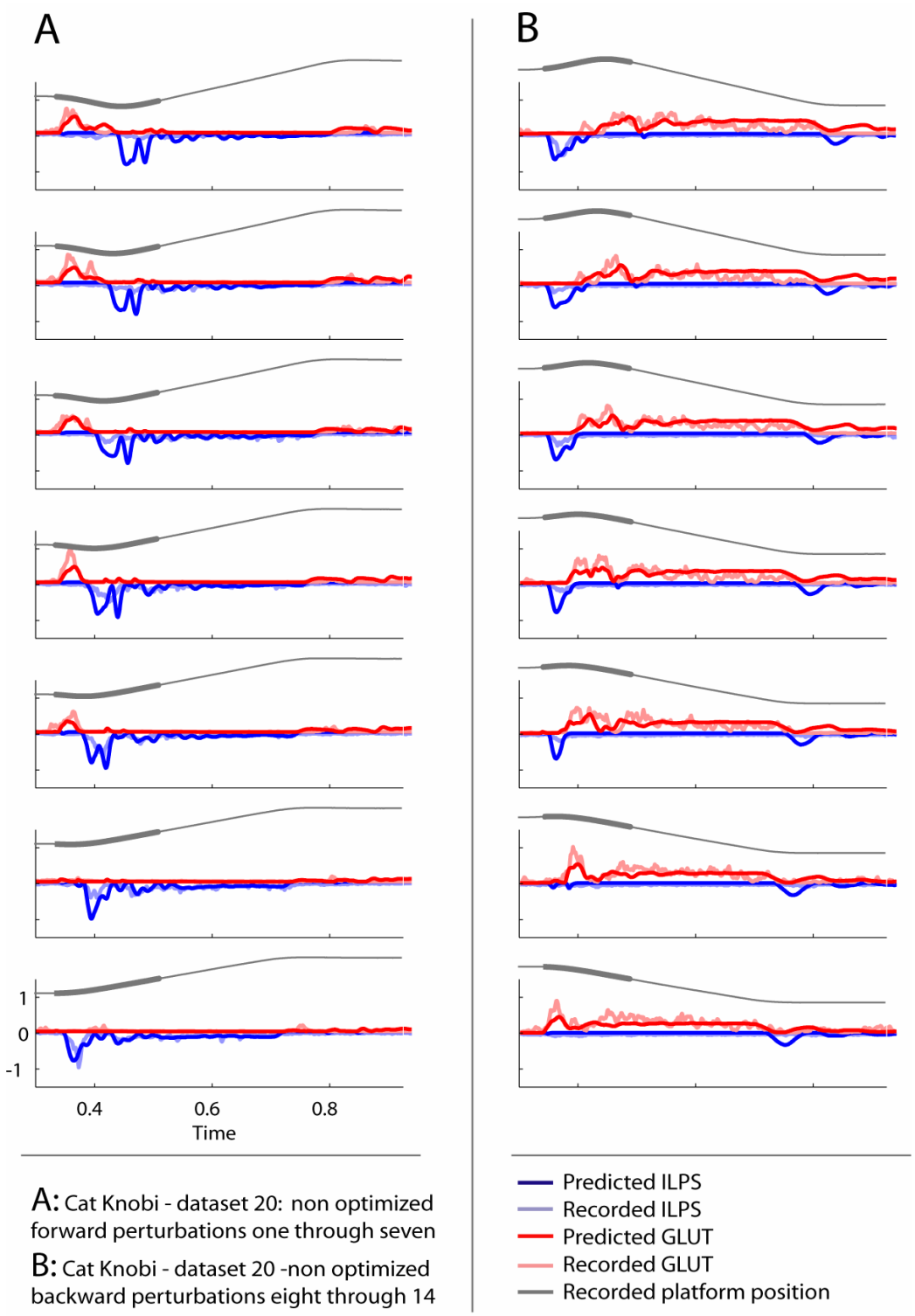

Figure 54: Cat Knobi, dataset 20, muscles ILPS vs. GLUT without further optimization: simulated with the gains of the unidirectional perturbations of trial seven and 14.

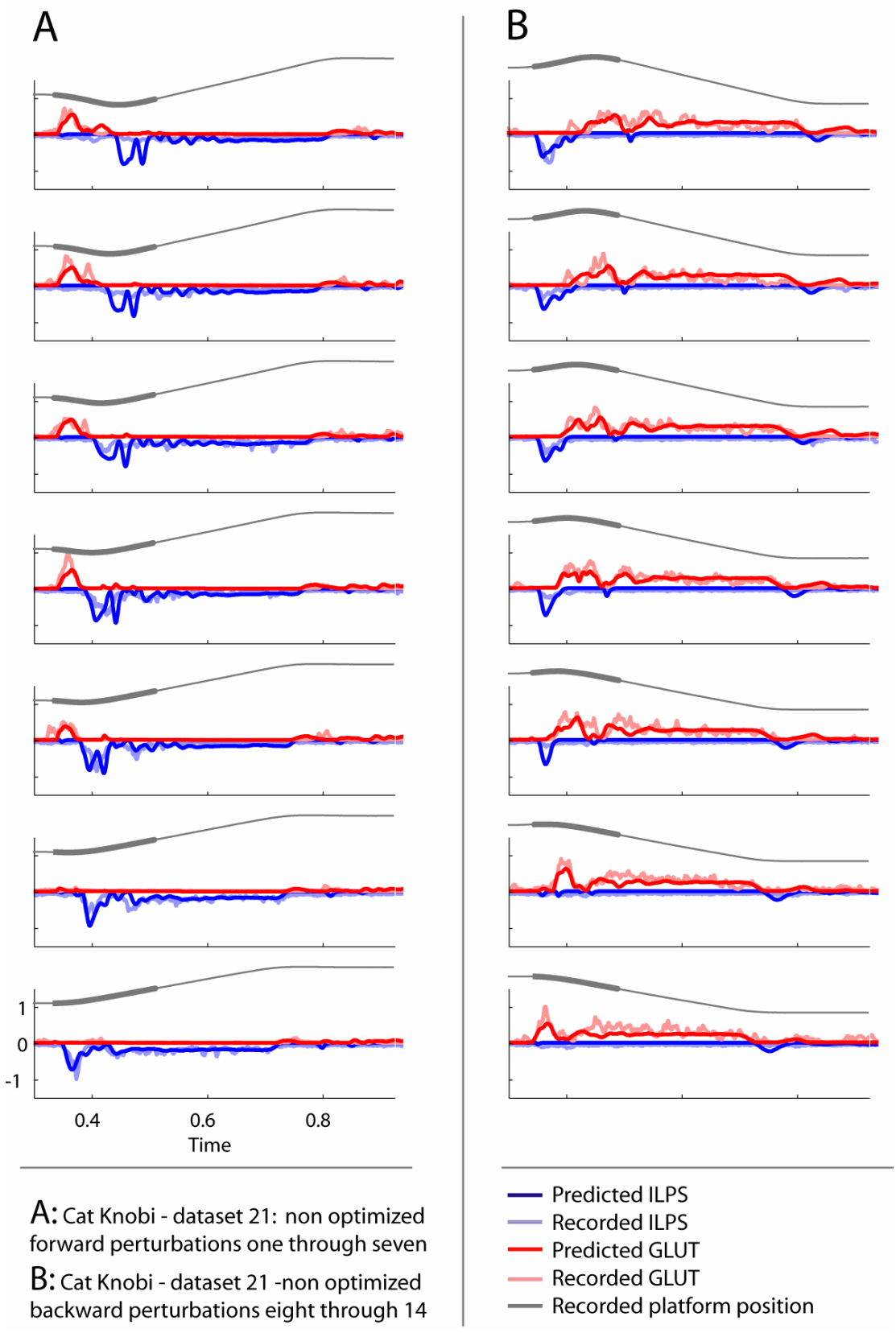

Figure 55: Cat Knobi, dataset 21, muscles ILPS vs. GLUT without further optimization: simulated with the gains of the unidirectional perturbations of trial seven and 14.

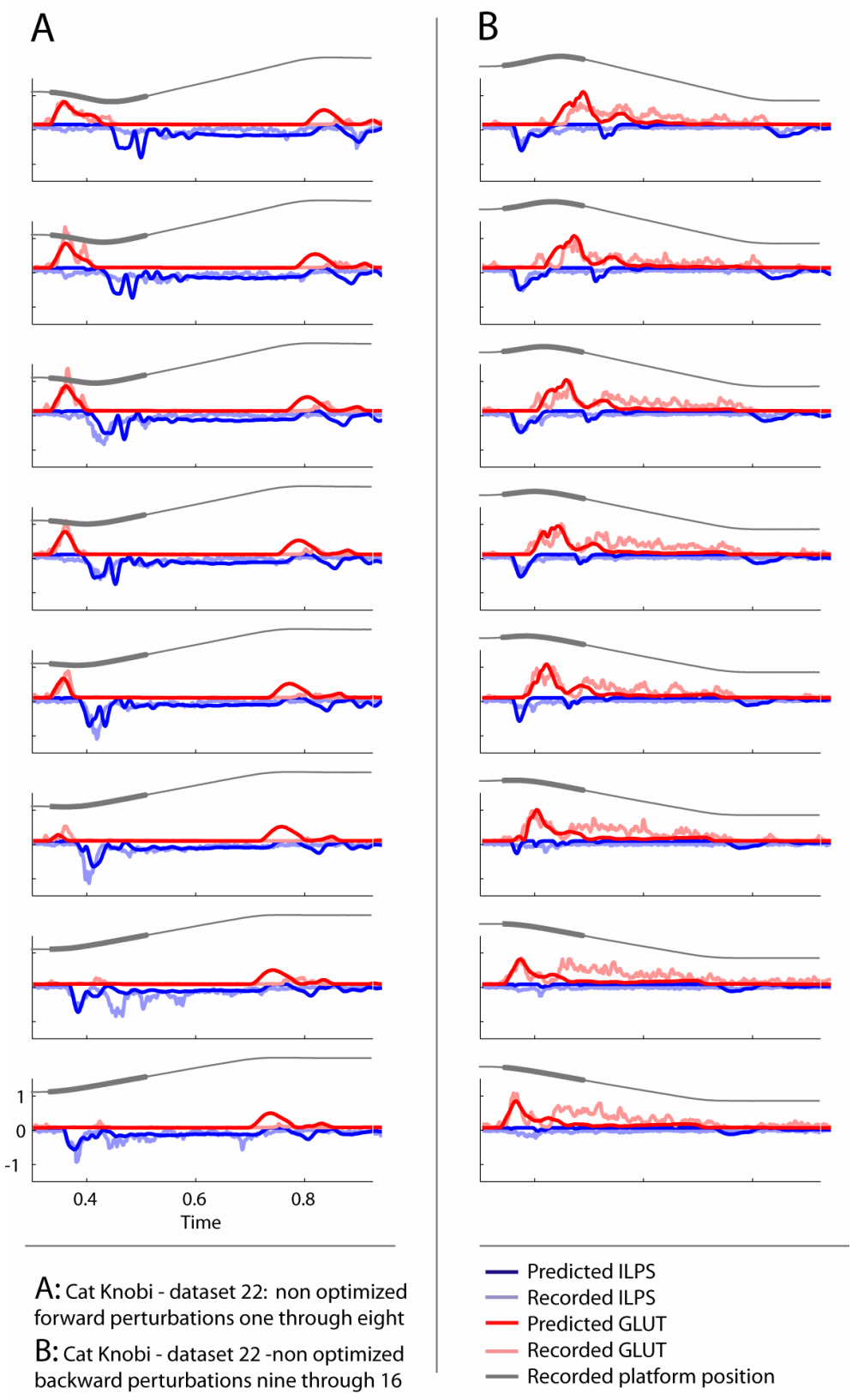

Figure 56: Cat Knobi, dataset 22, muscles ILPS vs. GLUT without further optimization: simulated with the gains of the unidirectional perturbations of trial eight and 16.

REFERENCES

Alexandrov AV, Frolov AA, and Massion J. Biomechanical analysis of movement strategies in human forward trunk bending. II. Experimental study. *Biol Cybern* 84: 435-443, 2001.

Audu ML, and Davy DT. The influence of muscle model complexity in musculoskeletal motion modeling. *J Biomech Eng* 107: 147-157, 1985.

Brown LA, Jensen JL, Korff T, and Woollacott MH. The translating platform paradigm: perturbation displacement waveform alters the postural response. *Gait Posture* 14: 256-263, 2001.

Fuglevand AJ, Winter DA, and Patla AE. Models of recruitment and rate coding organization in motor-unit pools. *J Neurophysiol* 70: 2470-2488, 1993.

Gordon AM, Huxley AF, and Julian FJ. The variation in isometric tension with sarcomere length in vertebrate muscle fibres. *J Physiol* 184: 170-192, 1966.

He JP, Levine WS, and Loeb GE. Feedback gains for correcting small perturbations to standing posture. *IEEE Trans Autom Control* 36: 322-332, 1991.

Hof AL, and Van den Berg J. EMG to force processing I: An electrical analogue of the Hill muscle model. *J Biomech* 14: 747-758, 1981.

Horak F, and Moore SP. The effect of prior leaning on human postural responses. *Gait Posture* 1: 203-210, 1993.

Horak FB, Dickstein R, and Peterka RJ. Diabetic neuropathy and surface sway-referencing disrupt somatosensory information for postural stability in stance. *Somatosensory and Motor Research* 19: 316-326, 2002.

Horak FB, and Hlavacka F. Somatosensory loss increases vestibulospinal sensitivity. *Journal of Neurophysiology* 86: 575-585, 2001.

Horak FB, and Macpherson JM. Postural orientation and equilibrium. In: *Handbook of Physiology, Section 12*. New York: American Physiological Society, 1996, p. 255-292.

Horak FB, Shupert CL, and Mirka A. Components of postural dyscontrol in the elderly: a review. *Neurobiol Aging* 10: 727-738, 1989.

Jo S, and Massaquoi SG. A model of cerebellum stabilized and scheduled hybrid long-loop control of upright balance. *Biol Cybern* 91: 188-202, 2004.

Kuo AD. An optimal control model for analyzing human postural balance. *IEEE Trans Biomed Eng* 42: 87-101, 1995.

Kuo AD, and Zajac FE. A biomechanical analysis of muscle strength as a limiting factor in standing posture. *J Biomech* 26 Suppl 1: 137-150, 1993.

Lieber RL. *Skeletal Muscle Structures and Functions, Implications for Rehabilitation and Sports Medicine*. Williams & Wilkins, 1992.

Lockhart DB. Prediction of muscle activation patterns during postural control using a feedback control model. In: *Woodruff School of Mechanical Engineering*. Atlanta, GA: Georgia Institute of Technology, 2005, p. 115.

Lockhart DB, and Ting LH. Prediction of muscle activation patterns for postural control using a linear feedback model. In: *American Society of Biomechanics Annual Meeting*. Portland, OR: 2004.

Macpherson JM. Strategies that simplify the control of quadrupedal stance. I. Forces at the ground. *J Neurophysiol* 60: 204-217, 1988.

Macpherson JM, and Fung J. Weight support and balance during perturbed stance in the chronic spinal cat. *Journal of Neurophysiology* 82: 3066-3081, 1999.

Macpherson JM, Lywood DW, and Van Eyken A. A system for the analysis of posture and stance in quadrupeds. *J Neurosci Methods* 20: 73-82, 1987.

Mazzaro N, Grey MJ, and Sinkjaer T. Contribution of afferent feedback to the soleus muscle activity during human locomotion. *J Neurophysiol* 93: 167-177, 2005.

Park S, Horak F, and Kuo AD. Effect of initial lean on scaling of postural feedback responses. In: *Key Engineering Materials*2005, p. 142-147.

Park S, Horak FB, and Kuo AD. Postural feedback responses scale with biomechanical constraints in human standing. *Exp Brain Res* 154: 417-427, 2004.

Partridge LD. Modifications of Neural Output Signals by Muscles: A Frequency Response Study. *J Appl Physiol* 20: 150-156, 1965.

Peterka RJ. Postural control model interpretation of stabilogram diffusion analysis. *Biol Cybern* 82: 335-343, 2000.

Peterka RJ. Sensorimotor integration in human postural control. *J Neurophysiol* 88: 1097-1118, 2002.

Peterka RJ, and Loughlin PJ. Dynamic regulation of sensorimotor integration in human postural control. *J Neurophysiol* 91: 410-423, 2004.

Roy A. Robust Stabilization of Multi-Body Biomechanical Systems: A Control Theoretic Approach. University at Little Rock, 2004.

Siegmund GP, Sanderson DJ, and Inglis JT. The effect of perturbation acceleration and advance warning on the neck postural responses of seated subjects. *Exp Brain Res* 144: 314-321, 2002.

Stapley PJ, Ting LH, Hulliger M, and Macpherson JM. Automatic postural responses are delayed by pyridoxine-induced somatosensory loss. *J Neurosci* 22: 5803-5807, 2002.

Szturm T, and Fallang B. Effects of varying acceleration of platform translation and toes-up rotations on the pattern and magnitude of balance reactions in humans. *J Vestib Res* 8: 381-397, 1998.

Tinetti ME. Clinical practice. Preventing falls in elderly persons. *N Engl J Med* 348: 42-49, 2003.

Tinetti ME, and Williams CS. The effect of falls and fall injuries on functioning in community-dwelling older persons. *J Gerontol A Biol Sci Med Sci* 53: M112-119, 1998.

Van der Helm F, and Rozendaal LA. *Musculoskeletal Systems with Intrinsic and Proprioceptive Feedback*. New York: Springer, 2000, p. 164-174.

van der Kooij H, Jacobs R, Koopman B, and Grootenboer H. A multisensory integration model of human stance control. *Biol Cybern* 80: 299-308, 1999.

van der Kooij H, Jacobs R, Koopman B, and van der Helm F. An adaptive model of sensory integration in a dynamic environment applied to human stance control. *Biol Cybern* 84: 103-115, 2001.

Widmaier EP, Raff H, and Strang KT. *Vander's Human Physiology - The Mechanisms of Body Functions*. McGraw Hill, 2006.

Winters JM, and Stark L. Analysis of fundamental human movement patterns through the use of in-depth antagonistic muscle models. *IEEE Trans Biomed Eng* 32: 826-839, 1985.